The Biogeochemical Controls on the Corrosion and Fate of Depleted Uranium

by

Stephanie Handley-Sidhu

A thesis submitted to the University of Plymouth in partial fulfilment for the degree of

DOCTOR OF PHILOSOPHY

School of Earth, Ocean & Environmental Sciences
Faculty of Science

October 2008

This copy of the thesis has been supplied on condition that anyone who consults it is understood to recognise that its copyright rests with its author and that no quotation from the thesis and no information derived from it may be published without the author's prior consent.

Signed:.....Shondly Sidha..............

Date:........16-03-09................

Dedicated in loving memory of Susan who was a great mum

and friend

AUTHOR'S DECLARATION

At no time during the registration for the degree of Doctor of Philosophy has the author been registered for any other University award without prior agreement of the Graduate Committee.

This study was financed with the aid of a studentship form the Natural Environment Research Council (Studentship number; NER/S/S/2004/13082) and carried out in collaboration with Universities of Manchester and Dundee. Relevant scientific seminars and conferences were regularly attended at which work was presented; external institutions were visited for consultation purposes and several papers were prepared for publication.

The work presented in this thesis is primarily the work of the author except where specified.

Word count of main body of thesis

28,871 words

Signed:....*S Hand Sidhu*.................

Date:......16-03-09.................

i

Abstract

The Biogeochemical Controls on the Corrosion and Fate of Depleted Uranium

Stephanie Handley-Sidhu

Depleted uranium (DU) is a by-product of the nuclear fuel industry and is used in anti-tank penetrators due to its high density, self-sharpening and pyrophoric properties. Military activities have left a legacy of DU waste in terrestrial and marine environments and presently there are no clean up procedures in place. In order to understand the fate of this DU, long term (500 days) microcosm experiments simulating key environments have been carried out for the first time to investigate the mechanisms and rates of DU corrosion as a function of the biogeochemical and environmental conditions.

The corrosion of DU was investigated in microcosms simulating organic-rich marine sediments of high and medium salinity. The results showed that the biogeochemical conditions control DU corrosion in both systems, with corrosion occurring under sub-oxic conditions (0.056 ± 0.006 g cm^{-2} y^{-1}) and ceasing under anoxic conditions due to passivation of the DU surface. During corrosion, oxidation of surface-bound UO_2 to U(VI) and its subsequent dissolution was identified as the main source of U to the surrounding water and sediment. The corroding DU was found to increase the rate of progression through the redox cascade (NO_3^-, Fe(III) and SO_4^{2-}) and decreased the diversity of the microbial community.

The corrosion of DU was also studied in microcosms simulating field-moist and waterlogged soil. Under waterlogged soil conditions, corrosion occurred under sub-oxic conditions at a rate of $0.010 - 0.020$ g cm^{-2} y^{-1} and the mechanism of DU corrosion was comparable to that in marine sediments. Again, passivation of the metal occurred under anoxic conditions, and the corroding DU increased the rate of progression through the redox cascade and decreased the diversity of the microbial community. However, under oxic field-moist conditions the DU corroded at a notably higher rate of 0.49 ± 0.06 g cm^{-2} y^{-1} to bright yellow metaschoepite, and this loosely bound product was the main source of U to the surrounding matrix. Despite the different mechanism of corrosion, the corroding DU again caused changes in the local biogeochemical environment and changed the microbial community profile.

Finally, the corrosion of DU was investigated in microcosms simulating field-moist dune sand and sand with seawater intrusion. This work confirmed the earlier hypotheses that the corrosion of DU and the products formed are dependent on the water content and geochemistry of the environment. In the field-moist sand DU corroded at a rate of 0.10 ± 0.01 g cm^{-2} y^{-1}, metaschoepite formed and changes were observed in the geochemical environment. The lower corrosion rate in the sand compared to the field-moist soil was attributed to differences in soil/sediment properties. Column experiments showed that metaschoepite transport through dune sand was dependent on its dissolution to dissolved U(VI). The majority of dissolved U(VI) adsorbed to the sand with very slow desorption kinetics and it is this behaviour that will dominate transport. In the sand with seawater intrusion, the mechanism of DU corrosion was the same as reported in organic-rich marine sediments; however the rate of corrosion was linear (0.020 ± 0.003 g cm^{-2} y^{-1}) due to the system remaining oxic.

Acknowledgements

Oral Presentations

Handley-Sidhu, S., Worsfold, P.J., and Keith-Roach, M.J. (2008). The corrosion of depleted uranium penetrators in grassland soils. Vancouver, Canada, Goldschmidt, 13 - 18th July 2008.

Vaughan D., Alvarez, R., Byran N., Formina, M., Gadd, G.M., Handley-Sidhu, S., Keith-Roach, M., Livens F., and Lloyd, J. (2008). Geochemical and microbial controls on the decomposition and dispersion of depleted uranium in the environment: Experimental Studies. Vancouver, Canada, Goldschmidt, 13 -18th July 2008.

Handley-Sidhu, S., Worsfold, P.J., and Keith-Roach, M.J. (2008). The corrosion and fate of depleted uranium in coastal sediment during progressively anoxic conditions. Cancun, Mexico, 2nd International Nuclear Chemistry Congress 13 -18th April 2008.

Handley-Sidhu, S., Worsfold, P.J., and Keith-Roach, M.J. (2008). The corrosion and fate of depleted uranium in coastal sediment during progressively anoxic conditions. Nottingham University, COGER Conference 7-9th April.

Handley, S., Worsfold, P.J., and Keith-Roach, M.J. (2007). Investigating the corrosion of depleted uranium in the environment. Loughborough University, COGER Conference 17-19th April.

Handley, S., Worsfold, P.J., and Keith-Roach, M.J. (2006). Experimental design and strategy for investigating the decomposition of depleted uranium in the environment. Westlakes Research Institute, COGER Conference 3-6th April.

Contents

Chapter 1. Introduction

Chapter 4. The Corrosion and Fate of Depleted Uranium Alloy in Grassland Soils

Chapter 5. The Corrosion and Transport of Depleted Uranium Alloy in Sand Environments

List of Abbreviations

DNA	Deoxyribonucleic acid
DU	Depleted uranium
Eh	Redox potential
ICP-MS	Inductively coupled plasma mass spectroscopy
K_d	Sorption coefficient
LOD	Detection limit (3 x standard deviations of the blank)
PEEK	Polyetheretherketone
RISA	Ribosomal intergenic spacer analysis
SEM-EDAX	Scanning electron microscopy - energy dispersive X-ray spectroscopy
TEA	Terminal electron acceptors
UO_2	Uraninite
U	Uranium
UO_2^{2+}	Uranyl
$UO_3.H_2O$	Schoepite
XRD	X-ray diffraction
XRF	X-ray fluorescence

Chapter 1

Introduction

1.1 Uranium

Uranium is a naturally-occurring, metallic element that is toxic and weakly radioactive. It is ubiquitous in the natural environment and present in varying concentrations in environmental matrices (Table 1.1). Natural U is a mixture of three alpha-emitting radioactive isotopes, ^{234}U, ^{235}U, and ^{238}U; with an isotopic composition of approximately 0.0054 %, 0.72 %, and 99.27 %, respectively (WHO, 2001). Uranium-234, ^{235}U, and ^{238}U decay with half-lives of 2.46 × 10^5, 7.04 × 10^8, and 4.47 × 10^9 years, respectively (BLEISE et al., 2003), and are in equilibrium with their decay series isotopes in most environments, thus U-containing materials emit alpha, beta and gamma radiation (JIA et al., 2004). Uranium-235 is fissile, a property used in nuclear reactors and nuclear weapons. Most reactors require the ^{235}U isotope to be enriched to 3-4% by mass, and this is achieved on the basis of isotopic mass difference through gas centrifugation.

Table 1.1 Concentration of U found in environmental matrices (BLEISE et al., 2003).

Environmental matrix	Typical concentrations
Soil	0.3 - 11.7 mg kg^{-1}
Air	2.5 × 10^{-8} - 2.5 × 10^{-7} mg m^{-3}
Surface water	3.0 × 10^{-2} - 2.1 µg L^{-1}
Ground water	3.0 × 10^{-3} - 2.0 µg L^{-1}
Seawater	3.0 µg L^{-1}

1.2 Depleted Uranium

Depleted uranium (DU) is a by-product of ^{235}U enrichment, thus it has a lower ^{235}U content than natural U: approximately 0.0006 % ^{234}U, 0.2 % ^{235}U, and 99.8 % ^{238}U (WHO, 2001). In the production of 1 kg of U fuel (3 % ^{235}U), 5 kg of DU is produced (BEM and BOU-RABEE, 2004). This waste DU is approximately 40 % less radioactive than naturally-occurring U (Table 1.2).

Table 1.2 The activity of natural U and DU (0.2 % ^{235}U) (BLEISE et al., 2003).

Isotope	Natural U activity (Bq mg^{-1})	DU activity (Bq mg^{-1})
^{234}U	12.40	2.26
^{235}U	0.57	0.16
^{238}U	12.40	12.40
Total	25.28	14.80

1.3 Applications of Depleted Uranium

DU has many civil applications such as counterweights for aircraft, alloy in special steels, catalysts in the oil and gas industries, oil-well sinker bars and for radiation shielding (BETTI, 2003; BLEISE et al., 2003). The known military applications of DU are DU munitions and protective amour for tanks (BLEISE et al., 2003).

1.4 Depleted Uranium Munitions in the Environment

DU metal has been developed as an anti-tank penetrator due to its high density, hardness and relatively low cost. It is alloyed with 0.75 % titanium (DU-Ti) to improve its strength, ductility and corrosion resistance. DU munitions have no explosive charge; they are "kinetic weapons", whereby the force of the impact comes from the high

3

kinetic energy of the dense DU penetrator travelling at speeds of up to 1.8 km s^{-1} (BAILEY et al., 2002). DU is pyrophoric and self sharpens on impact, giving it superior penetrative ability (BLEISE et al., 2003).

The UK Ministry of Defence (MOD) currently use 120 mm (Charm 3) anti-tank rounds, which are fired from Challenger tanks (POST, 2001). These munitions were used during the 1991 Iraq/Kuwait and the 2003 Iraq conflicts. The Charm 3 munitions contain a DU-Ti penetrator rod with radius of 1.5 cm, length of 30 cm and an approximate mass of 4500 g (BAILEY et al., 2002).

The USA forces have a wider range of DU rounds for use in tanks, aircraft and ships. The USA A-10 anti-tank aircraft fire 30 mm DU munitions, and these were used widely during the 2003 Iraq and 1999 Kosovo/Sebia conflicts (POST, 2001; BLEISE et al., 2003). The 30 mm DU munitions contains a conical DU-Ti penetrator rod with a base radius of 0.8 cm length of 9.5 cm and an approximate mass of 280 g (BLEISE et al., 2003).

1.4.1 Military Sources of Depleted Uranium into the Environment

In the UK, the experimental test firing of DU alloy penetrators began in the 1960s and intensified in the early 1980s following a programme to develop armour munitions. The UK MOD estimates that between 1981 and 1995, 15 tonnes of 120 mm penetrators were fired against armoured plate at Eskmeals in Cumbria, and 30 tonnes of DU rounds have been fired into the Solway Firth since testing began in 1982 at Kirkcudbright, Scotland (POST, 2001).

In the USA the experimental firing of DU alloy penetrators began in the early 1970s and has taken place at the Aberdeen and Yuma Proving Grounds. At the Aberdeen Proving Ground in Maryland, > 70 tonnes of DU has been deposited over an area of 1500 acres, into terrestrial, fresh water, brackish water and marine aquatic

environments (DONG et al., 2006; FAN et al., 2005). The Yuma Proving Ground in western Arizona is a general-purpose desert environmental test facility that has conducted test firing of DU weapons since the 1980s over an area of 12000 acres, although the amount of DU deposited has not been released (FAN et al., 2005; JOHNSON et al., 2006).

During Gulf War I, approximately 320 tonnes of DU munitions were used by the USA forces (BLEISE et al., 2003), and approximately 1 tonne of DU was fired from UK tanks (BLEISE et al., 2003). During the Bosnia-Herzegovina conflict in 1994 and 1995, approximately 3 tonnes of DU was fired in NATO airstrikes, and about 10 tonnes of DU was fired during the 1999 Kosovo conflict (BLEISE et al., 2003). During the recent 2003 Iraq War approximately 2 tonnes of DU was fired by the UK MOD (MOD, 2008), the amount of DU fired by the USA forces has not yet been released.

1.5 Environmental Impact of DU Penetrators

When a penetrator hits its target, an estimated 10 - 35 % (maximum of 70 %) of the DU mass is converted into an aerosol (BLEISE et al., 2003). However, it has been estimated that 90 % of penetrators fired from aircraft miss their targets (PAPASTEFANOU, 2002) and when penetrators hit soft targets such as soil, there is insignificant aerosol production. The depth that a penetrator can become embedded within a soil depends on the angle of impact and physical properties of the soil, with reported penetration depths of more than 2 m in clay soils (PAPASTEFANOU, 2002) and 6 - 7 m in soft soils (UNEP, 2001). Therefore, there are two primary source terms of DU entering the environment from fired DU munitions: (1) as aerosol dust generated from abrasions during firing or impact and (2) the corrosion of whole or part penetrators lodged in environmental matrices.

Aerosol dusts dilute and disperse, thus are not of significant concern beyond the immediate health considerations for exposed military personnel (UNEP, 2001). As the majority of DU deposited is as whole or part penetrators, the eventual corrosion and dissolution of these pose the key long term environmental concern (BAILEY et al., 2002). The DU penetrators are grey-black in colour but they corrode to black and yellowish-green oxides (UNEP, 2001). The concern for human exposure is mostly chemical rather than radiological, DU has low specific radioactivity and its emissions are mainly alpha particles that do not have the ability to penetrate skin (BLEISE et al., 2003; HAMILTON, 2001). The hazards of picking up a penetrator therefore come from not washing hands afterwards, keeping them in pockets for long periods, inhalation of DU dust/corrosion products and ingestion of DU debris, and DU contaminated soil, food and water (UNEP, 2001).

The presence of high U level in humans has been reported to effect renal functions and very high levels can lead to kidney failure (PRIEST, 2001). Therefore the World Health Organisation has recommended a maximum admissible concentration for U in drinking water of 15 μg L^{-1} (WHO, 2005). Currently there are no plans to clean-up the DU deposited during conflict, in light of this, agencies such as United Nations Environment Programme (UNEP) have undertaken post-conflict environmental assessments on targeted DU sites at Kosovo in 2000 (UNEP, 2001), Serbia and Montenegro in 2001 (UNEP, 2002), Bosnia and Herzegovina 2002 (UNEP, 2003). All these reports confirm that DU has impacted the environment but chemical and radiological harm to humans is likely to occur only under worse-case scenarios. Primarily, health risks will depend on the awareness of people coming into contact with DU. The reports therefore recommend precautionary actions such as signing, fencing and clean-up of impacted sites (UNEP, 2001; 2002; 2003).

6

1.6 The Corrosion of DU Alloy

The corrosion of a metal or alloy can be defined as the detrimental change of its fabric and structure due to interaction with its environment (BAILEY et al., 2002). Depleted U is thermodynamically unstable and will readily corrode in a natural system. The corrosion and dissolution of DU occurs in two stages; firstly, oxidation of zero valent U to U(IV), and then oxidation of U(IV) to U(VI). The first process is favorable under all earth surface conditions while the second is dependent on redox and pH conditions (BAILEY et al., 2002).

The corrosion behavior of U is shown in Equations [1.1] to [1.5]. In water [1.1] and air [1.2], U readily corrodes to the U(IV) mineral uraninite (UO_2) (DONG et al., 2006; LAUE et al., 2004). Further oxidation to U(VI) is dependent on local redox and pH conditions (BAILEY et al., 2002), and leads to the formation of soluble species such as the uranyl ion (UO_2^{2+}) [1.3] and minerals such as schoepite ($UO_3.2H_2O$) [1.4]. Dissolution of schoepite also occurs, with the release of soluble species such as UO_2^{2+} [1.5].

$$U_{(s)} + 2H_2O \rightarrow UO_{2(s)} + 2H_2 \qquad\qquad [1.1]$$

$$U_{(s)} + O_2 \rightarrow UO_{2(s)} \qquad\qquad [1.2]$$

$$UO_{2(s)} + 2H^+ + \frac{1}{2}O_2 \rightarrow UO_{2(aq)}^{2+} + H_2O \qquad\qquad [1.3]$$

$$UO_{2(s)} + \frac{1}{2}O_{2(g)} + 2H_2O \rightarrow UO_3.2H_2O_{(s)} \qquad\qquad [1.4]$$

$$UO_3.2H_2O_{(s)} + 2H^+ \rightarrow UO_{2(aq)}^{2+} + 3H_2O \qquad\qquad [1.5]$$
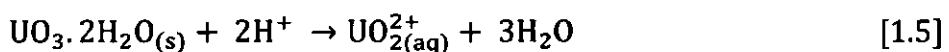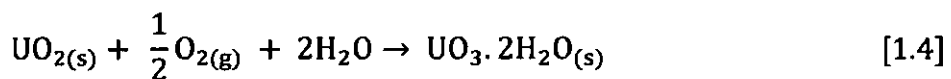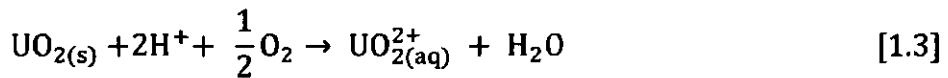
Uranium metal can undergo corrosion, immunity or passivation in water, according to the redox potential and pH conditions (Figure 1.1). In the domain of corrosion there is detrimental degradation of the metal, while in the domain of passivation the metal can become coated with an oxide, hydroxide, hydride or a salt, giving varying degrees of protection against corrosion, and in the domain of immunity the corrosion of a metal is thermodynamically impossible (POURBAIX, 1966). DU-Ti is more corrosion resistant than natural U; it will however corrode in a similar way to U metal (BAILEY et al., 2002). DU-Ti alloys have been observed to corrode by a pitting process involving localized areas on their surfaces (TOQUE and BAKER, 2006; 2007).
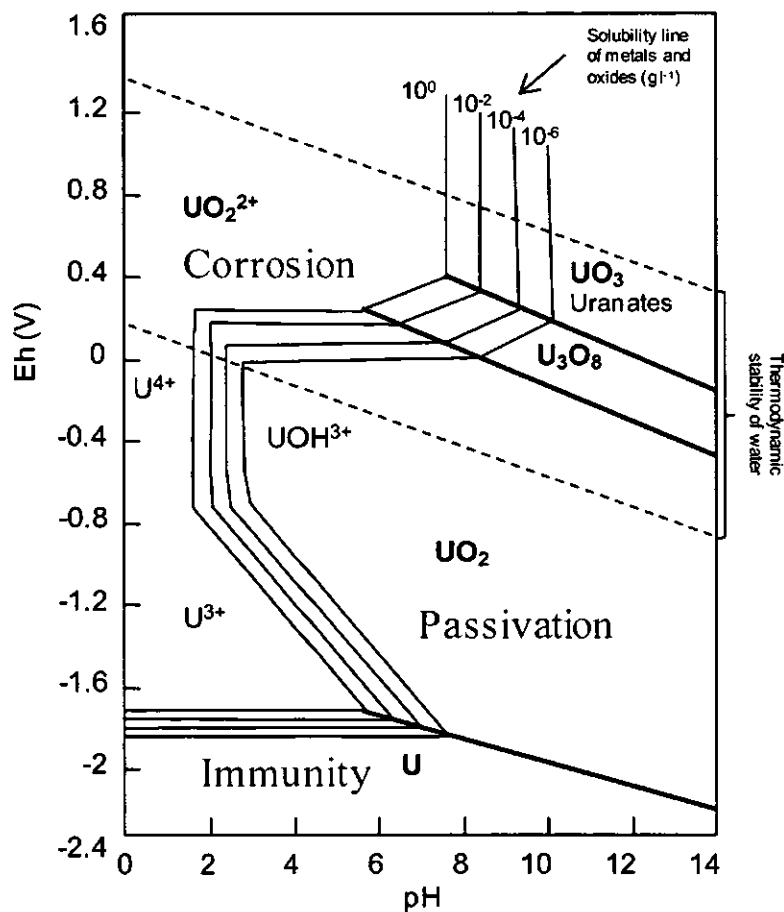
Figure 1.1 Adapted Pourbaix diagram for U metal in water (1atm, 25 °C) highlighting areas of corrosion, passivation and immunity (DE ZOUBOV, 1966).

1.6.1 Microbial Activity and Redox Potential

As highlighted in Figure 1.1 the redox potential is an important factor in the corrosion behaviour of U. Microorganisms can influence the redox potential of an environment by utilising a succession of terminal electron acceptors (TEA) for the oxidation of organic matter. The amount of energy gained from the use of each TEA influences the rate and sequence of TEA utilisation. The classical TEA sequence is reduction of: O_2, NO_3^-, Mn, Fe(III), SO_4^{2-} and methanogenesis (KONHAUSER et al., 2002). The dominant oxidation states for U at pH 7 are shown in Figure 1.2. During O_2, NO_3^-, and Mn reduction, relatively mobile U(VI) species dominate, whilst during Fe(III), SO_4^{2-}, and CO_2 reduction, the immobile U(IV) species dominate (KONHAUSER et al., 2002), thus highlighting the importance of the biogeochemical environment in the fate of DU.
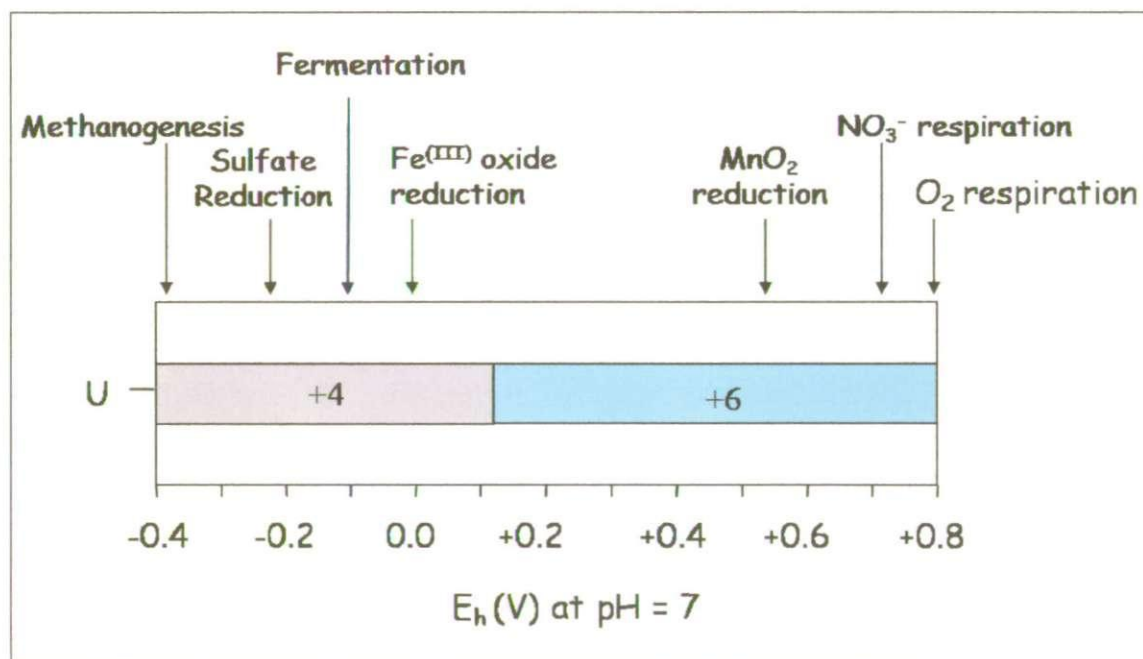
Figure 1.2 Adapted diagram showing the expected dominant oxidation states of U as a function of standard reduction potential in pH 7 water at equilibrium with atmospheric CO_2 (MORRIS and RAISWELL, 2002).

9

1.7 Experimental DU Corrosion Studies

Investigations into DU corrosion have included *in situ* and laboratory studies which provide an overview of corrosion rates and the corrosion products formed (Table 1.3). Laboratory-based dissolution studies (MCINTYRE et al., 1988; TRZASKOMA, 1982) have shown that DU alloy has a tendency to undergo pitting corrosion in the presence of chloride, with corrosion rates increasing with Cl⁻ concentration (DISPIRITO and TUOVINEN, 1982; TRZASKOMA, 1982). This is consistent with the remaining data in this table, which show the highest corrosion rates in marine environments (TOQUE and BAKER, 2007). In these *in-situ* marine experiments, scattered corrosion pits developed on the DU surface, with black uraninite (UO_2) corrosion products adhering to the surface.

Two *in situ* corrosion studies were carried out in silty clay soil at a test firing facility in Kirkcudbright, Scotland and in sand at a test facility in Eskmeals, Cumbria (TOQUE and BAKER, 2006). DU coupons were buried to a depth of 0.3 m and sampled periodically over 4.4 years. Black and yellow corrosion products characterised as UO_2 and schoepite, respectively, were observed on these DU coupons and in the surrounding soil at the first sampling time of 102 days. The corrosion rate of DU in the soil was faster than in sand, which was attributed to moisture content and soil parameters (TOQUE and BAKER, 2006). In general, soil parameter such as moisture content, anion concentrations, O_2 supply, pH, temperature and microbial community influence how corrosive conditions are in the environment (MATTSSON, 1989).

The corrosion of DU-Ti penetrators collected from Kosovo was studied in two soils (sandy-loamy and silty-loamy brown earth) in the laboratory at 20°C, with 16 mm week^{-1} of simulated rainfall (SCHIMMACK et al., 2007). Pitting corrosion occurred and black and yellow corrosion products were again reported. There was negligible difference in corrosion rates in these two different soils (0.19 ± 0.03 g cm^{-2} y^{-1}) which

had similar soil pH (5.6 vs. 5.8) and the same organic carbon content (2.1%) (SCHIMMACK et al., 2007).

Table 1.3 Summary of literature corrosion rates (g cm^{-2} year^{-1}) for DU-0.75Ti in soil, waters and sediments.

Environmental matrix	Corrosion rates (g cm^{-2} year^{-1})	Reference
Organic, clay-rich soil from Kirkcudbright	0.80 - 1.1	TOQUE and BAKER, 2006
Sandy-loamy and silty-loamy soil	0.19 ± 0.03	SCHIMMACK et al., 2007
Dune Sand, Eskmeals, Cumbria	0.080 - 0.17	TOQUE and BAKER, 2006
Sea Sediment, Solway Firth, Scotland	1.4 - 1.8	TOQUE and BAKER, 2007
H$_2$O	0.072	TRZASKOMA, 1982
3.5% NaCl	0.40	TRZASKOMA, 1982
5% NaCl	1.5	MCINTYRE et al., 1988
Seawater column, Solway Firth	2.6 - 3.1	TOQUE and BAKER, 2007

1.8 The Mobility of Corrosion Products

Studies of DU corrosion show that the predominant products formed in the environment are UO$_2$ and schoepite or similar phases (BUCK et al., 2004; JOHNSON et al., 2004; SCHIMMACK et al., 2007; TOQUE and BAKER, 2006; 2007). The transport of these corrosion products in the environment will depend on their size and on dissolution and subsequent transport of soluble U species. The geochemical speciation of U in the environment influences its solubility, mobility and fate. In oxidising and mildly

11

reducing environments the relatively soluble U(VI) species dominates, whereas in a reducing environment the less soluble U(IV) species dominates (LANGMUIR, 1997). A study from the Mojave Desert region of the YPG, investigated the migration of U from corroding penetrators (BUCK et al., 2004; JOHNSON et al., 2004). Distinct layers of U compounds were observed in the sandy loam soil; the surface contained yellow-orange schoepite, whereas at 2 - 4 cm depth bright yellow metaschoepite was observed and below 4 cm, U was present as secondary U silicate species (BUCK et al., 2004; JOHNSON et al., 2004). This highlights that dissolved U species are transported over longer distances than particulate corrosion products in the environment. However the mobility of soluble U species (predominately U(VI)) is a function of sorption, complexation and precipitation reactions occurring in the environment (Figure 1.3).
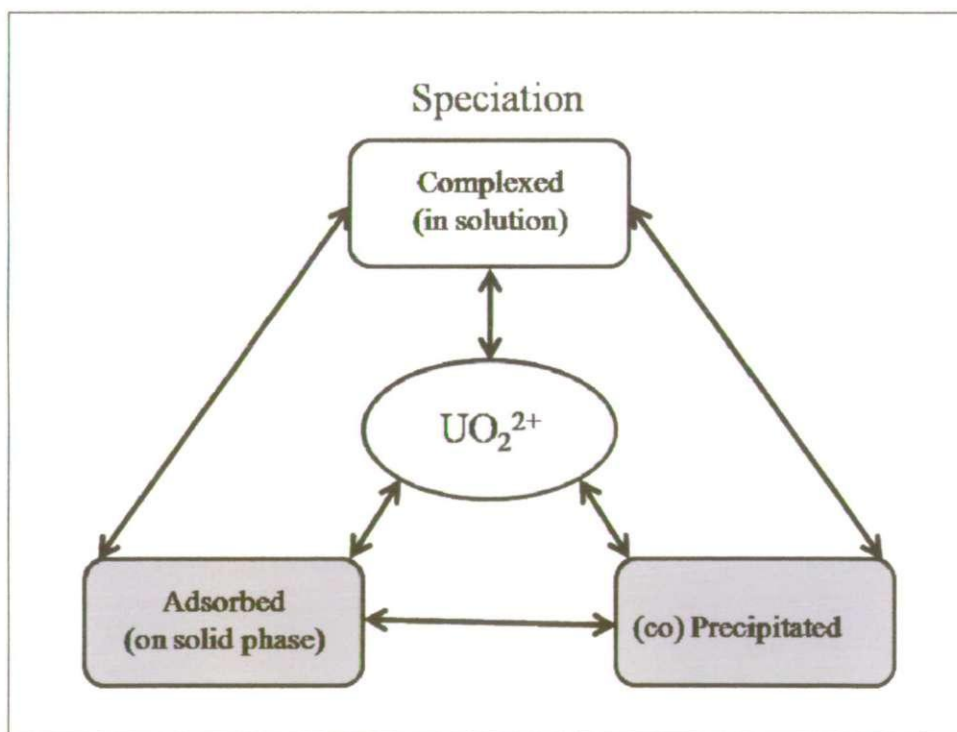
Figure 1.3 Adapted model showing the effect of chemical speciation on U(VI) mobility (BAILEY et al., 2002).

1.8.1 Sorption of U(VI)

The interaction of U(VI) ions with solid phases is an important factor limiting U mobility. Negatively charged surfaces of minerals and organic compounds adsorb uranyl ions (UO_2^{2+}). With increasing pH, protons are released and more negative charged binding sites are available to adsorb these U(VI) uranyl species. The sorption of U(VI) to minerals and organic matter occurs over a wide range of solution pH conditions (DUFF et al., 2002). Iron and Fe-containing minerals are important binding phases as they strongly adsorb UO_2^{2+} species; these minerals include iron oxyhydroxide (BRUNO et al., 1995) ferrihydrite ($Fe_5HO_8 \cdot 4H_2O$) (WAITE et al., 1994), Fe(III), hematite (α-Fe_2O_3) (MURPHY et al., 1999) and goethite (α-FeOOH) (GABRIEL et al., 1998). Uranyl also adsorbs to non Fe- containing minerals such as silica (SiO_2), alumina (Al_2O_3) and montmorillonite ($AlMg_2Si_4O_{10}OH_2 \cdot H_2O$) (SYLWESTER et al., 2000). Organic matter is another important binding solid phase as humic substances are often deposited on the surfaces of oxide and clay minerals of soils and sediments (CHOPPIN, 1992). Sorption to organic matter is very strong in soils and leads to the immobilisation of U (DUFF et al., 2002).

1.8.2 Influence of U speciation on Sorption

U(VI) has a high affinity for carbonate ligands, forming stable complexes such as $UO_2(CO_3)_2^{2-}$ or $UO_2(CO_3)_3^{4-}$ (Equations 1.6 - 1.7) (CHOY et al., 2006). These negatively charged complexes have a lower affinity than U(VI) ions for negatively charged surfaces and therefore increase the mobility of U(VI) in the environment.

$$UO_{2(aq)}^{2+} + 2HCO_3^- \rightarrow UO_2(CO_3)_{2(aq)}^{2-} + 2H^+ \qquad [1.6]$$

$$UO_2(CO_3)_{2(aq)}^{2-} + HCO_3^- \rightarrow UO_2(CO_3)_{3(aq)}^{4-} + H^+ \qquad [1.7]$$
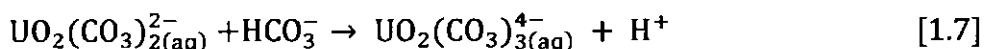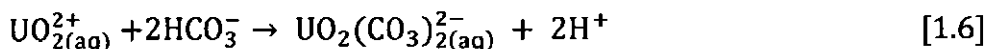
The speciation of dissolved U in the presence of inorganic carbon in summarised in Figure 1.4. In oxidising and mildly reducing environments at pH > 6 the negatively charged $UO_2(CO_3)_2^{2-}$ or $UO_2(CO_3)_3^{4-}$ dominate, between pH 5 - 6 the less soluble $UO_2(CO_3)$ species dominate and below pH 5 the uranyl ion dominants. The pH of a system is therefore a dominant control over U mobility (ECHEVARRIA et al., 2001).

The solubility of U is therefore enhanced by the presence of complexing ligands, including HCO_3^-, OH^-, PO_4^{3-}, NO_3^-, SO_4^{2-}, Fl^-, Cl^- and dissolved organics (humic and fulvic acids) (BOROVEC et al., 1979; LANGMUIR, 1997; SHANBHAG and CHOPPIN, 1981). The sorption of U onto minerals and organic matter tends to decrease in the presence of complexing ligands, for example U(VI) sorption onto clays is decreased in the presence of sulfate (BACHMAF et al., 2008) and fulvic acids due to complexation (KORNILOVICH et al., 2004).
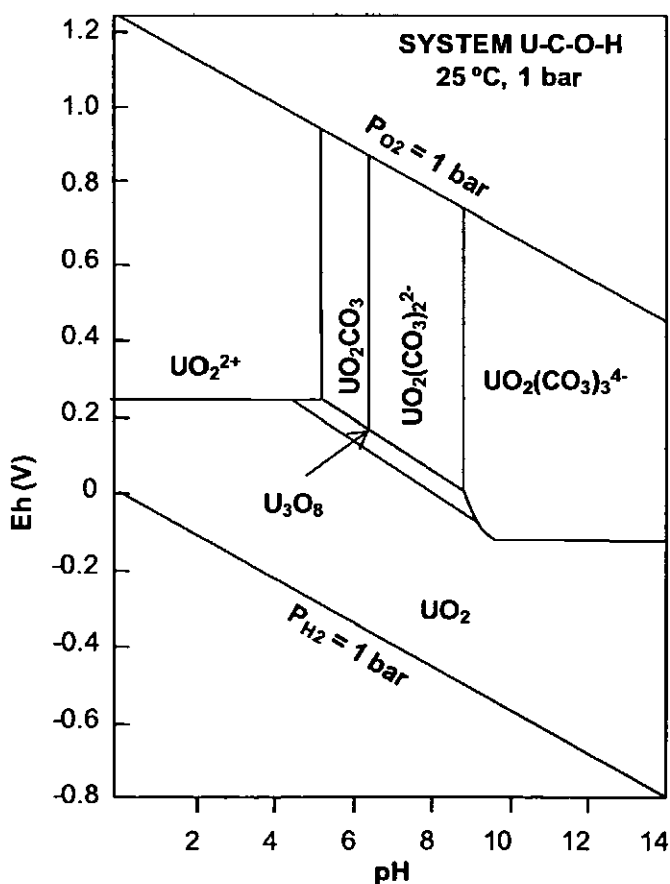
Figure 1.4 Redrawn Eh-pH diagram showing the U- C-O-H system. Assumed activities for dissolved species are: $U = 10^{-8, -6}$, $C = 10^{-3}$ (BROOKINS, 1988).

1.8.3 Reduction and Precipitation of U(VI)

The solubility of U is influenced by geochemical and microbially driven processes in a soil and sediment through co-precipitation and by direct or indirect microbial activities. The co-precipitation of U(VI) with Fe-oxides, carbonates and silicates occurs removing U from solution (BRUNO et al., 1995; DUFF et al., 2002; REEDER et al., 2000). However metals co-precipitated with Fe(III) can be released during the anaerobic respiration of Fe(III) (NEALSON and SAFFARINI, 1994). Fe(III)-reducing bacteria such as *Geobacter metallireducens* strain GS-15 and *Shewanella putrefaciens* can reduce U(VI) to U(IV) directly as a terminal electron acceptor in respiration, conserving energy in the process (LOVLEY et al., 1991). Other microorganisms such as the sulfate-reducing *Desulfovibrio vugaris* and *Desulfovibrio desulfuricans* are able to reduce U(VI) enzymically without conserving energy (LOVLEY and PHILLIPS, 1992; LOVLEY et al., 1993). Equally, since the oxidation state of U(VI) is controlled by the Eh of the system it can be reduced indirectly as anaerobic microbial respiration occurs (Figure 1.2) (KONHAUSER et al., 2002).

1.9 Uranium Minerals

Uranium (VI) minerals such as soddyite $((UO_2)_2SiO_4.2H_2O)$, schoepite $(UO_3.2H_2O)$ and rutherfordine (UO_2CO_3) form in oxic environments, whereas U(VI) minerals such as uraninite (UO_2) and coffinite $(USiO_4)$ are stable under reducing conditions (FINCH and EWING, 1992). The solubility (mg L^{-1}) of U(IV) and U(VI) minerals in water equilibrated with atmospheric CO_2 are shown in Table 1.4. The U(IV) mineral UO_2 which is a corrosion product of DU metal (TOQUE and BAKER, 2006; 2007) has a particularly low solubility of 0.00010 mg L^{-1}. However, in the environment UO_2 can be chemically oxidised to the more mobile U(VI) species by O_2 (ABDELOUAS et al., 1999; MOON et al., 2007; ZHENG et al., 2002), NO_2^- (SENKO et al., 2002; 2005), the

intermediates of NO_3^--reduction (NO_2^-, N_2O, and NO) (SENKO et al., 2002) and Fe(III) (hydr)oxides (NEVIN and LOVLEY, 2000; SENKO et al., 2005). The U(VI) mineral schoepite is much more soluble than uraninite and has been reported as a corrosion product of DU in oxic environments (TOQUE and BAKER, 2006).

Table 1.4 Adapted table showing the solubility (mg L^{-1}) of selected U minerals. At fixed temperature (15°C) and pH (7), in pure water at equilibrium with atmospheric CO_2 (BAILEY et al., 2002).

Oxidation State	Mineral	Solubility in H_2O under atmospheric CO_2 equilibrium (mg L^{-1})
U(IV)	Uraninite (UO_2)	0.00010
U(IV)	Coffinite ($USiO_4$)	0.096*
U(VI)	Soddyite (($UO_2)_2SiO_4.2H_2O$)	0.060
U(VI)	Schoepite ($UO_3.2H_2O$)	2.4
U(VI)	Rutherfordine (UO_2CO_3)	2700000¤

* Solubility controlled by the precipitation of uraninite
¤ Solubility controlled by the precipitation of schoepite and other U(VI) minerals

1.10 The Impact of Depleted Uranium on the Microbial Community

Although few studies have been carried out investigating the effect of DU on natural microbial communities, there is a body of knowledge from U contaminated environments, such as U mine waste heaps. These studies show that even in heavily polluted uranium wastes, microbial community can be diverse (CERDA et al., 1993; SCHIPPERS et al., 1995).

The effect of corroded DU (schoepite) on three measures of soil function (biological activity, decomposition and mineral N availability) were carried out in soil with DU over a concentration range of 0 to 25000 mg kg^{-1} (MEYER et al., 1998). The

16

biological activity deceased significantly as DU contamination reached 500 mg kg^{-1}. In another study, addition of DU (U_3O_8) to a soil at concentrations > 200 mg kg^{-1} resulted in a drastic loss of biomass and community diversity (RINGELBERG et al., 2004). The only genera of species identified that was able to grow in laboratory studies at the highest concentrations of U (20,000 mg kg^{-1}) was the Bacilli species. In *situ* characterisation of exposed DU soil sites have also shown the presence of Bacilli and an increase in the sulfate reducing bacteria *Desulfovibrio* (RINGELBERG et al., 2004).

The release of H_2 from corroding DU can also impact the microbial community, in a low O_2 environment the corrosion of U metal occurs with the release of H_2 (Equation 1.8) (LAUE et al., 2004) and this H_2 can be used as an electron donor by some microorganisms to support NO_3^-- (TILL et al., 1998) Fe(III)- (CACCAVO et al., 1994) and SO_4^{2-}-reduction (LIAMLEAM and ANNACHHATRE, 2007; OREMLAND and POLCIN, 1982). The biogeochemical indicators NO_3^-, Fe(III) and SO_4^{2-} can also be reduced abiotically by H_2, as shown in equations [1.9 - 1.11] (MARSH and MCINERNEY, 2001). Therefore the DU may impact the microbial community by changing the local geochemical environment and/or by the addition of corrosion products.

Reaction	ΔG (KJ/Mol of e−)
$U + 2H_2O \rightarrow UO_2 + 2H_2$	$= -139.53$ [1.8]
$\frac{1}{5}NO_3^- + \frac{1}{5}H^+ + \frac{1}{2}H_2 \rightarrow \frac{1}{10}N_2 + \frac{3}{5}H_2O$	$= -86.44$ [1.9]
$Fe(OH)_{3(am)} + 2H^+ + \frac{1}{2}H_2 \rightarrow Fe^{2+} + 3H_2O$	$= -43.89$ [1.10]
$\frac{1}{8}SO_4^{2-} + \frac{1}{8}H^+ + \frac{1}{2}H_2 \rightarrow \frac{1}{8}HS^- + \frac{1}{2}H_2O$	$= -0.42$ [1.11]
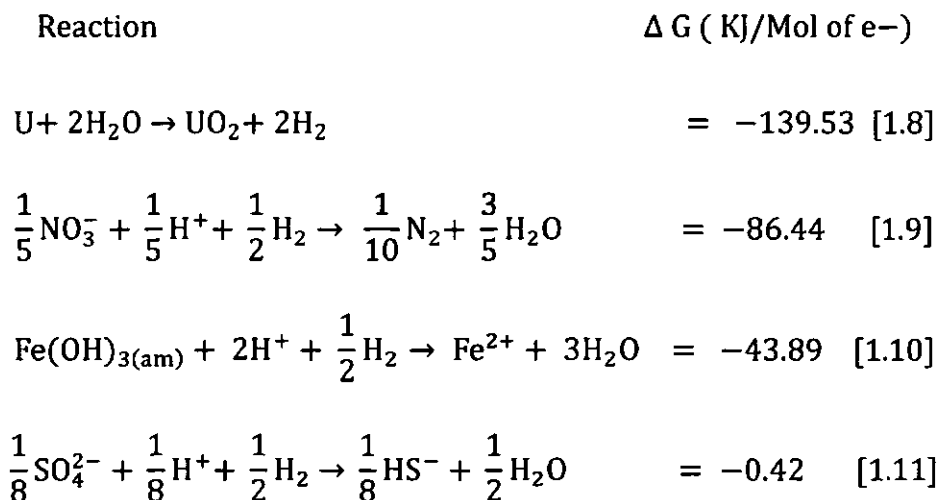
1.11 Microcosm Studies

A microcosm is defined as an intact, minimally disturbed piece of an ecosystem brought into the laboratory for study under controlled experimental conditions (PRICHARD and BOURQUIN, 1984). Microcosm have been used extensively to study the biotic and abiotic transformation of radioactive contaminants (BEGG et al., 2007; BURKE et al., 2005; REINOSO MASET et al., 2006) the fungal transformation of DU (FOMINA et al., 2008) and the effects of DU on microbial communities (MEYER et al., 1998; RINGELBERG et al., 2004). The advantages of using microcosm experiments for DU studies are that reproducible replicates and controls can be employed; changes in a sealed microcosm can be tracked over time in detail without interference from outside forces; and the study of radioactive and toxic substances can be carried out without contaminating the environment. The limitations of using microcosm experiments are that the ecosystem structure is disturbed and it does not represent a true environment, i.e. there is no groundwater flow, seasonal change or physical disturbance.

1.12 Transport Experiments

When predicting the movement of chemical species through soil, rock or sediment, the chemical interactions controlling sorption to the matrix (equilibria and kinetics) and the physical movement of the material (transport) need to be considered. The simplest way of describing the chemical interactions is through an operationally defined sorption coefficient (K_d) value, which describes the measured partitioning of the species between the solid and aqueous phase. The equation for measuring K_d values in laboratory batch experiments is shown in Equation [1.12] (EPA, 1999), where K_d is the partition coefficient (L kg^{-1}), V_w is the volume of water (L), C_o is the initial bulk concentration of contaminant (mg L^{-1}), C_i is the bulk concentration remaining in solution after sorption

18

(mg L^{-1}) and M$_s$ is the mass of soil/sediment (kg). The K$_d$ values for U in environmental matrices differ considerably, for example in one summary report the geometric mean K$_d$ (L kg^{-1}) of U in sandy soil was reported as 40, in loam and clay soil as 200; and in organic soil as 2000 (SHEPPARD et al., 2006).

$$K_d = \frac{V_w \times (C_o - C_i)}{M_S \times C_i} \qquad [1.12]$$

The K$_d$ values alone cannot describe kinetically controlled processes, thus in dynamic systems with groundwater flow, interactions with the solid phase need to be characterised in terms of uptake and desorption rate constants, unless sorption processes are rapidly exchangeable. Physical transport of a material depends on three processes, advection, dispersion and diffusion. Advection is the movement of the dissolved species in solution as a result of the linear flow. The velocity of groundwater in sand and gravel aquifers typically range from 1 - 1000 m y^{-1} (MACKAY et al., 1985). However, under a natural gradient groundwater velocities are between 10 - 100 m y^{-1} (MACKAY et al., 1985). Dispersion is the spread of species as they move through the environment as a result of following different flow paths, and diffusion is the spread of molecules down the concentration gradient due to the random movement of molecules (HEMOND and FECHNER-LEVY, 2000).

Column experiments and numerical modelling are becoming increasingly important tools for understanding the fate and transport of contaminants in the subsurface environment. Column experiments can be used to quantify the movement of dissolved species through a homogenous porous medium. The k1D transport code is a suitable tool for modelling one dimensional (1-D) column experiments because it

incorporates simple advection-dispersion 1-D transport, and allows chemical processes to be described with a mixture of equilibrium and rate constants (SCHÜßLER et al., 2001). At groundwater flow rates the effect of diffusion is swamped by advection and dispersion processes and is therefore not included in the k1D code. Its development, testing and application have been described elsewhere (SCHÜßLER et al., 2001), it has been used to define metal transport in column experiments (BRYAN et al., 2005; SCHÜßLER et al., 2001; WARWICK et al., 2000) and to make predictions of contaminant metal ion transport at the field scale (BRYAN et al., 2007).

1.13 Aims and Objectives

Much of the understanding of DU corrosion processes in the environment comes from long term *in situ* studies at sites where munitions have been tested (TOQUE and BAKER, 2006; 2007). The environmental conditions, including the local biogeochemical conditions, varied over time, and were not monitored in detail during the corrosion process. Therefore, although there is information on rates of corrosion and the products formed, the environmental controls affecting DU corrosion have not been identified. Limited studies have investigated the impact of corrosion products on the microbial community and none have investigated the impact of corrosion products on anaerobic bacteria. There have also been no column transport experiments to date using DU corrosion products.

In order to characterise the environmental hazards of DU, it is essential to know the mechanisms and rates of DU corrosion under different conditions, the U corrosion products formed (dissolved, suspended, or immobilised in sediment), their transport in the environment and how these corrosion products impact the local microbial community. Microcosm experiments have therefore been carried out to obtain detailed characterisation of key environmental variables alongside DU corrosion, to test the

hypothesis that the rate of DU corrosion, and the corrosion products formed, are dependent on the local biogeochemical environment. The key objectives of the project were to investigate:

(1) The long term corrosion rates of DU within representative soils and sediments (that have received fired DU munitions) as a function of biogeochemical conditions

(2) The dissolved and particulate corrosion products formed under different conditions and their transport in the environment

(3) The impact of corroding DU on the natural microbial community

1.14 Collaborator Contributions

This PhD was funded as part of a NERC/MOD consortium grant between the universities of Manchester, Plymouth and Dundee. To carry out this multidisciplinary project, training was received in the fields of microbiology, surface science and mathematical modelling. However, aspects of the work were carried out by collaborators, as follows:

(1) Ribosomal intergenic spacer analysis (RISA) and DNA profiling techniques were carried out by Christopher Boothman at the Environmental Geochemistry and Geomicrobiology group at the University of Manchester under the supervision of Professor Jonathan Lloyd.

(2) The isolation and characterisation of corrosion products (Autoradiography, ESEM-EDAX and XRD) were carried out by members of the Centre for Radiochemistry Research and Williamson Research Centre for Molecular Environmental Science at the University of Manchester under the supervision of Professor Francis Livens.

(3) The k1D modelling of DU transport was carried out by Dr Nick Bryan at the Centre for Radiochemistry Research and at the Williamson Research Centre for Molecular Environmental Science at the University of Manchester.

Chapter 2

Experimental Methods

2.1 Introduction

This chapter is composed of seven sections: field sampling, experimental design and strategy, chemical analytical methods, microbial community analysis, analysis of DU coupons, characterisation of corrosion products, and transport experiments involving DU corrosion products. The field sampling section describes the selection of appropriate soil and sediment matrices and natural waters, their locations, and the collection and storage protocols. The experimental design and strategy section describes the design of microcosm experiments to investigate DU corrosion over time as a function of the biogeochemical environment. The analytical methods section gives comprehensive details of the methods used for the characterisation of the soil/sediment matrices and the analysis of samples from the microcosm. The microbial community analysis describes the use of ribosomal intergenic spacer analysis (RISA) and DNA profiling for observing changes in the microbial community profile. The analysis of DU coupons section gives details on mass loss determination and the calculation of the complete corrosion time of a 120 mm Charm penetrator. The characterisation of corrosion products section describes the isolation of corrosion particles and their characterisation by scanning electron microscopy X-ray spectroscopy (SEM-EDAX) and X-ray diffraction (XRD). Finally, the transport of DU corrosion products section describes the column experiments used to simulate the transport of DU corrosion products through sand.

2.1.1 Experimental Strategy

The strategy to simulate in the laboratory, environments and environmental conditions that have been impacted by DU. A grassland soil was selected to investigate DU corrosion in organic soil areas such as the Kirkcudbright test fire range in Scotland and conflict impacted areas (e.g. Iraq, Kosovo and Bosnia). A dune sand was selected to investigate DU corrosion in a sand-rich environment such as the Eskmeals test firing range in Cumbria and conflict impacted sand-rich desert areas (e.g. Iraq and Kuwait). A estuarine sediment was selected to investigate marine systems impacted by DU such as Solway Firth in Scotland.

2.1.2 Analysis of Data

All analyses were based on three replicate samples, the analytical quality assurance of the analyses are stated in the method sections below. The statistical t-tests had an acceptance criteria of being statistically significant when $P < 0.05$.

2.2 Field Sampling

2.2.1 Site Selection

Soil, sediments and waters were selected to give a comprehensive study of DU corrosion in biogeochemically contrasting environments. A summary of the target systems, biogeochemical environments, time scales and time points are shown in Table 2.1.

Table 2.1 Summary of the experimental systems.

Model system	Soil/ sediment and water	Target biogeochemical conditions	Ratio of matrix: water (g:mL)	Experimental period (days)	Number of time points
Grassland, agriculture or rural land impacted by DU munitions, e.g. Kirkcudbright test fire range in Scotland.	Grassland soil and drainage water	Oxic field-moist	15:1	510	5
		Sub-oxic waterlogged	15:15	510	5
		Anoxic waterlogged	15:15	510	10
Marine environments impacted by DU munitions, e.g. Kirkcudbright test fire range in Scotland.	Estuarine sediment with seawater of salinity 16.5 and 31.5	Anoxic medium salinity	20:10	500	10
		Anoxic high salinity	20:10	500	10
Sand dunes, beach or desert locations that have received DU munitions, e.g. Eskmeals test firing range in Cumbria.	Dune sand and seawater at salinity 31.5	Oxic field-moist	15:1	500	5
		Oxic waterlogged	15:15	500	5

2.2.2 Soil, Sediment and Water Sampling

A grassland soil (silt loam) from the North Wyke Research Station, Okehampton, Devon (Lat: 50.777451 °N Long: 3.920402 °W GB; 26.01.05) was sampled from a depth of 10-40 cm to avoid the upper organic horizon and root material. The soil was wet sieved (2 mm), stored at 15 °C in the dark and used within 6 months. Water was collected from a drain channel at the same site, stored in polypropylene container at 4

°C and used within one week of collection.

Estuarine sediment was sampled from Bowness-on-Solway, Solway Firth (Lat: 54.951070 °N Long: 3.214709 °W GB; 02.04.06). Care was taken to collect only the aerobic surface layer (0.5 cm), which was light in colour. The sediment was hand homogenised, stored at 10 °C and used within 2 weeks of collection.

Dune sand sediment from Drigg Sands in Cumbria (Lat: 54.372143 °N Long: 3.470030 °W GB; 03.02.05) was sampled from a depth of 5 - 40 cm to avoid the upper layer and root material. The soil was wet sieved (2 mm), stored at 15 °C in the dark and used within 6 months.

Seawater was sampled from Plymouth Sound (Lat: 50.460211 °N Long: 4.063914 °W GB; 02.04.06) and river water from the River Tamar (Lat: 50.522302 °N Long: 4.209116 °W GB; 02.04.06). These waters were stored in polypropylene containers at 4 °C and used within one week of collection.

2.2.3 Soil, Sediment and Water Characterisation

2.2.3.1 Particle Size Analysis

The average particle size distributions of the soil and sediments (n = 3) were measured by low angle laser light scattering (Malvern Mastersizer Long-bed X with MS17 autosampler, Worcestershire, UK). The soils and sediments required preparation to remove organic matter which can interfere with particle size distribution results. Approximately 10 g of air dried soil or sediment that had been sieved to < 2 mm was placed into a shallow glass basin. Approximately 30 mL of 6 % hydrogen peroxide (H_2O_2) was added to the sample and the mixture was heated on hot plate. The resultant effervescence indicated organic matter digestion, H_2O_2 was added until this reaction ceased. Any floating fibrous material which was not broken down by H_2O_2 was

removed using a porous pad. The basin was half filled with distilled water and left on hot plate to completely break down the H_2O_2. The soil/sediments were allowed to dry to a moist paste and mixed to homogenise the paste. Sub-samples were taken and placed into plastic autosample pots and analysed by laser diffraction.

2.2.3.2 Cation Exchange Capacity

The unit of cation exchange capacity is milliequivalents of exchangeable positive ions per 100 g of dry soil (mEq/100 g of dry soil). The following procedure was used to characterise the cation exchange capacity of each matrix and was carried out in triplicate (EPA, 1986). Approximately 5 g of air-dried, soil/sediment sample, pre-sieved to <2 mm, was weighed accurately, using a five figure balance, into a 10 mL centrifuge tube. The soil cation sites were saturated by adding 30 mL of 1 M sodium acetate solution, capping the tube and shaking mechanically for 5 min. The mixture was centrifuged at 4000 rpm for 4 min. The supernatant liquid was then decanted from the tube. The soil/sediments were then soaked in 30 mL industrial methylated spirit, shaken and centrifuged as before. This procedure was repeated twice more. The available Na^+ from the soil was extracted by shaking with 30 mL of 1 M ammonium acetate for 15 min, and centrifuged as described above.

The Na^+ concentration was determined using a flame photometer (Corning 400), calibrated with NaCl standards. A volume of supernatant liquid was diluted with high purity water (MQ water, 18.2 MΩ cm^{-1}, Millipore Ltd, Hertfordshire, UK) to within the calibration range. Blanks were included to ensure good quality control. The cation exchange capacity values were calculated according to equation [2.1]. Where C is the concentration of Na^+ (mg/L), V is the volume of added reagent (L), AW is the atomic mass of Na^+ and W is mass of added soil/sediment (g).

Cation exchange capacity (mEq/100 g of Dry Soil/Sediments)

$$= C \times \left(\frac{V}{AW}\right) \times \left(\frac{100}{W}\right) \qquad [2.1]$$

2.2.3.3 Carbon Analysis

Sedimentary total carbon content of soil/sediments was quantified using a CHNS analyzer (EA 1110, CE Instruments, Wigan, UK). Ethylenediamine tetraacetic acid (VWR, analytical reagent. UK) was used to calibrate the instrument and a certified reference sediment, PACS-1 (National Research Council of Canada), was used to validate the procedure. Accurately measured sample weights of approximately 6 - 11 mg were placed in tin capsules and analysed for total carbon analysis. A proportion of wet soil/sediment was placed in a glass Petri dish and fumed in 4 M HCl for > 48 h to digest the inorganic carbon; sub-samples were air dried and analysed for organic carbon, the %RSD between replicate (n = 3) standards was < 1%.

2.2.3.4 X-Ray Fluorescence Analysis

The bulk mineral composition of the sediments and soils were determined by X-ray Fluorescence (XRF) (Axios, Panalytical, Almelo, The Netherlands) was carried out by the Environmental Geochemistry and Geomicrobiology group at the University of Manchester. An accurately weighed mass of approximately 12.0 g soil/sediment was added to an agate mill with 3.0 g of Hoechst Wax C Micropowder (Merck Ltd, Dorset, UK). The mixture was ground to a fine powder by milling for 5 min at 100 rpm. The powder was transferred to a die and pressed at 20 tonnes for approximately 10 s. The retrieved pellet was subsequently analysed by XRF.

2.2.3.5 Extracted and Dissolved Inorganic carbon Analysis

Inorganic carbon analysis was carried out by a member of the Environmental Geochemistry and Geomicrobiology group at the University of Manchester. The water samples were filtered (0.45 μm), diluted and analysed using a total organic carbon T5000 analyzer (Shimadzu Ltd, Milton Keynes, UK). The inorganic carbon content of the soils and sediments (n = 3) was determined following a MQ water extraction. An accurately weighed mass of approximately 5 g of soil/sediment was added to a polypropylene vial and 20 mL of MQ water was added. The vials were sealed and mechanically swirled horizontally at 200 rpm for 60 min at room temperature. The samples were then ultrasonicated for 15 min, then syringe filtered (0.45 μm) prior to dilution and analysis. Carbon standards were prepared in MQ water using iron potassium hydrogen phthalate (Sigma-Aldrich Co Ltd, Dorset, UK).

2.3 Experimental Design and Strategy

2.3.1 Microcosm Design

Microcosm experiments were designed to investigate the corrosion of DU as a function of the biogeochemical environment, according to Table 2.1. Selected microcosm were sealed to allow the development of progressively anaerobic conditions, whereas others were left open to the atmosphere, maintaining oxic/suboxic conditions. Three different microcosm designs (Figure 2.1) were implemented, which are denoted here as field-moist, open waterlogged and closed waterlogged systems. The field-moist microcosm simulated oxic sub-surface conditions; the open microcosm enabled O_2 exchange with the atmosphere as indicated by the air-filled macro-pores in the soil/sediment structures. The open waterlogged microcosm produced sub-oxic conditions, due to limited diffusion of O_2, defined here as a region of measurably low dissolved oxygen

concentrations and no observed SO_4^{2-}-reduction. The closed waterlogged microcosm were sealed to produce progressively anoxic conditions.
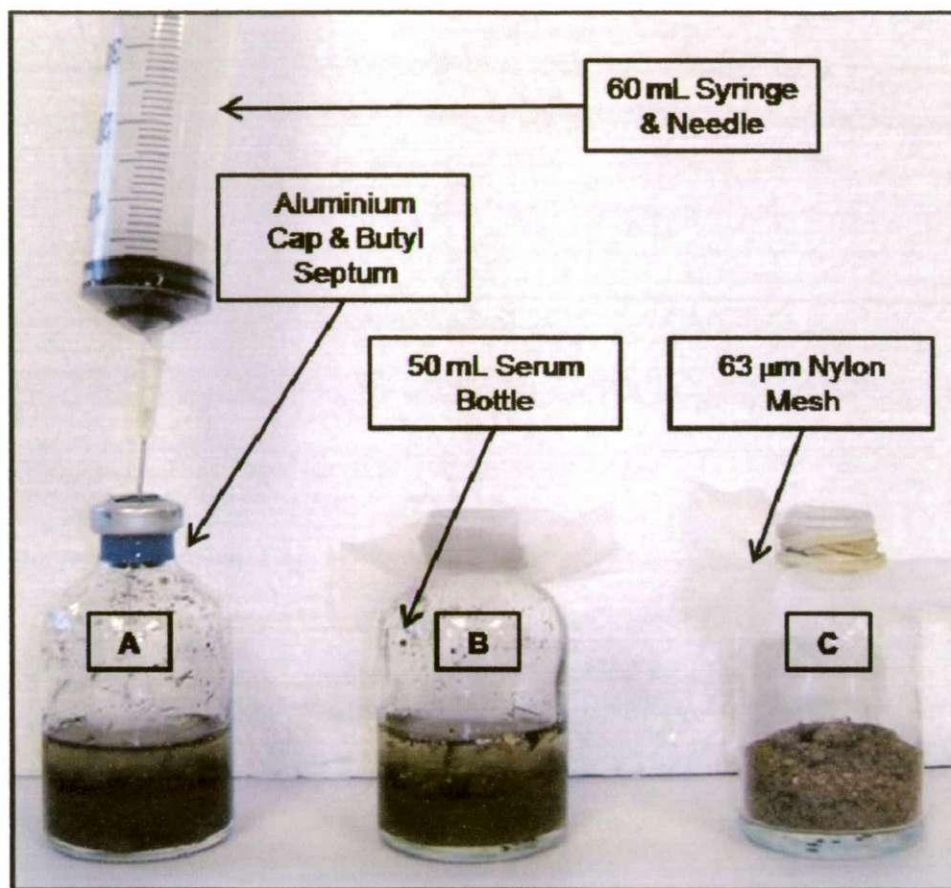
Figure 2.1 Representative microcosm designs, showing (A) closed waterlogged, (B) open waterlogged and (C) field-moist microcosm.

2.3.2 The Preparation of Depleted Uranium Coupons

DU from a penetrator was supplied by DSTL (Porton Down, UK) and cut into triangular 'coupons' (size *ca* 1.5 x 1.5 x 1.0 x 0.5 cm and mass 5 - 10 g) by AWE (Aldermaston, UK). The DU coupons were cleaned prior to use to remove any cutting oil or surface contaminants. This involved ultrasonication in dichloromethane (10 min), air drying and ultrasonication in isopropanol (10 min). The coupons were then air dried on absorbent paper (Kimberly-Clark, Kent, UK), accurately weighed to 4 decimal places and stored in polyethylene bags prior to use. Figure 2.2 shows a sliced section of the DU penetrator which has been cut into eight coupons.
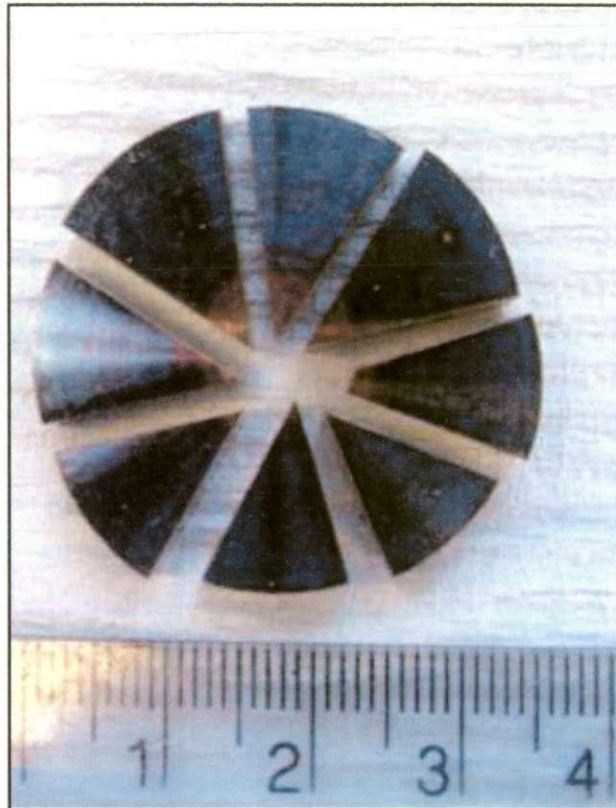
Figure 2.2 DU~0.75%Ti coupons cut from a DU penetrator.

2.3.3 Microcosm Setup

The microcosm model systems were planned and implemented according to the solid matrix used (see Table 2.1).

2.3.3.1 Grassland Soil

The grassland soil microcosms were designed to model the corrosion of DU under field-moist, open waterlogged and closed waterlogged subsurface conditions. All experimental microcosms were prepared on the same day. Each microcosm consisted of a 50 mL glass serum bottle (Wheaton Scientific, New Jersey, USA), containing 15 g of

sieved grassland soil. Waterlogged conditions were simulated by adding 15 mL of drainage water, whereas field-moist soil conditions were achieved by the addition of 1 mL of this water. For the open systems (open waterlogged and field-moist soil) fifteen microcosm containing a DU coupon were prepared, together with an equivalent number of controls without a DU coupon. Nylon mesh was tied around the neck of each of the open bottles to allow gas exchange. The microcosms were weighed each month and any water loss was corrected by the addition of deoxygenated MQ water. Deoxygenated MQ water was used so that the redox state of the microcosm was preserved. For the closed waterlogged system, thirty microcosms containing a DU coupon were prepared, together with an equivalent number of controls without a DU coupon. The microcosms were sealed with a butyl rubber stopper (Bellco Glass Inc, New Jersey, USA) and aluminium seals (Sigma-Aldrich, Dorset UK). An 18 gauge needle was inserted, attached to a syringe to prevent pressure build-up (none observed). All microcosms were incubated in the dark at 10 °C.

2.3.3.2 Estuarine Sediment

The estuarine sediment microcosms were designed to model the corrosion of DU in the subsurface and progressively anoxic environments of high and medium salinity. All experimental microcosms were prepared on the same day. Each microcosm consisted of a 50 mL glass serum bottle, 20 g of sieved sediment, and 10 mL of either seawater, to mimic conditions in the Solway Firth, or a 1:1 mix of river and seawater, to mimic areas with a freshwater influence. For each salinity, thirty microcosms each containing a DU coupon were prepared, together with an equivalent number of controls without a DU coupon. The microcosms were sealed with a butyl rubber stopper and aluminium seals. An 18 gauge needle and syringe was inserted and the microcosms were incubated in the dark at 10 °C.

2.3.3.3 Dune Sand

The dune sand microcosms were designed to model the corrosion of DU in field-moist, terrestrial sand and sand that had been inundated with seawater. All experimental microcosms were prepared on the same day. Each microscosm consisted of a 50 mL glass serum bottle and 15 g of sieved dune sand. Seawater inundation was simulated by the addition of 15 mL of Plymouth Sound seawater, whereas field-moist conditions were maintained by the addition of 1 mL of MQ water. Nylon mesh was tied around the neck of each of the open bottles to allow gas exchange. The microcosms were weighed each month and any water loss was corrected by the addition of MQ water. The microcosms were incubated in the dark at 10 °C.

2.3.4 Microcosm Sacrifice and Isolation of Waters

The approach taken involved using entire microcosm for analysis and characterisation, and the opening of each microcosm for this process is termed a "sacrifice". At each time point of interest over a period of up to 510 days, microcosms were sacrificed in triplicate, along with three controls. To preserve redox conditions within the microcosm, all sacrifices and further manipulation was carried out within an anaerobic chamber (Coy Laboratory Products Inc, Michigan, USA; 95% N_2, 5% H_2).

The closed microcosm systems were mechanically swirled for 15 min at 200 rpm to homogenise the entire sample, placed in the anaerobic chamber and the butyl rubber stopper removed. For the open systems, the microcosm were weighed and the water volume adjusted to 15 mL by addition of deoxygenated MQ water, a butyl rubber stopper was added and microcosm were mechanically swirled for 15 min at 200 rpm and then placed in the anaerobic chamber.

The entire content of each microcosm was then transferred to a nylon mesh (65 µm) in a funnel, to separate the bulk sediment from the water slurry. The water slurry

was then further filtered through a disposable syringe filter (0.45 μm, mixed cellulose esters, Millipore, Hertfordshire, UK) and collected in acid-washed polypropylene vials. The DU coupons, solution and solid phase were then prepared for further analysis (Figure 2.3) as described in Section 2.4.
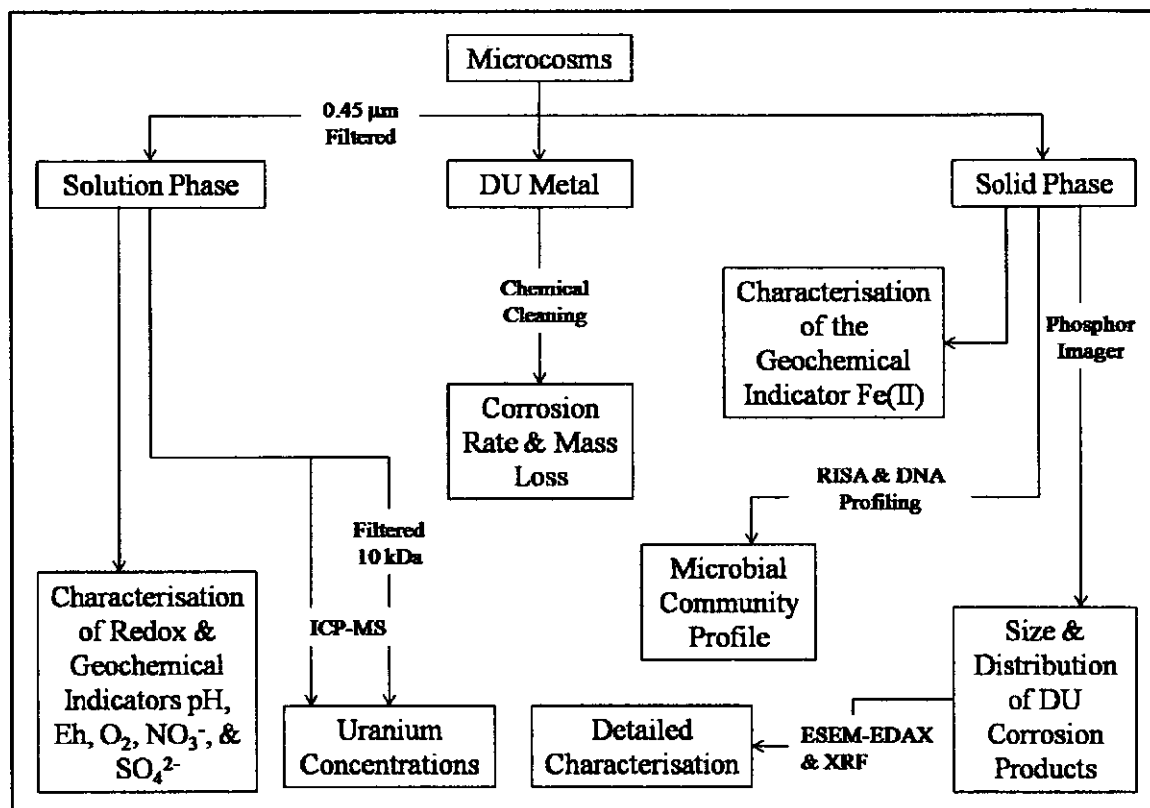
Figure 2.3 Schematic of the analysis strategy, showing the separation of the microcosm into three sections: solution phase, solid phase and DU coupon.

2.4 Analytical Methods

2.4.1 Apparatus Preparation

All glassware and plasticware was washed in 2% Decon for at least 24 h, rinsed in MQ water, washed in 10% hydrochloric acid (HCl) for 24 h and then rinsed again in MQ water. Plasticware and glassware were then left to dry in a laminar flow hood and double sealed in zip lock plastic bags.

2.4.2 Analysis of Redox Indicators

The biogeochemical environment of the microcosm environment was characterised over time by analysing the redox indicators. The redox indicators chosen and the biogeochemical process they signify are summarised in Table 2.2.

Table 2.2 Redox indicators and the biogeochemical environment they signify.

Redox indicators	Biogeochemical environment
Eh	Decreasing Eh indicates progressively reducing conditions.
Oxygen	O_2 depletion indicates O_2 reduction
Nitrate	NO_3^- depletion indicates NO_3^- reduction
Iron(II)	Ingrowth of Fe(II) onto soil indicates Fe(III) reduction.
Sulfate	SO_4^{2-} depletion indicates SO_4^{2-} reduction

2.4.2.1 Determination of O_2, Eh, pH and Salinity

The oxygen content (MI-730; O_2.ADPT, Microelectrodes Inc, New Hampshire, USA), pH (MI-410, Microelectrodes Inc, New Hampshire, USA) and Eh (MI-800, Microelectrodes Inc, New Hampshire, USA) of the waters were determined using electrochemical probes that were calibrated on use and a bench meter (pH 210, Hanna Instruments, Leighton Buzzard, UK) within the anaerobic chamber, using an aqueous sub-sample from each microcosm. The O_2 electrode was calibrated through two points (0 % and 100 % O_2) using a solution of sodium sulfide (500 mg L^{-1}) and MQ water in equilibrium with atmospheric O_2. The pH electrode was calibrated through two points (pH 4.01 and 7.01) and the OPR electrode was corrected (+ 228 mV) to the standard hydrogen electrode using the experimental Eh reading determined from an Fe(II)/Fe(III) solution (Table 2.3) (LIGHT, 1972). The salinity of waters was determined using a portable refractometer (DIGIT-100 ATC, Medline Ltd, Oxford, UK).

Table 2.3 Standard ferric-ferrous solution for Eh measurements.

Composition	Concentrations	Relative mass
Fe(II) ammonium sulfate	0.10 M	39.21 g L^{-1}
Fe(III) ammonium sulfate	0.10 M	48.22 g L^{-1}
Sulfuric acid	1.00 M	56.20 mL L^{-1}

2.4.2.2 Determination of Anions by Ion Chromatography

Detectable anions (Cl^-, NO_3^- and SO_4^{2-}) in waters were determined by ion chromatography. The calibration series was prepared from a stock anion solution (1000 mg L^{-1}) prepared from salts (Table 2.4) and stored for < 1 month at 4 °C. Inside the anaerobic chamber, filtered samples were diluted within the calibration range (1 - 150 mg L^{-1}) using MQ water. The vials were sealed and analysed within 12 h (Dionex DX-500, Dionex Co, Camberley, UK) with set instrument parameters (see Table 2.5) (DIONEX, 2001). The instrument was calibrated using anion standards (1-150 mg L^{-1}); with calibration checks and blanks run after every 10 samples to check that the instrument drift was within 10%, if drift was over 10% samples were rerun. The analytical figures of merit for anion determination are shown (Table 2.6).

Table 2.4 Masses of compounds to prepare 0.1 L of 1000 mg L^{-1} anion standard.

Anion	Compound	Supplier	Relative Mass (g)
Chloride	NaCl	Sigma-Aldrich (Analytical Grade)	0.1648
Nitrate	$NaNO_3$	Sigma-Aldrich (Analytical Grade)	0.1371
Sulfate	Na_2SO_4	Sigma-Aldrich (Analytical Grade)	0.1479

Table 2.5 Ion chromatography parameters for the determination of anion.

Instrument:	Dionex DX-500
Matrix:	Isolated microcosm waters
Eluent:	1.9 mM sodium carbonate
Columns:	Dionex IonPac AG9-HC, IonPac AS9-HC
Run time:	< 20 min
Flow rate:	1 mL min^{-1}
Detection:	100 mA current.
System backpressure:	~ 2200 psi
Background conductance:	~ 30 µS

Table 2.6 Analytical figures of merit for anion determination*

	Chloride	Nitrate	Nitrite	Sulfate
Blank	0.011 ± 0.008	0.26 ± 0.1	0.40 ± 0.06	0.27 ± 0.1
Detection limit	0.02	0.3	0.2	0.3
Precision, %RSD ¤	0.3	0.4	0.6	0.2
Sensitivity (5 point calibration slope)	0.98	0.99	0.99	0.99
Linear range	0.2 - 200	0.3 - 100	0.4 - 100	0.3 - 200

* All data given in mg L^{-1}, n = 3. Error bounds indicate ± one standard deviation. ¤ The precision is calculated as the percent relative deviation (%RSD) and based on the repeatability between replicate measurements of a 10 mg L^{-1} standard.

2.4.2.3 Determination of Ferrous Iron (Fe(II))

Fe(III)-reduction is known to occur in sediments 10 - 20 days before it is observed in the porewaters (BURKE et al., 2005). Iron(II) was therefore extracted from soils/sediments (LOVLEY and PHILLIPS, 1986) and analysed using the ferrozine method (STOOKEY, 1980). Stored soil/sediment (-18 °C) samples were defrosted within the anaerobic chamber and an accurately weighed mass of approximately 0.1 g was added to a polypropylene vial. An aliquot of 0.1 M HCl (5 mL) was pipetted into each polypropylene vial, sealed and mechanically swirled horizontally at 200 rpm (Orbital Shaker, GFL 3017, Progen Scientific Ltd, South Yorkshire) for 30 min (soils) or 60 min (sediments) at room temperature (LOVLEY and PHILLIPS, 1986). The samples were immediately syringe filtered (0.45 µm), and 100 µL of this filtered sample was pipette into 5 mL of the ferrozine solution (1 g L^{-1}) prepared in 50 mM HEPES (Fisher BioReagents, Leicestershire, UK) buffer (pH 7.3 ± 0.1). The samples were mixed and measured spectrophotometrically (Cecil CE 1010, Cecil Instruments Ltd, Cambridge, UK) at absorbance 562 nm. Standards were prepared in MQ water using iron (II) chloride (Fluke Chemika, Buchs, Switzerland) and analysed as above. The analytical figures of merit for Fe(II) determination are shown in Table 2.7.

Table 2.7 Analytical figures of merit for Fe(II) determination*

	Fe(II)
Blank	0.0020 ± 0.003
Detection limit	0.01
Precision, %RSD ¤	0.5
Sensitivity (5 point calibration slope)	0.98
Linear range	0.1 - 2

* All data given in mg L^{-1}, n = 3. Error bounds indicate ± one standard deviation. ¤ The precision is calculated as the percent relative deviation (%RSD) and based on the repeatability between replicate measurements of 0.5 mg L^{-1} standard.

2.4.3 Uranium Determination

Uranium was determined in the filtered (0.45μm) and ultrafiltered (< 10 kDa; polyethersulfone membrane, Vivaspin Sartorius Group, Epsom, UK) fractions to identify the colloidal + dissolved (< 0.45μm) and the dissolved (< 10 kDa) fractions. There was no retention of U on filters (n = 3) with recovery of 103 ± 0.92 % for the 0.45μm mixed cellulose ester filters and 103 ± 0.51 % for the polyethersulfone membrane filter. This recovery is within the 10 % drift of the ICP-MS instrument. Following the initial filtration, an aliquot of water was pipetted into a Vivaspin filter, sealed and immediately centrifuged (Sorvall Legend RT, Massachusetts, USA) outside the anaerobic chamber (4000 g force, 5 min). Accurately known volumes of the filtrate and ultrafiltrate were then pipetted into polypropylene vials (Fisherbrand, Leicestershire, UK), acidified with 50 μL of concentrated nitric acid (Fisherbrand, Specified Grade, Leicestershire, UK), sealed and stored (< 6 months) in a fridge (4 °C) for future analysis.

On the day of analysis, samples were diluted within the calibration range using 2% (v/v) nitric acid and analysed for U by ICP-MS (Plasmaquad PQ2+ Turbo; Thermo Elemental, Cheshire, UK) with set parameters (see Table 2.8), using 200 μg L^{-1} of thorium (Alfa Aesar, Karlsruhe, Germany) as an internal standard. The instrument was calibrated using U (Spex Certiprep, New Jersey, USA) standards (0.5 to 50 μg L^{-1}), with calibration checks and blanks run after every 10 samples to check the instrument drift was within 10%, if the drift was over 10% samples were rerun. The analytical figures of merit for U determination are shown in Table 2.9.

Table 2.8 ICP-MS parameters for the determination of uranium.

Instrument:	Plasmaquad PQ2+ Turbo
Matrix:	Isolated microcosm waters
Eluent:	Argon
Power:	1350 W
Coolant gas:	12 L min^{-1}
Auxiliary flow:	1 L min^{-1}
Nebulizer gas:	0.9 L min^{-1}
Nebulizer:	Sturman-Masters VGroove
Wavelength detection	238 λ
Sample analysis time:	1024 ms

Table 2.9 Analytical figures of merit for uranium determination*

	Uranium
Blank	0.20 ± 0.1
Detection limit	0.3
Precision, %RSD ¤	1.5
Sensitivity (5 point calibration Slope)	1.0
Linear range	0.5 - 200

* All data given in µg L^{-1}, n = 3. Error bounds indicate ± one standard deviation. ¤ The precision is calculated as the percent relative deviation (%RSD) and based on the repeatability between replicate measurements of a 10 µg L^{-1} standard.

2.4.3.1 Geochemical Modelling

The geochemical speciation of uranium under the experimental microcosm conditions (inorganic carbon concentration, pH and Eh) were modelled using the Hydra hydrochemical database with the MEDUSA software (by I Puigdomenech, Inorganic Chemistry Royal Institute of Technology, Stockholm, Sweden).

2.5 Microbial Community Analysis

Microcosm soil/sediment samples were selected for ribosomal intergenic spacer analysis (RISA) so that changes in the microbial profile could be identified over time and/or as a result of the presence of DU. Positive observed changes in the microbial community warranted further analysis of amplified product by DNA profiling. Both techniques were carried out by the Environmental Geochemistry and Geomicrobiology group at the University of Manchester by Christopher Boothman under the supervision of Professor Jon Lloyd.

2.5.1 Ribosomal Intergenic Spacer Analysis

DNA was extracted from sediment samples using a Fast DNA spin kit, Powersoil DNA Isolation Kit, (Cambio, Cambridge, UK). The 16S-23S rRNA intergenic spacer region from the bacterial RNA operon was amplified as described previously using primers ITSF and ITSReub (ISLAM et al., 2004). The amplified products were separated by electrophoresis in Tris-acetate-EDTA gel. DNA was stained with ethidium bromide and viewed under short-wave UV light using a BioRad Geldorganic carbon 2000 system (BioRad, Hertfordshire, UK). Once the purity of the amplified products were established, the 16S-23S intergenic spacer region from the bacteria RNA operon was further amplified, using primers ITSF (eubacterial 16 S rRNA), and ITSReub (eubacterial 23S rRNA) following published reactions conditions (CARDINALE et al., 2004). DNA was stained and viewed as before.

2.5.2 DNA Profiling

Positive microbial community changes identified by the RISA justified further investigation by DNA sequencing of 16S rRNA gene clone libraries and phylogenetic

analysis. Here, approximately 1490 base pairs of the 16S rRNA gene was amplified using the broad-specificity 16S rRNA gene primers 8F and 1492R following published PCR reaction conditions (CARDINALE et al., 2004), cloned into a pSC-A-amp/kan cloning vector and reamplified using primers complementary to the flanking regions of the PCR insertion site of the vector. Restriction fragment length polymorphism and DNA sequencing was carried out on the reamplified product following the method of Islam et al., (2004). Sequences (typically 850 base pairs in length) were analysed against the NCBI (USA) database using BLAST program packages and matched to known 16S rRNA gene sequences.

2.6 Analysis of Depleted Uranium Coupons

Coupons retrieved from the matrix were gently rinsed with MQ water to remove bulk soil/sediment material. Coupons were then air dried on absorbent paper (Kimberly-Clark, Kent, UK), placed in an open polypropylene bag. With the knowledge that corrosion is greater in water than in air (TRZASKOMA, 1982), coupons were air dried and stored in a desiccator to prevent further corrosion for a maximum period of 1 month. During this period the DU coupons were photographed under a light microscope (Kyowa Stereo Microscope, SDZ-TR-PL) fitted with a digital camera (Nikon Coolpix 4500), for a visual record. Selected coupons were imaged by scanning electron microscopy and analysed using energy dispersive X-ray spectroscopy (SEM-EDAX; Jeol JSM-6100, Tokyo, Japan). Any loose corrosion material was removed from the coupon with a polypropylene spatula and collected in a clean glass vial for future transport experiments (Section 2.8). The remaining corrosion products were removed within 1 month to calculate the mass loss. Corrosion products were removed by washing the coupon three times for 30 min in 12 M formic acid, rinsing with ethanol,

and then dipping the coupons in concentrated nitric acid (Analytical Grade, Fisherbrand, Leicestershire, UK) for 30 s and rinsing with MQ water. Once dried, the coupons were re-weighed to give mass loss (g) and mass loss (%) (TOQUE and BAKER, 2006), using an analytical balance (Salter Electronic Balance, ER-182A, Salter Brecknell, UK) with a balance accuracy of ± 0.0001 g.

The acid cleaning process has low associated uncertainties. No uncertainties are associated with the formic acid cleaning step because only uranium oxides are partially soluble in formic acid at room temperature (TOQUE and BAKER, 2006). However nitric acid removes DU alloy metal as well as adherent oxides. The extent to which replicate DU coupons were dissolved in concentrated nitric acid during a 30 s immersion has been quantified. Nine DU coupons were cleaned in conc nitric acid for 5 min to remove the oxide layer. The coupons were rinsed in MQ water, air dried and accurately weighed. The coupons were then individually placed in concentrated nitric acid for 30 s emersions, immediately washed with MQ water, air dried, and accurately reweighed to determine mass loss. The extent to which nitric acid dissolves DU was calculated as 0·27 ± 0.06 mg of the total mass. This therefore gives an overall uncertainty budget of less than ± 0.005 % per average sized coupon (7.5 g) for the coupon acid cleaning process and weighing errors.

2.6.1 Calculation of Corrosion Rate and Complete Corrosion Time

The rate of corrosion (g cm^{-2} y^{-1}) was calculated using equation [2.2] using replicate coupons. When calculating the surface area of each coupon, the slightly irregular curved side of the coupon was assumed to be straight for simplicity, the exact area was calculated by weighing cardboard (160 grams per square meter) cut to the same area (n = 9), the uncertainty of this assumption was calculated as ± 2 %.

$$\text{Corrosion Rate (g cm}^{-2}\text{y}^{-1}) = \frac{365 \times \text{Weight loss (g)}}{\text{Coupon Area (cm}^2) \times \text{Time (days)}} \qquad [2.2]$$

The rate of corrosion can be used to estimate how long a complete penetrator will take to corrode in the environment. A 120 mm DU penetrator has a radius of 1.5 cm, height of 30 cm, and approximate weight of 4500g (BAILEY et al., 2002). The penetrator's surface area (300 cm^2) was calculated from a perfect cylinder. The corrosion rate (g cm^{-2} y^{-1}), mass and the mean surface area of a penetrator during corrosion (i.e. 150 cm^2) can be used to estimate the total corrosion time for a complete penetrator using equation [2.3].

Total Corrosion Time of 120 mm Penetrator

$$= \frac{4500 \text{ (g)}}{\text{Corrosion Rate (g cm}^{-2}\text{y}^{-1})} \times \frac{1}{150 \text{ (cm}^2)} \qquad [2.3]$$

2.7 Characterisation of Corrosion Products

Characterisation of corrosion products in soil/sediment provides information on how the corroding DU will disperse within the environment. The isolation and characterisation of these corrosion products is also important in determining the fate and transport of DU. All techniques (Autoradiography, ESEM-EDAX and X-ray diffraction) were carried out by a member of the Centre for Radiochemistry Research and Williamson Research Centre for Molecular Environmental Science at the University of Manchester under the supervision of Professor Francis Livens.

2.7.1 Isolation of Uranium Particles by Autoradiography

Autoradiography (phosphor imaging) maps the position of "hot spots" of uranium in a sample through its α-emissions. A portion of representative dried soil/sediment (1 g) was spread thinly onto a grid plate; a clean phosphor screen was then placed on top for 2 - 12 h, depending on the intensity of the radioactivity. The phosphor screen images were recorded on a Typhoon 9410 Variable Mode Imager (Amersham Biosciences, Buckinghamshire, UK). The images were used as a map to identify areas of enhanced radioactivity.

2.7.2 ESEM-EDAX of Isolated Corrosion Products

Particles of enhanced radioactivity identified by phosphor image maps were isolated using tweezers and stored on conductive carbon adhesive tabs and mounts. Samples were loaded into the ESEM-EDAX (Philips XL30 ESEM-FEG, Oregon, USA) using set instrument parameters (see Table 2.10). Spot scans and whole scans of particles were analysed by EDAX and resulting particle images and spectra stored.

Table 2.10 Parameters for the characterisation of radioactive corrosion products.

Instrument:	ESEM-EDAX; Philips XL30 ESEM-FEG
Matrix:	Isolated particles of enhanced radioactivity
Resolution:	2 nm
Accelerator voltage:	0.2 to 30 kW
Electron gun:	Field emission
Stage movement:	Tilt of -15° to +75°
Detector:	Galileo Channeltron 4870V electron multiplier
EDAX	EDS Prism X-ray detector

2.7.3 X-ray Diffraction Analysis of Isolated Corrosion Products

For characterisation of DU corrosion products by X-ray diffraction (XRD) the uranium content of the matrix was required to be above 3 % m/m. Only the field-moist microcosm had sufficient DU corrosion products for XRD analysis. The corrosion products were isolated from soil/sediment using tweezers and stored in a glass container prior to analysis. The instrument (Bruker X'Pert diffractometer) was calibrated using the instrument parameters given in Table 2.11 and a silica standard. Samples were dispersed onto the polished side of the face of a pure silicon substrate and adhered using "Wacker Siliconpaste P4" (Wacker-Chemie GmbH, Munich, Germany). Spectra were baseline subtracted and compared against a library of diffraction patterns to characterise sample using EVA software (DIFFRACplus Evaluation Package, 2001, Bruker AXS, Karlsruhe, Germany).

Table 2.11 Parameters for the characterisation of DU corrosion products.

Instrument:	XRD with Bruker X'Pert diffractometer
Matrix:	Isolated particles of enhanced radioactivity
Radiation:	Cu-K
Radiation generated:	40 kW and 30 mA
In step scan mode:	$10 - 80°$ 2θ 107.7 s/step
Step size mode:	$0.010°$ 2θ
Step time:	107.7 s

2.8 Transport of DU Corrosion Products

The transport of the characterised DU corrosion products (metaschoepite) through dune sand was simulated using column experiments. The experimental setup is shown in

Figure 2.4. The equipment consisted of a column (Polyetheretherketone [PEEK]; self pack®; 50 mm × 10 mm; Applied Biosciences, Foster City, USA), 0.2 μm inline filter frit, peristaltic pump (Multiflow Lambda, Zurich, Switzerland), Rheodyne valve (Bergstrasse, Germany) 50 μL injection loop for UO_2^{2+} and Br⁻, injection port, fraction collector (Omnicoll, Lambda, Zurich, Switzerland), and 2 mm PVC tubing (Nalgene, Hereford, UK). Synthetic rainwater was used as the most relevant mobile phase for the terrestrial, field-moist system, in which corrosion to metaschoepite was observed. A synthetic rainwater with major anion and cation concentrations equivalent to those found in UK rainwater, was prepared in MQ water (ANDERSON et al., 2000). The pH of the rainwater (Table 2.12) was adjusted to pH 5.5 using 0.01M HCl.
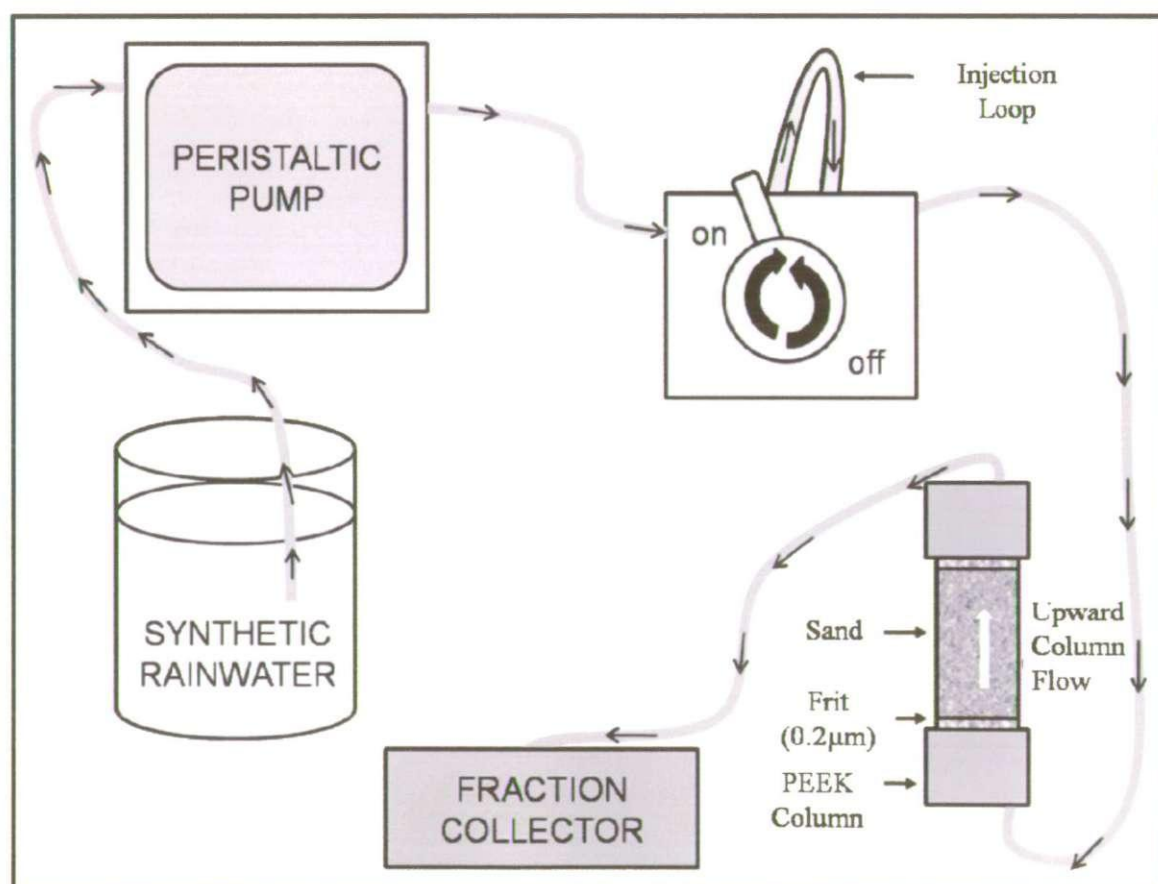
Figure 2.4 Schematic showing the transport experiment setup.

Table 2.12 Composition of synthetic rainwater used in column experiments (ANDERSON et al., 2000).

Stock solution salts	Supplier	Concentration in stock solution (g L^{-1})	Rainwater
NaCl	Aldrich	1.8	Dilute stock solution
KCl	Fisher	0.075	100-fold using MQ
NH$_4$Cl	Fisher	0.054	water. Adjusted to pH
MgCl$_2$.6H$_2$O	Fisher	0.24	5.5 using 0.01 M HCl
CaCl$_2$.2H$_2$O	Fisher	0.15	
NaNO$_3$	Aldrich	0.085	
Na$_2$SO$_4$	Aldrich	0.36	

2.8.1 Sand and Column Preparation

The dune sand was sieved mechanically for > 24 h to obtain the 63 μm – 2 mm sand fraction. This was washed three times for 30 min in simulated rainwater (10 g solid: 100 mL solution) and left to equilibrate in the simulated rainwater for >1 week. The damp sand slurry was then packed into the column. The column was tapped gently to dislodge air bubbles and allow the sand to settle into place, and more sand was packed until the column was full (3.9 cm^3). The column was sealed and synthetic rainwater was pumped upwards at a steady flow rate of 0.14 mL h^{-1} for > 48 h to equilibrate the column prior to transport experiments. This flow rate in dune sand corresponds to a flow velocity of 19.04 m y^{-1} which is at the lower end of the range found in sand and gravel aquifers with a natural gradient (10 - 100 m y^{-1}) (MACKAY et al., 1985). Low flow rates allow detailed experimental data of reactive species to be obtained using packed columns, and this data can then be used to predict behaviour under higher flow conditions. An upward flow direction avoids artefacts due to gravity and ensures that the column remains

saturated. All calculations were performed using the k1-D coupled chemical transport code. Transport simulations of uranium were defined at 30 fixed sub-divisions of the column. The k1D modelling of DU transport was carried out by Dr Nick Bryan at the Centre for Radiochemistry Research and at the Williamson Research Centre for Molecular Environmental Science at the University of Manchester. Two columns were prepared to investigate the transport behaviour of UO_2^{2+} and DU corrosion products separately, and both were characterised physically (porosity, dispersivity and K_d) using a tracer Br^- injection after the transport experiments were complete. The eluant profiles from the UO_2^{2+} columns were used to define the U(VI) sorption kinetics for transport modelling of metaschoepite.

2.8.2 Transport of UO_2^{2+}

The sand column was used to define the transport behaviour of dissolved UO_2^{2+} and identify the kinetics of its interactions with the sand matrix. A U solution (1000 mg L^{-1}) was prepared from a certified standard solution of U (Spex Certiprep, New Jersey, USA), adjusted to pH 5.7 using 0.5 M ammonium acetate (HPLC Grade, Fisher Scientific, Leicestershire, UK) and was injected (50 µL) into the column. Eluent flow rates were checked weekly by mass (0.14 ± 0.005 mL h^{-1}) and was collected continuously in 4 h fractions over 32 days, diluted to 5 mL with 2 % nitric acid and refrigerated (4 °C) for future analysis (< 1 month). On the day of analysis filtered samples were spiked with thorium as an internal standard and analysed for U by ICP-MS. After the column experiment involving UO_2^{2+} was complete, a tracer of KBr (2000 mg L^{-1}) was injected onto the column, this concentrations was required for good resolution of the Br^- breakthrough curve. Fractions were collected every 1.5 h, diluted to 5 mL with 2 % nitric acid and analysed by ICP-MS using indium as an internal standard (Spectrosol Grade, Merck Ltd, Dorset, UK).

2.8.3 Transport of Depleted Uranium Corrosion Products

A newly prepared, equilibrated sand column was opened and a portion of sand (2 mm depth) was taken out and replaced with metaschoepite corrosion product (50.8 mg), and the remaining space immediately refilled with sand. The column was closed and the oxic rainwater pumped, as before, at an upward flow rate of 0.14 mL h^{-1} from the corrosion product source. Fractions were collected from the sand column every 8 h over 98 days, diluted to 5 mL with 2 % nitric acid and analysed as described in Section 2.8.2. After the column experiment was complete, a tracer of KBr (2000 mg L^{-1}) was injected into the column, fractions were collected every 1 h and analysed as described in Section 2.8.2.

The column was then opened and the sand was pushed through the column using a polypropylene rod and collected at approximate 0.5 cm intervals into preweighed perfluoroalkoxy containers (Savillex, Minnetonka, USA). The sand was freeze dried, reweighed and refluxed with concentrated nitric acid for 8 h to digest the DU. The dissolution of this quantity of uranium metal is favourable in boiling concentrated nitric acid (GATES-ANDERSON et al., 2004; LAUE et al., 2004). The digest was filtered (Whatman 540, Ashless filter, Kent, UK) and diluted within calibration range using (2 % Nitric acid) and analysed by ICP-MS using thorium (200 µg L^{-1}) as an internal standard.

2.9 Summary

This project utilised a range of analytical techniques to study the corrosion of DU under various environmental conditions, including different biogeochemical environments. The LODs for the redox indicators NO_3^-, NO_2^-, Fe(III) and SO_4^{2-} were < 0.5 mg L^{-1}. These techniques have been used previously and were found to be a good method for

detecting changes in environmental redox indicator concentrations (REINOSO MASET et al., 2006). The impact of DU corrosion products on the microbial community was determined using established techniques at a world class facility (CARDINALE et al., 2004; ISLAM et al., 2004). The analysis of DU corrosion products is another important part of this project. The background levels of U in environmental matrices such as soil, groundwater and seawater are 0.3 - 11.7 mg kg^{-1}, 0.003 - 2.0 µg L^{-1} and 3.0 µg L^{-1} (BLEISE et al., 2003), respectively. The LOD of U analysed by ICP-MS was 0.3 µg L^{-1}, and is therefore suitable for detecting U contamination above the environmental background levels. The use of autoradiography (Phosphor imaging) for isolating DU particles (LO et al., 2006) and SEM-EDAX and XRD for the analysis of DU corrosion products are well established, proven techniques (TOROK et al., 2004) and were again carried out at a world class facility. The removal of corrosion products from DU by chemical cleaning has been used previously (TOQUE and BAKER, 2006; 2007) and the overall uncertainty budget of this method was ± 0.005 %. Finally the transport of DU corrosion products was mathematically modelled using the k1D code (SCHÜßLER et al., 2001). Therefore it is concluded that all the techniques used for this project are appropriate to achieve the aims of this work.

Chapter 3

The Corrosion and Fate of Depleted Uranium Penetrators under Progressively Anaerobic Conditions in Estuarine Sediment

3.1 Introduction

The UK Ministry of Defence has estimated that, since weapons testing began at their firing range near Kirkcudbright in Scotland in the early 1980s, approximately 30 tonnes of DU has been deposited into the waters of the adjacent Solway Firth (HAMILTON, 2001). While at the Aberdeen Proving Ground in the USA, > 70 tonnes of DU has been deposited into ecosystems of varying salinity (DONG et al., 2006). Laboratory studies have shown that DU alloy has a tendency to undergo pitting corrosion in the presence of Cl^-, and corrosion rates increase with increasing Cl^- concentrations. However, U metal corrosion is also dependent on the Eh/pH conditions of the surrounding environment, thus the relationship of Cl^- concentrations and U corrosion may be more complex in the natural environment (Figure 1.1). Once corroded, the mobility of uranium is dependent upon its oxidation state, with U(VI) being more soluble than U(IV). In environments containing (bi)carbonate, stable, mobile uranyl(U(VI)) complexes such as $UO_2(CO_3)_2^{2-}$ or $UO_2(CO_3)_3^{4-}$ form (CHOY et al., 2006).

The long term fate of DU-Ti alloy in the water column and surface sediments of the Solway Firth has been investigated previously through *in situ* studies (TOQUE and BAKER, 2007). The reported corrosion rates were 2.9 g cm^{-2} y^{-1} in the water column and 1.6 g cm^{-2} y^{-1} in the surface sediments. Fine grained, organic-rich marine sediments inhibit diffusion of dissolved oxygen, thus, the biogeochemical environment is likely to be controlled by anaerobic respiration processes. The corrosion of U (Equation 1.1) can occur in low O_2 environments (LAUE et al., 2004) and the H_2 released can further impact on the biogeochemical conditions as it can be used as an electron donor by some microorganisms to support NO_3^-- (TILL et al., 1998) Fe(III)- (CACCAVO et al., 1994) and SO_4^{2-}-reduction (LIAMLEAM and ANNACHHATRE, 2007; OREMLAND and POLCIN, 1982). The geochemical indicators NO_3^-, Fe(III) and SO_4^{2-} can also be reduced abiotically by H_2 (Equations 1.9 -1.11) (MARSH and MCINERNEY, 2001).

There is a need to investigate the corrosion of DU-Ti alloy under conditions such as those represented by the Solway Firth in order to define the controls and mechanisms involved. We intend to test the hypothesis that the rate of DU corrosion, and the corrosion products formed, are dependent on the local biogeochemical conditions.

Laboratory microcosm experiments have therefore been carried out to investigate the fate of DU penetrator material in undisturbed estuarine sediment. The aims of the study were to investigate: (1) the long-term corrosion of DU within sediments of the Solway Firth under progressively anaerobic conditions; (2) the dissolved and particulate products of the corrosion processes, and (3) the impact of DU on the natural microbial community.

3.2 Experimental Section

3.2.1 Sampling and Characterisation

Estuarine sediment was sampled from Bowness-on-Solway, Solway Firth. Sub-samples of the sediment were dried to determine the water content and the size distribution of the < 2 mm sediment fraction. The organic carbon, inorganic carbon, cation exchange capacity and the bulk chemical composition of the sediment were determined. Seawater was sampled from Plymouth Sound and the salinity, pH, inorganic carbon and anions concentrations determined. All methods were carried out as described in Section 2.2.3.

3.2.2 Microcosm Experiments

The variation in salinity was designed to model the corrosion of DU in the subsurface and progressively anoxic environments of estuarine influence, denoted here as 'high salinity' and 'medium salinity'. All experimental microcosm (n = 120) were prepared

on the same day as described in Section 2.3. For both the high and medium salinity, thirty microcosms containing a DU coupon were prepared, together with an equivalent number of controls without a DU coupon. At selected intervals over a period of 500 days, microcosms were sacrificed in triplicate, along with three controls inside an anaerobic chamber (see Section 2.3). The DU coupons, solution and sediment were then prepared in the anaerobic chamber for further analysis as described below; all errors stated are one standard deviation of three replicates.

3.2.3 Geochemical Methods

The oxygen content, pH and Eh of the solution phase were determined using calibrated electrochemical probes. The redox indicators, SO_4^{2-} and NO_3^-, were quantified by ion chromatography. Microbially-produced Fe(II) was extracted from the sediments (LOVLEY and PHILLIPS, 1986) and determined using the ferrozine method (STOOKEY, 1980). The U in the liquid phase was quantified by ICP-MS in two fractions, the colloidal + dissolved (< 0.45 µm) and the dissolved (< 10 kDa) and the geochemical speciation of U was modelled using Hydra/MEDUSA software with experimental inorganic carbon, Eh and pH measurements. All methods were carried out as described in Section 2.4.

3.2.4 DU Coupon Analysis

The DU coupons were retrieved and rinsed to remove sediment. Coupons were photographed, analysed by SEM-EDAX and the corrosion products were removed to calculate the percentage mass loss. All methods were carried out as described in Section 2.6.

3.2.5 Microbiological Methods

Three time points of the high salinity series and their controls were selected for RISA and DNA profiling so that changes in the microbial profile could be identified over time and/or as a result of the presence of DU. All methods were carried out as described in Section 2.5.

3.2.6 Sediment DU Distribution and Particle Analysis

The sediment from day 500 of each series of microcosm was screened using Phosphor Imaging to identify areas of enhanced radioactivity or "hot" particles. The particles were subsequently isolated and analysed by Environmental SEM-EDAX. All methods were carried out as described in Section 2.7.

3.3 Results and Discussion

3.3.1 Sediment and Water Characterisation

The sediment is 31% (w/w) water, with a particle size distribution of 58 % sand, 39% silt and 2.5 % clay, organic carbon by mass of 3.2 ± 0.1 % and a cation exchange capacity of 4.0 ± 0.4 meq/100 g and an initial inorganic carbon content of 370 ± 20 mg kg^{-1}. Manganese and iron oxides comprised 0.10 % (m/m) and 3.3 % (m/m) of the sediment, respectively. Manganese reduction was not investigated because its reduction potential is close to that of nitrate reduction (Figure 1.2).

The pH and salinity of the water phases were characterised prior to mixing with the sediment. The high and medium salinity waters were pH 8.0 and 8.1, had salinities of 31.5 and 16.5; and inorganic carbon content of 72 ± 0.2 and 42 ± 0.1 mg L^{-1}, respectively. The anion concentrations (mg L^{-1}) in the high salinity water were: chloride 21000 ± 140, nitrate 92 ± 0.7; and sulfate 3100 ± 2, and in the medium salinity water were: chloride 10000 ± 70; nitrate 40 ± 0.8 and sulfate 1600 ± 5.

3.3.2 Redox Indicators

In both the high and medium salinity DU-amended and control experiments, the microcosm became progressively more anoxic over 500 days as redox indicators were utilised (Figure 3.1). The development of anoxic conditions was also indicated by the Eh values, which decreased from its initial value of +400 mV to -190 mV on day 500. Dissolved oxygen was fully depleted from the initial value of ~70 % to 0 % by day 47, and the pH increased over the duration of the experiment from 6.4 to 8.0.
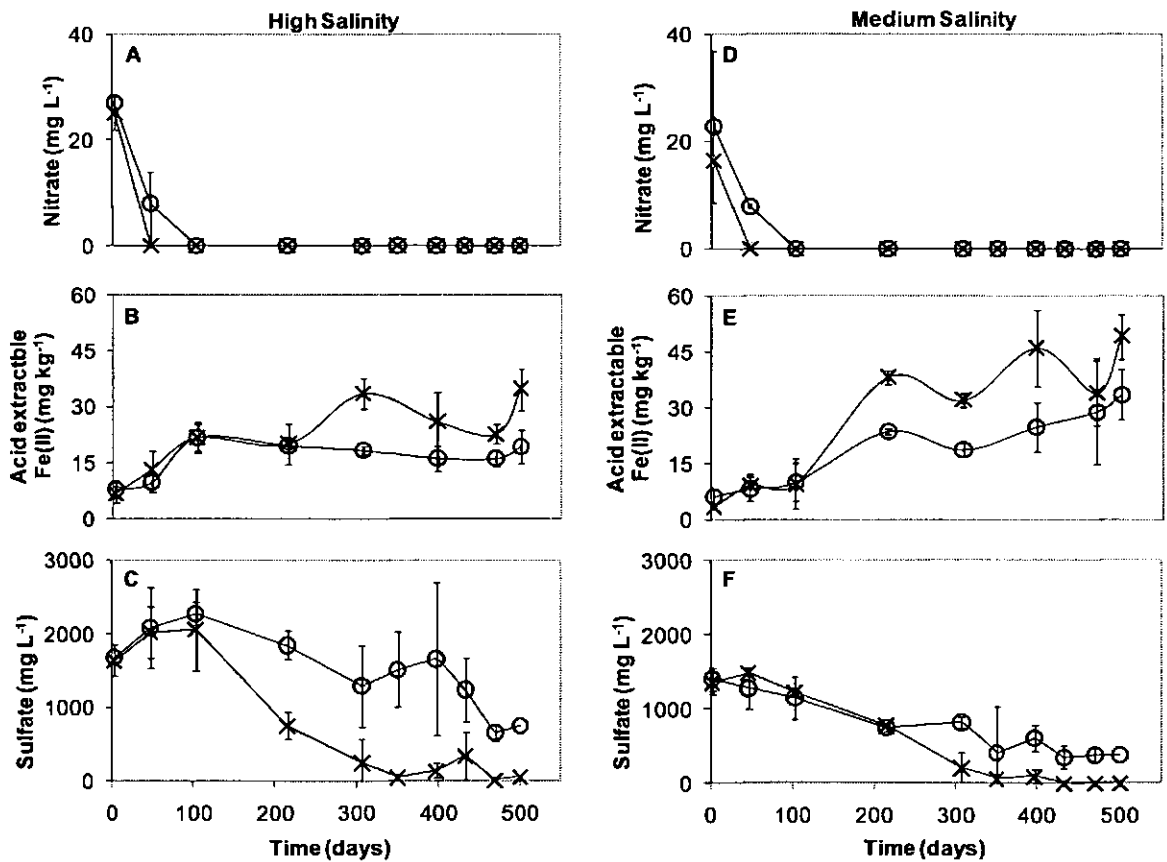
Figure 3.1 Biogeochemical time series data for the high salinity (A - C) and medium salinity (D - F), DU-amended (×) and control (○) microcosm. (A) and (D) show nitrate concentrations, (B) and (E) acid extractable Fe(II), and (C) and (F) sulfate concentrations over time. Error bars show ± 1s.d (n=3).

Both the control samples and DU-amended microcosm progressed through the redox cascade in order of NO_3^--, Fe(III)- and finally SO_4^{2-}-reduction, indicating microbial activity in the sediments. However, when comparing the control and DU-

amended microcosm, variations were observed in the concentration of the TEAs over time for both the high and medium salinity series. Nitrate depletion was more rapid in the DU-amended experiments than the controls, and occurred within 47 days and 103 days, respectively. Ingrowth of Fe(II) was observed in all sediments by day 47; however, as Fe(III)-reducing conditions progressed, significantly more Fe(II) was observed in the DU-amended sediments. Initially SO_4^{2-} concentrations increased in the high salinity series, which is consistent with an increase in pH, possibly due to desorption of SO_4^{2-} or organic sulfur mineralization (NEVELL and WAINWRIGHT, 1986). However, SO_4^{2-}-reduction was observed in all sets of microcosm by day 215. Sulfate was then depleted to a greater extent in the DU-amended microcosm than the controls. This increase in the rate of NO_3^--, Fe(III)- and SO_4^{2-}-reduction in the DU-amended experiments can be explained by abiotic or biotic processes. As DU corrodes to UO_2 it releases H_2 which can be used as an electron donor to support microbial reduction of NO_3^- (ACHTNICH et al., 1995), Fe(III) (CACCAVO et al., 1994) and SO_4^{2-} (OREMLAND and POLCIN, 1982). The H_2 released can also abiotically reduce NO_3^-, Fe(III) and, to a lesser extent, SO_4^{2-} (see Equations 1.9 - 1.11). Typically, 4.6×10^{-4} moles of U oxidised to UO_2 in each microcosm, potentially releasing 9.1×10^{-4} moles of H_2. This amount of H_2 is sufficient to abiotically reduce 53 % of the total available NO_3^- (6.5×10^{-6} moles), labile Fe(III) (7.6×10^{-6} moles) and SO_4^{2-} (3.8×10^{-4} moles) in these microcosms.

3.3.3 Corrosion of DU Coupons

The DU coupons corroded with formation of shallow pits on the surface of the coupon, together with strongly adhering black/grey corrosion products (Figure 3.2), SEM-EDAX analysis of the coupon surface indicated a uranium oxide, which is most likely to be UO_2; this has previously been reported in a similar DU sediment corrosion study (TOQUE and BAKER, 2007). Corrosion of DU was not measured until day 47 (Figure

3.3), and then rapid corrosion was observed until day 215. There was no statistical difference between the high (p = 0.077) or medium (p = 0.47) salinity system from day 215 - 500. The experimental geochemical conditions (day 215 - 500; Eh < 0; pH > 7) fall within the zone of uraninite on the relevant Pourbaix diagram (Figure 1.1), which suggests that the oxide formation protects against further corrosion by a process of passivation.
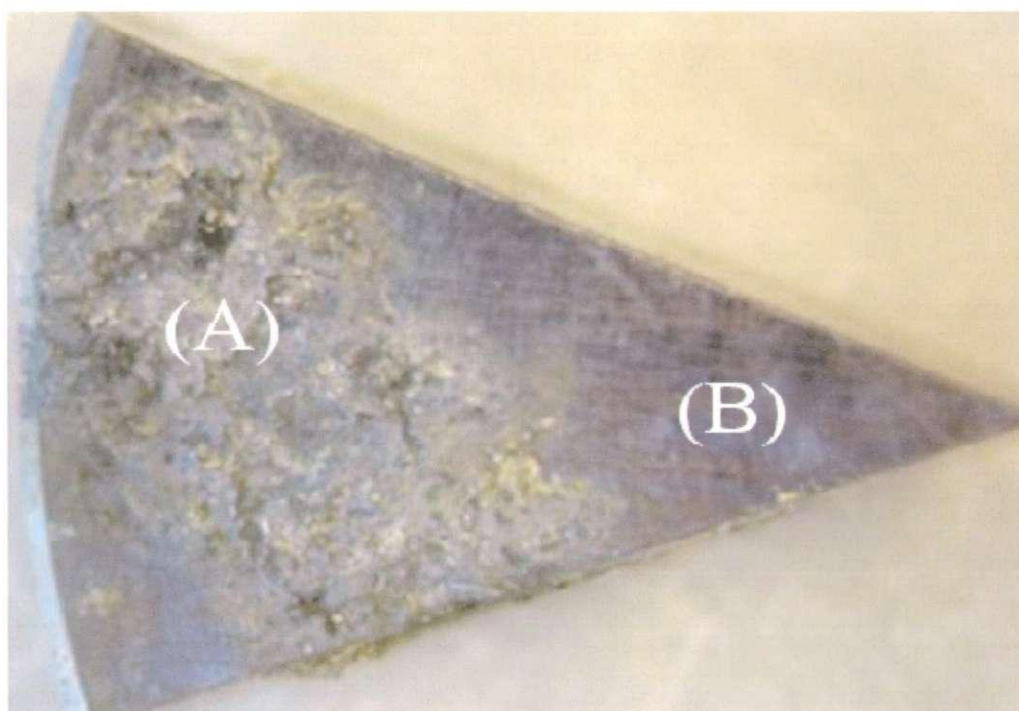
Figure 3.2 Colour photograph of a DU coupon retrieved from a sulfate-reducing microcosm (day 351), showing: (A) areas of heavily pitted corrosion and (B) areas of preserved metal.

The corrosion rate of the DU-Ti coupons (g cm^{-2} y^{-1}) was calculated using Equation 2.2 (Section 2.6.). The DU coupons only corroded measurably when dissolved oxygen concentrations were low and before SO_4^{2-}-reduction was observed, i.e. corrosion occurred predominately under sub-oxic conditions, suggesting that biogeochemical conditions control the rate of DU corrosion. The experimental uncertainties on the day 215 data were used to calculate the uncertainties associated with the corrosion rates over

the 0 - 215 day period. Thus, the corrosion rates for high and medium salinity series under sub-oxic conditions (days 0 to 215) were calculated as 0.056 ± 0.002 and 0.056 ± 0.009 g cm^{-2} y^{-1}, respectively; the difference in the salinities did not significantly (p = 1.00) affect the rate of DU corrosion.
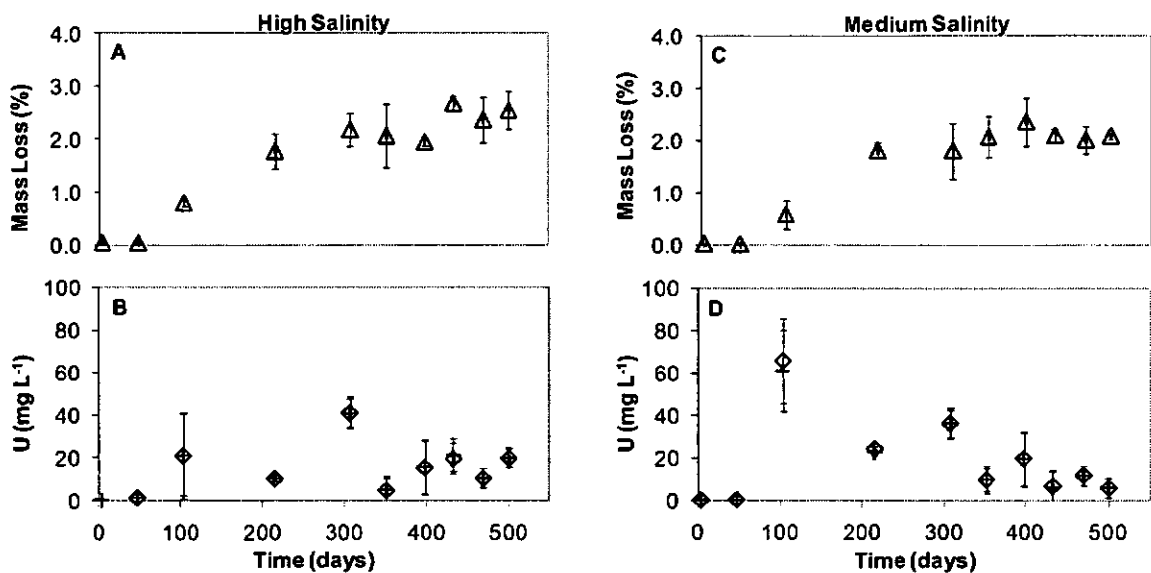
Figure 3.3 Time series data of DU corrosion and dissolved U concentrations in the high (A-B) and medium (C-D) salinity microcosm. (A) and (C) show mass loss (%) of DU corrosion products from coupon (Δ). (B) and (D) show changes in < 0.45 μm (+) and < 10 kDa (◊) uranium fractions. Error bars show ± 1s.d (n=3).

The sub-oxic corrosion rates were 7 times lower than the literature value for DU-Ti alloy in a synthetic 3.5% NaCl solution (TRZASKOMA, 1982) of equivalent salinity, and from 30 - 40 times lower than the rates calculated from the *in situ* data (TOQUE and BAKER, 2006). The higher corrosion rate in the 3.5% NaCl solution may be due to other factors such as oxic conditions and the pH, which is more acidic in the NaCl solution than in the marine microcosm (pH ~ 6.4 - 7.8) as compared to the NaCl which would have the pH of MQ water (pH 5.5). It is more difficult to explain the large difference between our microcosm corrosion rates and the previously reported *in situ* rates; the *in situ* biogeochemical conditions were not characterised due to unsuitable conditions at the time of sampling (TOQUE and BAKER, 2006). Additionally, the *in situ* experiments

involved a device to hold the penetrators at sediment depths of 0 - 15 cm (TOQUE and BAKER, 2007), so that the coupons experienced an uncharacterised level of physical disturbance. The slower corrosion rates in the microcosm experiments reported here reflect not only the local biogeochemical conditions but also minimal physical disturbance, as would be experienced when penetrators sink through fine-grained Solway Firth sediments.

The corrosion rate (g cm^{-2} y^{-1}), mass and the mean surface area of a penetrator during corrosion were used to estimate the total corrosion time for a complete penetrator (see Equation 2.3; Section 2.6). Under sub-oxic conditions, the complete corrosion times for a penetrator in both high and medium salinity systems were calculated as approximately 540 ± 80 years.

3.3.4 Uranium in the Solution Phase

The dissolved U concentrations are shown in Figure 3.3. The data show that there was no statistical difference between the U concentrations in the <0.45 μm and < 10 kDa fractions for the high (p = 0.058) and medium (p = 0.057) salinities, i.e. colloidal DU-oxides are not an important source of DU to the system. During the period when DU corrosion was negligible, the dissolved U concentration was less than 2 mg L^{-1}. The concentration then increased by day 103, co-incident with the onset of measurable corrosion when NO_3^--reduction was complete, and Fe(III) reducing conditions prevailed (Figure 3.1). At this time point, the concentration of uranium in the medium and high salinity microcosm was 66 and 21 mg L^{-1}, respectively. Using the inorganic carbon concentrations measured on day 1, the geochemical modelling suggests that U would be present in both the high salinity (pH: 7.1, Eh: 45 mV) and medium salinity (pH: 7.6, Eh: 30 mV) microcosm as mixture of soluble uranyl carbonate species ($UO_2(CO_3)_3^{4-}$; $UO_2(CO_3)_2^{2-}$; $(UO_2)_2CO_3(OH)_3^-$). By day 351 the uranium concentration had decreased

to a stable concentration, representing < 0.1 % of the total corroded U, in both the high salinity (pH: 7.8, Eh: -150 mV) and medium salinity microcosm (pH: 7.9, Eh: -170 mV). Results of speciation modelling suggests that the low mobility UO_2 species dominates under these conditions, with a minor contribution from soluble uranyl species $(UO_2(CO_3)_3^{4-}; UO_2(CO_3)_2^{2-}; U(OH)_5^-)$.

3.3.5 Microbial Community Profile

The high salinity sediments at days 6, 215 and 433 which were selected for RISA and the results suggested that DU had impacted the microbial community (Figure 3.4). The RISA profiles indicated a change in the microbial profile in both the DU-amended and controls over time. They also highlighted a change in the microbial community. This warranted further investigation by DNA profiling which was undertaken on the selected samples of control day 6, control day 433 and DU-amended day 433.
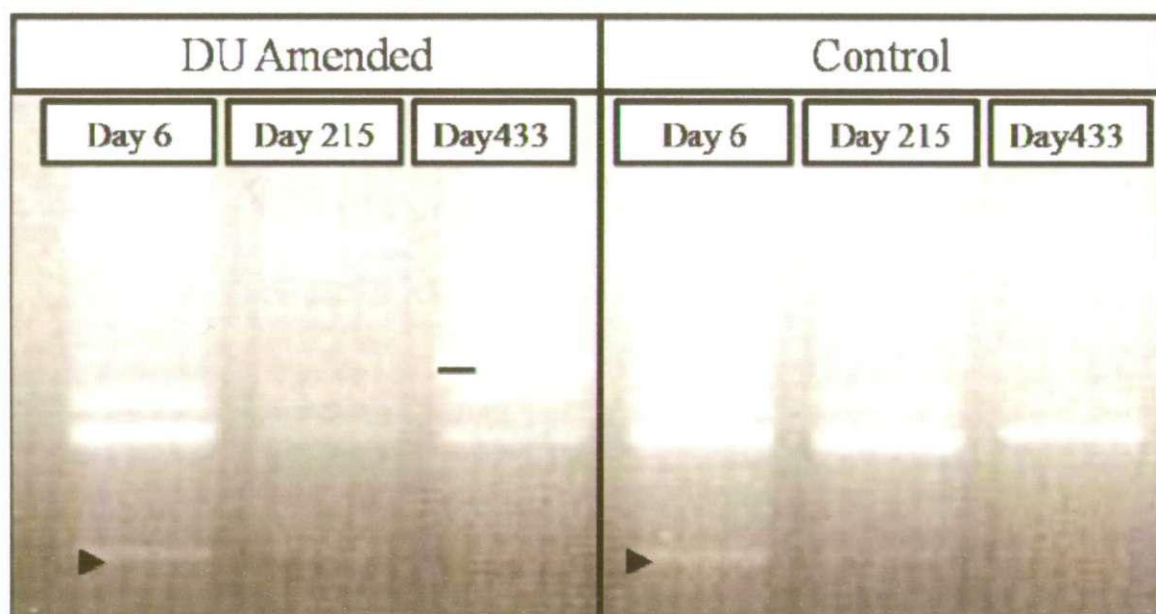
Figure 3.4 RISA profiles for the high salinity, DU-amended and control microcosm, at 6, 215 and 433 days, showing: (▶) the band that disappears over time as anoxic conditions develop and (—) the band that appears by day 433 in the DU-amended experiments.

Phylogenetic analysis (Figure 3.5) identified the bacterial groups present in the control day 6 (A), control day 433 (B) and DU-amended day 433 (C) samples. The controls show an increase in microbial diversity from day 6 to 433, as conditions became progressively anoxic, with four new phylogenetic groups detected in the clone library prepared from this sample. However, the DU-amended sample from day 433 shows a lower microbial diversity compared to those in either of the controls, due largely to the appearance of a new dominant member of the microbial community affiliated with the Epsilonproteobacteria group (representing 36% of the 16S rRNA genes detected in the clone library). Drastic loss in microbial diversity has been reported in soil when exposed to DU oxide (U_3O_8) (RINGELBERG et al., 2004). In our case, there would seem to be at least one member of the microbial community that is able to adapt to the DU contamination. Microbial adaptation even in heavily contaminated uranium sites has been previously observed (CERDA et al., 1993; SCHIPPERS et al., 1995; SELENSKA-POBELL et al., 1999). The dominant organism detected in the DU impacted microbial community was most closely related to *Sulfurovum lithotrophicum* (95% match over 925 bases), characterised as a sulfur-oxidizing chemolithoautotroph able to grow with elemental sulfur or thiosulfate as a sole electron donor and oxygen (5 % in the gas phase) or nitrate as the electron acceptor. It is difficult to extrapolate the physiological profile of the organism detected from 16S rRNA gene homology, especially at only 95% homology, but selection of this dominant end member of the community could be due to resistance to potentially toxic soluble uranium corrosion products liberated in the local environment, or adaptation to the chemical environment associated with the DU e.g. through utilisation of hydrogen produced by DU corrosion, or even direct use of the depleted uranium itself as an electron donor.
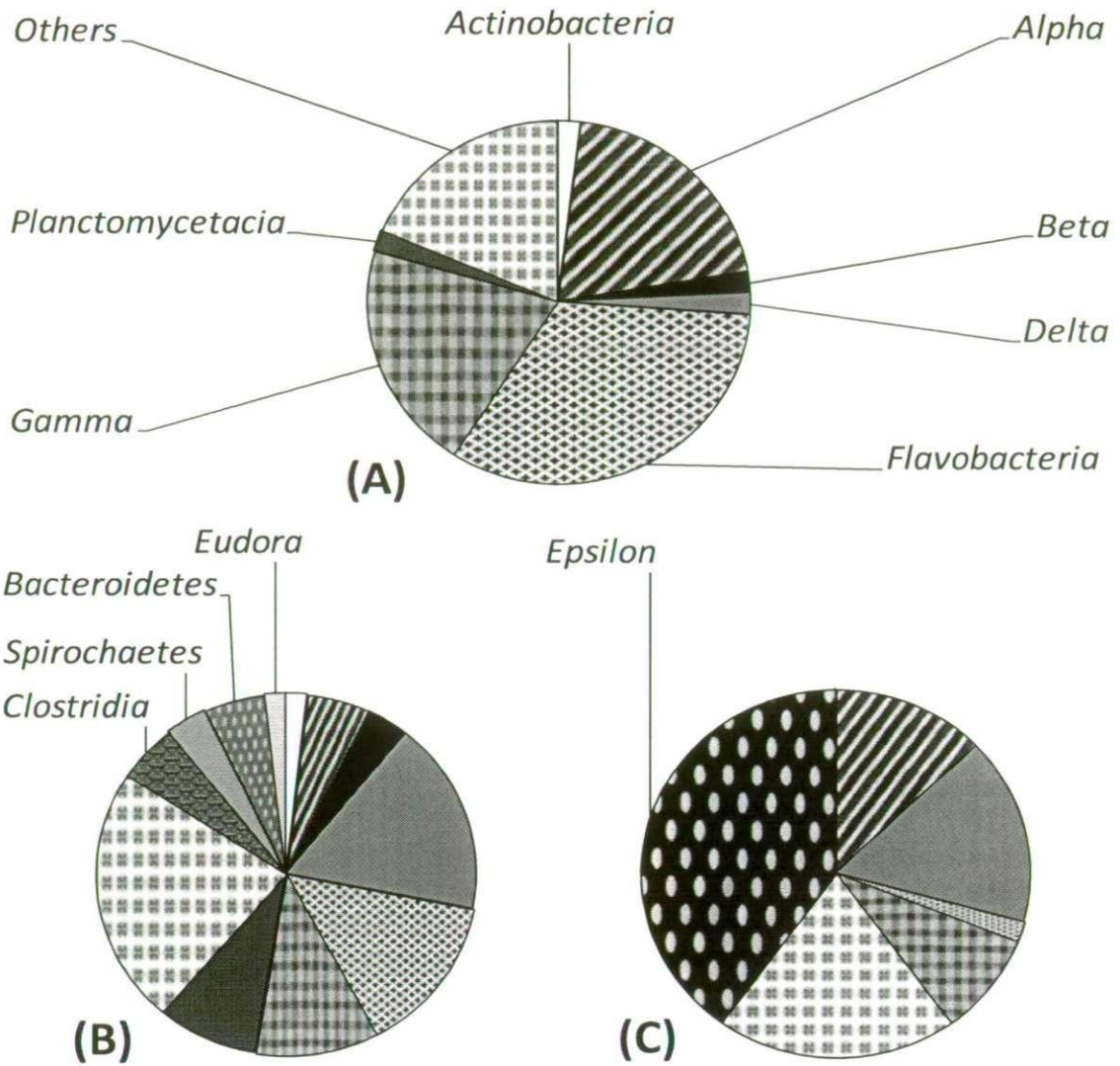
Figure 3.5 Phylogenetic affiliations of clones in high salinity sediments for (A) control day 6, (B) control day 433 and (C) DU-amended day 433. Phylogenetic groups are labelled once in order of (A) to (C). Alpha, Beta, Delta, Epsilon and Gamma represent proteobacterial divisions.

3.3.6 Sediment Uranium Distribution and Particle Analysis

The Phosphor Image data for the sediment from the long term microcosm (day 500) showed a homogeneous distribution of uranium in the sediment, with sparse localised hotspots corresponding to aggregated sediment. Representative particles were selected and analysed by Environmental SEM-EDAX, and a typical spectrum is shown in Figure 3.6. The spectrum shows elements typical of marine sediments such as Fe, C, Mg, Al, Si and Na, alongside U. The strong U and Si peaks suggest the formation of uranium

silicate species, possibly in association with a range of stable metal ions, although the product has no characteristic morphology. Similar species have been reported in sub-surface DU contaminated soils, following SEM-EDAX analysis (BUCK et al., 2004) and sequential extraction (JOHNSON et al., 2004). The U-O-C-Si Pourbaix diagram (BROOKINS, 1988) is also consistent with formation phases such as coffinite (USiO$_4$) under these experimental Eh/pH conditions.
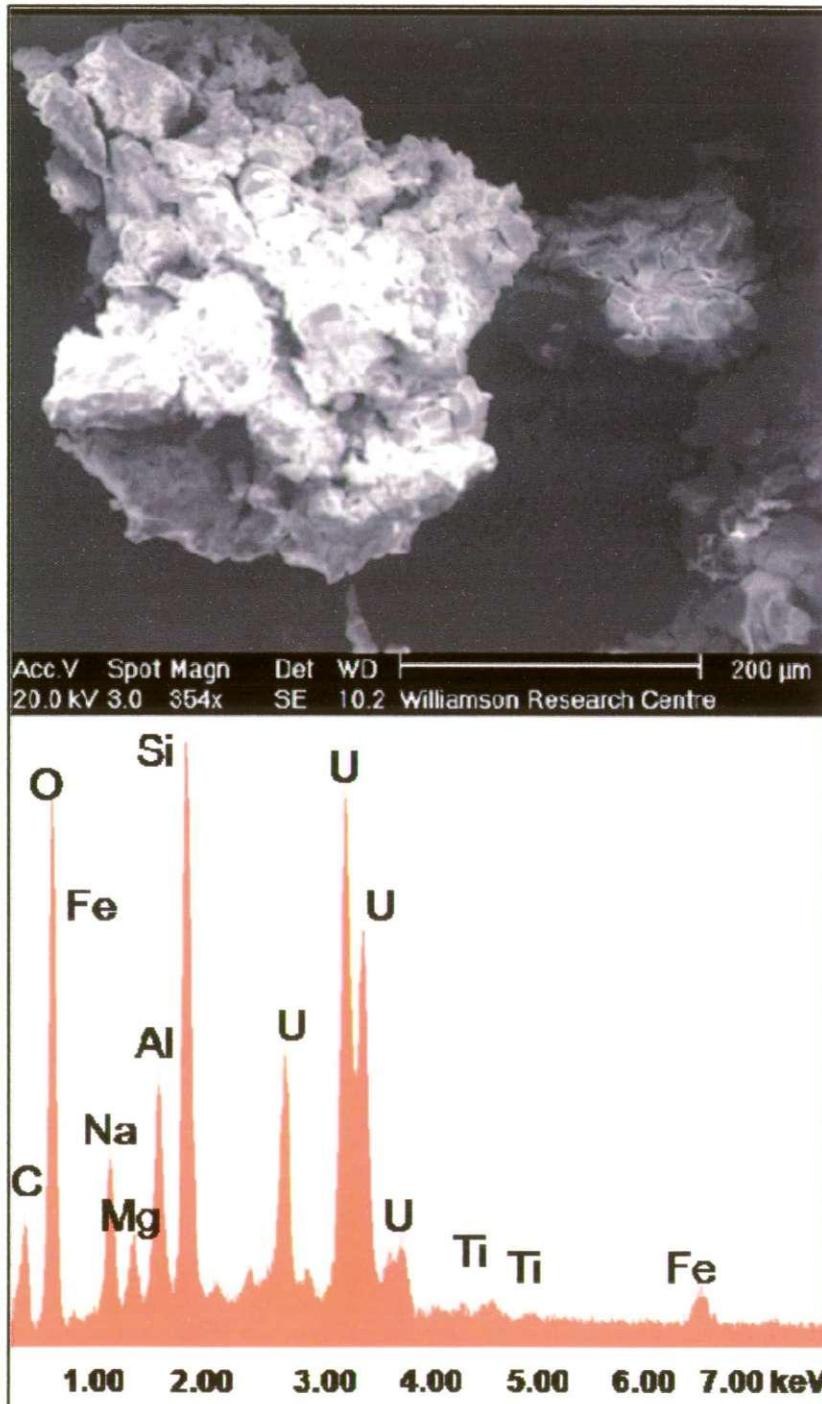
Figure 3.6 Backscattered electron image and SEM-EDAX spectrum of uranium-rich particle.

3.4 Conclusions

The results from this study suggest that, as DU penetrators fired from the Kirkcudbright range sink into the fine sediments of the Solway Firth, the biogeochemical conditions in those sediments will control the rate at which they corrode. The salinity (16.5 and 31.5) did not affect the corrosion rate or corrosion products formed, thus the chloride concentration, which has previously been identified as important in laboratory dissolution studies (MCINTYRE et al., 1988; TRZASKOMA, 1982), is superseded by biogeochemical conditions. Under sub-oxic conditions, penetrators will corrode at approximately 0.056 ± 0.006 g cm^{-2} y^{-1} by localised pitting and the formation of black/grey adhering UO_2. The main mechanism for U release from the penetrator is dissolution of U(VI) and dispersion of uranyl carbonate species ($UO_2(CO_3)_3^{4-}$; $UO_2(CO_3)_2^{2-}$; $(UO_2)_2CO_3(OH)_3^{-}$). Under more strongly reducing conditions, passivation of the penetrator occurs, preventing further corrosion. Colloidal or particulate corrosion products are not an important source of DU entering the sediment or aqueous phase under either sub-oxic or anoxic conditions. Dissolved U species can form uranium silicate species through interaction with sediment minerals. Additionally, the corroding DU results in more reducing local biogeochemical conditions and decreases the diversity of the microbial population.

Chapter 4

The Corrosion and Fate of Depleted Uranium Alloy in Grassland Soils

4.1 Introduction

Terrestrial environments have been impacted widely by depleted uranium fired during weapons testing and active conflicts, for example, the 1991 Gulf War resulted in the deposition of approximately 321 tonnes of DU in the terrestrial environment (BLEISE et al., 2003). Therefore, it is important to understand the corrosion and fate of this DU.

The moisture content, O_2 supply, pH, temperature, anions, cation exchange capacity and microbial community influence how corrosive conditions are in a soil (MATTSSON, 1989). At Kirkcudbright in the UK, DU coupons were buried to a depth of 0.3 m in an organic, silty clay soil and sampled over 4.4 years. Black and yellow corrosion products characterized as uranium dioxide and schoepite, respectively, were observed on the DU coupons and in the surrounding soil at the first sampling time (102 days), and corrosion rates over 4.4 years were 0.8 - 1.1 g cm^{-2} y^{-1} (TOQUE and BAKER, 2006). In the laboratory, DU corrosion has been studied in two soils (sandy-loam and silty-loam) at 20 °C, with simulated rainfall (16 mm $week^{-1}$). Black and yellow corrosion products formed, and there was negligible difference in corrosion rates for the two soils (0.19 ± 0.03 g cm^{-2} y^{-1}) (SCHIMMACK et al., 2007).

In soils, DU penetrators can become embedded to a depth of up to 7 m (PAPASTEFANOU, 2002; UNEP, 2001). Sub-surface soils can become waterlogged as a result of heavy rain, flooding, poor drainage, rising water tables or soil compaction. The diffusion rate of O_2 in soils ranges from 10^{-2} cm^2 s^{-1} to 10^{-6} cm^2 s^{-1} for dry soil aggregates and water saturated aggregates, respectively (SMITH, 1980). The limited diffusion of O_2 into waterlogged soils results in anaerobic conditions, and under these conditions, soil microorganisms utilize alternative terminal electron acceptors (TEAs) for organic matter oxidation. The energy gained from each TEA influences the order of utilization, giving rise to a classical TEA sequence of: O_2, NO_3^-, Mn, Fe(III), SO_4^{2-} and CO_2 (KONHAUSER et al., 2002).

69

Hydrogen released from the corrosion of DU can reduce geochemical indicators abiotically (MARSH and MCINERNEY, 2001), as shown in (Equations 1.9 - 1.11). However, it can also be used as an electron donor by some microorganisms to support NO_3^-- (TILL et al., 1998) Fe(III)- (CACCAVO et al., 1994) and SO_4^{2-}-reduction (LIAMLEAM and ANNACHHATRE, 2007; OREMLAND and POLCIN, 1982), and thus may alter the microbial community in an impacted sediment. DU corrosion products can also affect microbial diversity, with reduced microbial diversity reported in estuarine sediment (Chapter 3) and in soil (RINGELBERG et al., 2004).

To date, DU corrosion studies in soils have not considered waterlogging or biogeochemical conditions when characterising corrosion processes, leaving a level of uncertainty when extrapolating from oxic corrosion to other soil environments. Laboratory microcosm experiments have therefore been carried out to investigate the fate of DU penetrator material in field-moist soil and progressively anoxic waterlogged soils to test the hypothesis that the rate of DU corrosion, and the nature of corrosion products formed, are dependent on the local biogeochemical conditions. The aims were to investigate: (1) the corrosion of DU under different biogeochemical conditions and water status (field-moist and waterlogged); (2) the dissolved and particulate products formed in these corrosion processes, and (3) the impact of DU on the natural microbial community.

4.2 Experimental Section

4.2.1 Sampling and Characterisation

A grassland soil (silty-loam) was sampled from the North Wyke Research Station, Okehampton, Devon. Sub-samples of the soil were dried to determine the water content and the size distribution of the dried < 2 mm soil fraction. The organic carbon, inorganic

carbon, cation exchange capacity and the bulk chemical composition was determined. Water was collected from a drain channel at the same site and the pH, inorganic carbon and anion concentrations determined. All methods were carried out as described in Section 2.2.3.

4.2.2 Microcosm Experiments

Experiments were designed to investigate the corrosion of DU under sub-surface soil environments. The variation in water content and O_2 content was designed to generate three distinct sub-surface biogeochemical environments, denoted here as 'field-moist', 'open waterlogged' and 'closed waterlogged'. All experimental microcosm were prepared on the same day (n = 150) as described in Section 2.3. For the open systems (open waterlogged and field-moist), fifteen microcosms each containing a DU coupon were prepared, together with an equivalent number of controls without a DU coupon. For the closed waterlogged system, thirty microcosms each containing a DU coupon were prepared, together with an equivalent number of (DU absent) controls. At selected intervals over a period of 510 days, microcosms were sacrificed in triplicate, along with three controls inside an anaerobic chamber (Section 2.3.4). The DU coupons, solution and sediment were then prepared for further analysis as described below; all errors stated are one standard deviation of three replicates.

4.2.3 Geochemical Methods

The oxygen content, pH and Eh of the solution phase were determined using calibrated electrochemical probes and a bench meter within the anaerobic chamber, using a sub-sample from each microcosm. The redox indicators, SO_4^{2-} and NO_3^-, were quantified by ion chromatography. Microbially-produced Fe(II) was extracted from the sediments (LOVLEY and PHILLIPS, 1986) and determined using the ferrozine method (STOOKEY,

71

1980). The uranium in the liquid phase was quantified in two fractions, the colloidal + dissolved (< 0.45 μm) and the dissolved (< 10 kDa) uranium by ICP-MS. Sub-samples of each soil from day 510 were refluxed with concentrated nitric acid for 8 h and total U analysed by ICP-OES (0.1 mg L^{-1} detection limit, Varian 725-ES Axial, CA). The geochemical speciation of uranium was modelled using experimental inorganic carbon, Eh and pH measurements. All methods were carried out as described in Section 2.4.

4.2.4 DU Coupon Analysis

The DU coupons were retrieved and rinsed to remove soil, air dried and stored in a desiccator to prevent further corrosion. Coupons were photographed, analysed by SEM-EDAX and the corrosion products were removed to calculate the percentage mass loss. All methods were carried out as described in Section 2.6.

4.2.5 Microbiological Methods

Microbial analysis was carried out on DU-amended and control samples for the field-moist and closed waterlogged microcosm at day 435. This time point was selected to determine the long term impact of corroding DU on the microbial community. All methods were carried out as described in Section 2.5.

4.2.6 Sediment DU Distribution and Particle Analysis

The soil from day 337 of each series of microcosm was screened using Phosphor Imaging to identify areas of enhanced radioactivity or "hot" particles. The particles were subsequently isolated and analysed by ESEM-EDAX. Particles from the field-moist soil contained enough uranium which was sufficiently crystalline to allow further analysis by XRD. All methods were carried out as described in Section 2.7.

4.3 Results and Discussion

4.3.1 Soil and Water Characterisation

The soil moisture content was 22% (w/w), with a particle size distribution of 54 % sand, 41% silt and 5.0 % clay, organic carbon by mass of 12 ± 0.1 %, CEC of 21 ± 0.4 meq/100 g and an initial inorganic carbon content of 80 ± 1 mg kg^{-1}. Manganese and iron oxides comprised 0.2 % (m/m) and 6.0 % (m/m) of the sediment, respectively. Manganese reduction was not investigated because its reduction potential is near to that of nitrate reduction (Figure 1.2). The pH of the water prior to mixing with the soil was 7.4, with an inorganic carbon content of 73 ± 2 mg L^{-1}, and the anion concentrations (mg L^{-1}) were: chloride 130 ± 2, nitrate 120 ± 2; and sulfate 100 ± 1.

4.3.2 Redox Indicators in the Field-moist Microcosm

The pH (5.2 - 5.8) and Eh (+500 - +600 mV) stayed fairly constant over the 510 day experimental period. The changes in the redox indicator concentrations over time are shown in Figure 4.1 A, D & G. In the control microcosm, the TEAs were not reduced over the experimental period, suggesting that oxic conditions were maintained. This is consistent with the visible, air-filled macro-pores in the soil structure. However, in the DU-amended experiments, depletion of NO_3^- was observed from day 242 (510 ± 70 mg L^{-1}) to day 510 (17 ± 5 mg L^{-1}). In-growth of Fe(II) into soils was also observed from 242 days, possibly due to the reducing environment caused by corroding DU as U is known to be a strong reducing agent (LAUE et al., 2004). The SO_4^{2-} concentrations in both the DU-amended and control microcosm were fairly constant throughout the course of the experiment, indicating that SO_4^{2-}-reduction did not occur.
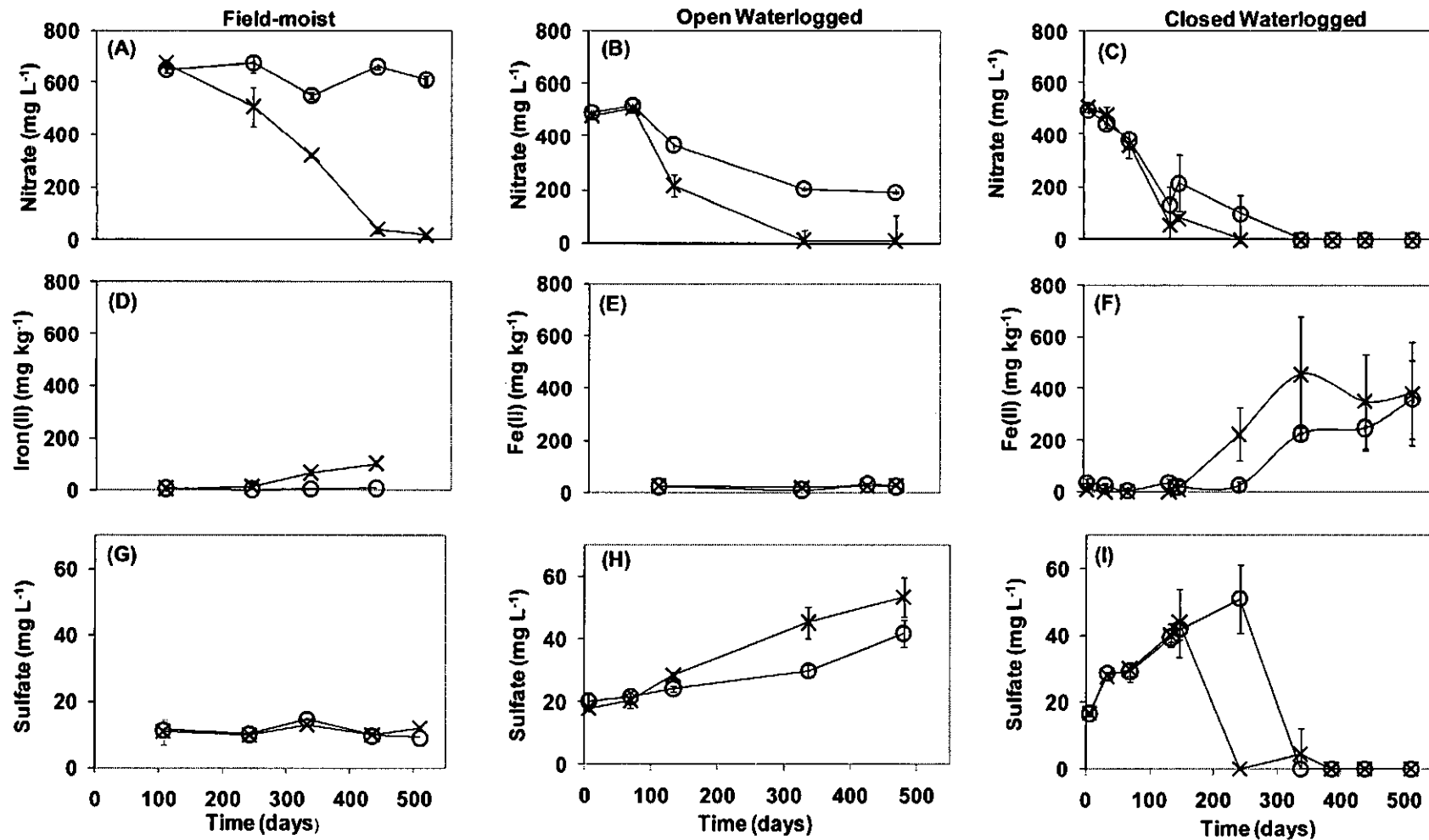
Figure 4.1 Biogeochemical time series data for DU-amended (x) and control (o) field-moist microcosms (A, D & G) and the open (B, E & H) and closed (C, F & I) waterlogged microcosms. Nitrate (A - C), acid extractable Fe(II) (D - F) and sulfate (G - I) concentrations over time. Error bars show ± 1 s.d (n = 3).

4.3.3 Redox Indicators in the Waterlogged Microcosm

Sub-oxic conditions developed in the open waterlogged microcosm and controls over time due to the limited diffusion of oxygen through waterlogged soils (SMITH, 1980). The dissolved oxygen decreased from its initial value of 84 % to 35 % on day 133. The Eh decreased slightly from +610 mV to +570 mV and the pH increased slightly over the duration of the experiment from pH 5.0 to 5.2 in the controls and pH 4.9 to 5.5 in the DU-amended experiments, which is consistent with waterlogged conditions (LU et al., 2004). Nitrate-reduction, as indicated by a decrease in the NO_3^- concentration, was observed in both the DU-amended experiments and controls after 133 days (Figure 4.1 B) although NO_3^- depleted to a greater extent in the DU-amended microcosm. Iron(III)-reduction was not observed and the SO_4^{2-} concentrations increased in both systems, consistent with the increase in pH (NEVELL and WAINWRIGHT, 1986).

The closed waterlogged microcosm and controls became progressively anoxic, with a decrease in the Eh from +610 mV to -170 mV by day 510. The dissolved oxygen rapidly depleted from its initial value of 85 % to 5 % by day 34 and the pH increased over the duration of the experiment from 4.9 to 6.5. When comparing the control and DU-amended microcosm, differences were observed in the concentrations of the TEAs over time. The onset of NO_3^--reduction was observed on day 34, and was complete by day 242 and 337 in the DU-amended microcosm and controls, respectively. In-growth of Fe(II) into soils was observed on day 242 and 337 for the DU-amended microcosms and controls, respectively. Sulfate initially increased in both the DU-amended and control microcosm, again due to the increase in pH (NEVELL and WAINWRIGHT, 1986). After this initial increase, SO_4^{2-}-reduction was observed concurrently with Fe(II)-reduction in the DU-amended and control microcosm between days 242 - 337 and 337 - 510, respectively. Therefore, the presence of DU increased the rate of progression through the redox cascade.

4.3.4 Corrosion of DU Coupons in Field-moist and Waterlogged Soils

The DU coupons from the field-moist soil microcosm are shown in Figure 4.2 A & B after 242 and 337 days incubation, respectively, and the % mass loss over time is shown in Figure 3A. Localised pitting initially developed on the metal surface by day 242, and by day 337 the coupon was covered with protruding, predominately yellow corrosion products; the coupon also had some adherent black corrosion products. Corrosion of DU as indicated by % mass loss (Figure 4.3) was not significant until day 242 (0.75 ± 0.2 %; $p = 0.0012$), indicating a latent period prior to the onset of corrosion. After day 242 corrosion progressed linearly ($r^2 = 0.99$), with a mass loss of ~ 21 % by day 510. As has been indicated previously for DU corrosion in soils (SCHIMMACK et al., 2007). Latent periods can reflect the presence of a protective oxide layer (750 Å or 10 μg cm^{-2} for pure uranium), which thickens over time and eventually cracks, accelerating the corrosion process (LAUE et al., 2004).

Nitrate depletion and in-growth of Fe(II) were observed in the DU-amended field-moist soil microcosm with the onset of measurable DU corrosion. Since the controls did not become NO_3^--reducing during the experimental period, oxygen supply to the soils was good, thus the corroding DU appears to drive these geochemical changes. A plausible reason for this is that the supply of H_2 from the corroding DU (Equation 1.8) drives the abiotic reduction of NO_3^- and Fe(III) (see Equation 1.9 - 1.10). By day 332, typically, 2.3×10^{-3} moles of U had oxidised to UO_2 in each microcosm, potentially releasing 4.7×10^{-3} moles of H_2. This H_2 is sufficient to reduce 100 % of the total NO_3^- (1.5×10^{-4} moles) and bioavailable Fe(III) (1.7×10^{-5} moles) abiotically. These induced changes did not, in turn, influence the rate of mass loss (i.e. indicator of corrosion) DU, which progressed linearly from day 242 ($r^2 = 0.99$) during NO_3^- and Fe(III) reduction.
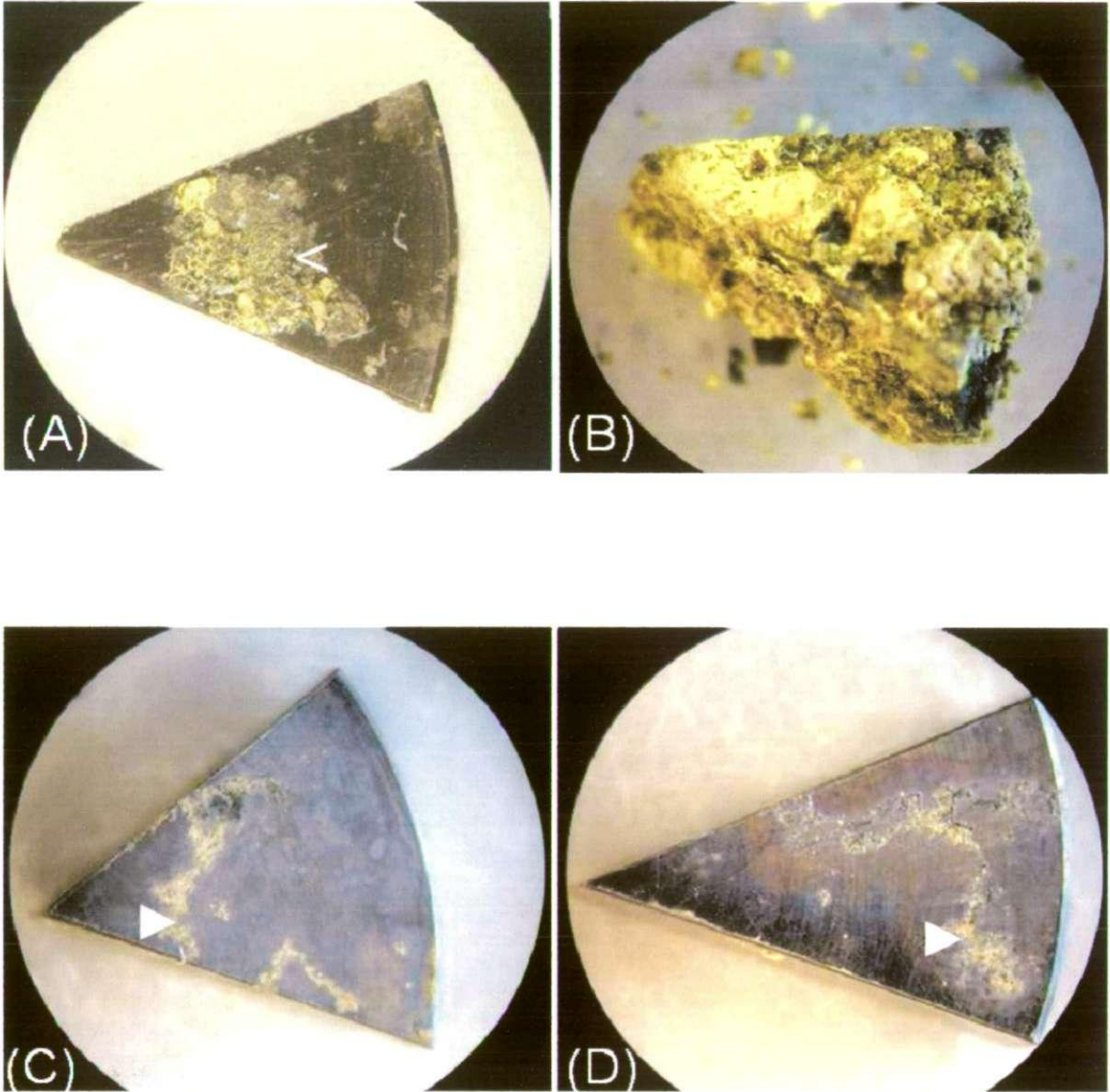
Figure 4.2 Colour photographs of retrieved DU coupons for (A) field-moist coupon after 242 days with highlighted area (<) of pitting corrosion and (B) a heavily corroded field-moist coupon after 337 days. Also DU coupons for (C) closed and (D) open waterlogged DU after 337 days with highlighted area (▶) of pitting.
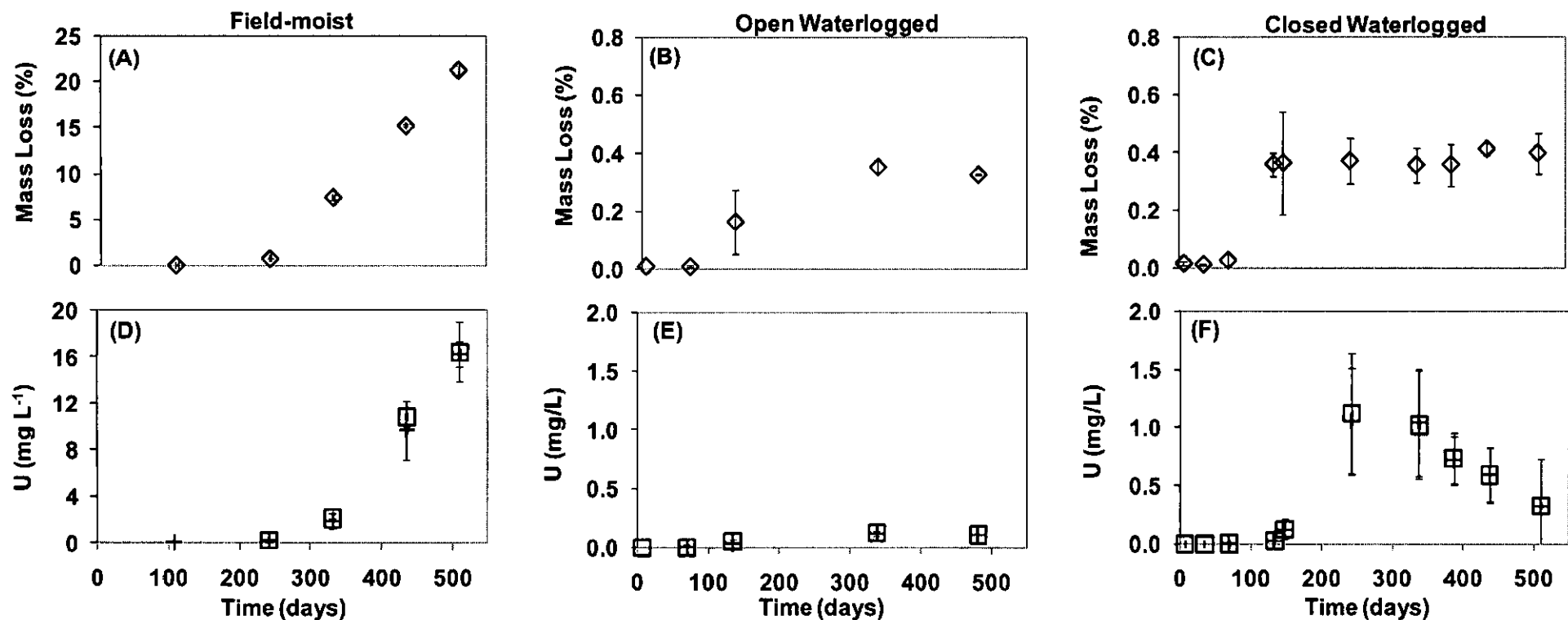
Figure 4.3 Time series for DU corrosion in the field-moist (A,D), open waterlogged (B,E) and closed waterlogged (C,F) microcosms. Figures A-C show mass loss (%) of DU metal from the DU coupon (◊) and figures D-F show changes in uranium concentration in the <0.45 μm (+) and <10 kDa (□) fractions. Error bars ± 1s.d (n=3).

Coupons retrieved from the open waterlogged and closed waterlogged microcosm on day 337 are shown in Figure 4.2 C and D, respectively. The corrosion pattern was similar in both systems with the formation of shallow, crevice-shaped pits on the surface of the alloy. The corrosion of DU as indicated by % mass loss (Figure 4.3) was not significant for the open waterlogged ($p = 0.59$) and closed waterlogged ($p = 0.43$) microcosm until day 133, which corresponded to NO_3^--reducing conditions. Once NO_3^--reduction was complete (by days 337 and 242 for the open and closed waterlogged systems respectively), the % mass loss was similar ($p = 0.84$) at 0.36 ± 0.02% and 0.37 ± 0.08%, respectively. The concomitant uranium corrosion and nitrate depletion in these systems suggests that the two processes are related. In fact, the intermediates of NO_3^--reduction are reported to oxidise UO_2 to more mobile U(VI) species (SENKO et al., 2002). For the remaining experimental period, no further corrosion was observed in the open waterlogged ($p = 0.10$) and closed waterlogged ($p = 0.86$) microcosm. Therefore corrosion in the waterlogged systems took place during NO_3^- reduction and ceased during Fe(III) and SO_4^{2-} reduction. A similar biogeochemical control on DU corrosion has been observed in estuarine sediments, with corrosion ceasing during SO_4^{2-}-reducing conditions (Chapter 3). In this and the current study (day 248 - 510; Eh < 0; pH >7), the Eh/pH conditions were consistent with uraninite (UO_2) formation and subsequent passivation of the metal surface (Figure 1.1). The presence of corroding DU in waterlogged conditions also altered the biogeochemical environment relative to the controls. The systems showed accelerated progression through the redox cascade, leading to quicker passivation and, in turn, protection against further corrosion.

The corrosion rates (g cm^{-2} y^{-1}), excluding the latent period, were calculated using Equation 2.2 (Section 2.6), with time periods of corrosion as follows: field-moist, day 242 – 510; open waterlogged, day 69 - 337; closed waterlogged, day 33 - 133. In each

case, the experimental uncertainties on the replicate microcosm for the two timepoints have been used to estimate the total uncertainties in the corrosion rates.

Corrosion in the field-moist microcosm proceeded at a rate of 0.49 ± 0.06 g cm^{-2} y^{-1}. This rate is intermediate between that reported by Schimmack et al. (2007) (0.19 ± 0.03 g cm^{-2} y^{-1}), for corrosion in silty loam soil at 20 C$^{\circ}$ with 16 mm week^{-1} of simulated rainfall, and the *in situ* rate in soil of $0.8 - 1.1$ g cm^{-2} y^{-1} reported by Toque and Baker (2006).

The corrosion rates in the open and closed waterlogged systems were 0.0092 ± 0.0005 g cm^{-2} y^{-1} and 0.020 ± 0.005 g cm^{-2} y^{-1}, respectively. This corrosion only occurred under sub-oxic conditions and was at least an order of magnitude slower than in field-moist soils.

The corrosion rate (g cm^{-2} y^{-1}), mass and mean surface area of a penetrator during corrosion were used to estimate the total corrosion time for a complete 120 mm penetrator (see Equation 2.3; Section 2.6). Under field-moist conditions the total corrosion time for a penetrator is therefore 55 - 69 years. Under waterlogged, NO_3^--reducing conditions, the total corrosion times for a penetrator in the open and closed systems is therefore 3100 - 3400 and 1200 - 1900 years, respectively.

4.3.5 Analysis of DU Particles from the Field-moist and Waterlogged Soils

The field-moist soils had a heterogeneous distribution of uranium with scattered intense radioactive hot spots of uranium, as indicated by Phosphor Imaging. The hotspots related to bright yellow corrosion products that were partially covered in soil, but still suitable for XRD analysis. XRD evidence suggested the presence of metaschoepite or a similar phase, as has previously been reported in surface and sub-surface soils (BUCK et al., 2004; TOQUE and BAKER, 2006). A representative ESEM image and EDAX spectrum of the selected particles are shown in Figure 4.4A & B. The ESEM image

shows desiccation cracks, indicative of a dehydrated metaschoepite phase (BUCK et al., 2004). The ESEM-EDAX spectrum shows major peaks from U and O alongside minor peaks from common matrix elements (Si, Al and Fe).

Phosphor Imaging showed that the waterlogged soils had a dispersed, homogenous and less intense radioactivity. This was consistent with corrosion of < 0.5 % of the DU. A representative ESEM image of these particles is shown, with the EDAX spectrum, in Figure 4.4 C and 4.4 D, respectively. The spectrum shows minor peaks from U together with signals from Si, Al and Fe. Collectively these results indicate that the DU is present in the soil as sorbed ions, rather than as discrete corrosion products.
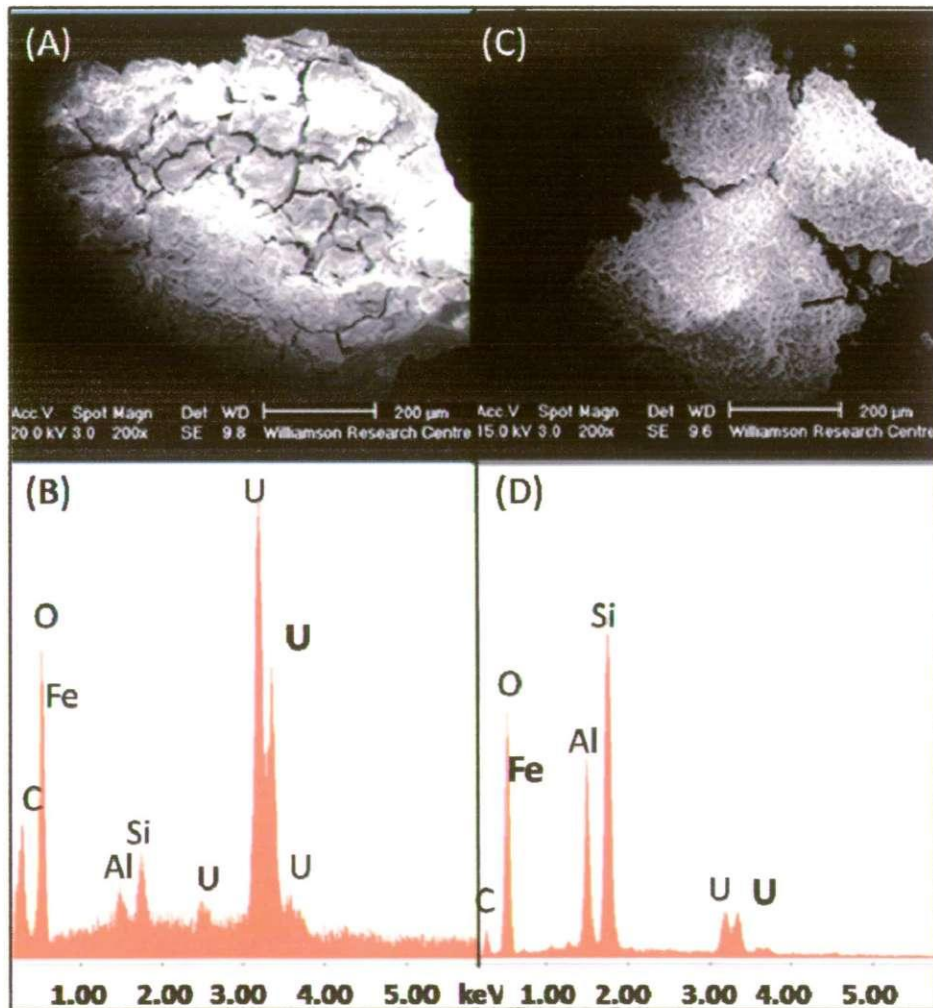
Figure 4.4 Backscattered electron image and ESEM-EDAX spectrum of a corroded DU particles isolated from the field-moist (A - B) and the progressively anoxic waterlogged microcosm (C - D).

4.3.6 Solution Phase Uranium in Field-moist and Waterlogged Soils

The dissolved U concentrations are shown in Figure 4.3. Colloidal U oxides were not important in these systems, since the U concentrations in the <0.45 μm and < 10 kDa fractions were not significantly different in the field-moist (p = 0.10), open waterlogged (p = 0.13) or closed waterlogged (p = 0.11) microcosm.

In the field-moist soil microcosm, the concentration of dissolved U (Figure 4.3 A) correlated linearly with the % mass loss (r^2 = 0.96) (Figure 4.3 D). By day 510, approximately 0.03% (16 ± 1 mg L^{-1}) of the corroded U was in solution, following a 15 min extraction in degassed MQ water. The low percentage of soluble uranium reinforces the dominance of the particulate corrosion products observed. This small amount of U will be readily transported away from the vicinity of a corroding penetrator by percolating rainwater. Small colloidal U oxides were not important in this system, since the U concentrations in the <0.45 μm and <10 kDa fractions were not significantly different (p = 0.10). However, large particulate DU-oxides were observed and, in the environment, these large fragile particles would probably break down due to natural weathering processes.

By day 337, 0.36% and 0.37% of the DU had corroded in the open and closed waterlogged microcosms, respectively. This corresponded to a dissolved U concentration in the open waterlogged system of 0.12 ± 0.01 mg L^{-1} (< 0.01% of the corroded DU), with a pH of 5.7, Eh of 600 mV and NO_3^--reducing conditions. In the closed waterlogged systems, the dissolved U concentration was 1.02 ± 0.47 mg L^{-1} (<0.1% of the corroded DU), with a pH of 6.4, Eh of -65 mV and Fe(III)- and SO_4^{2-}-reducing conditions. Using the initial inorganic carbon concentrations, the geochemical model Hydra/Medusa suggests that the U will be predominantly in low solubility forms in both systems by day 337. In the open system, low solubility UO_2CO_3 would dominate, with some soluble species such as $UO_2(CO_3)_2^{2-}$ present. In contrast, the

reduced UO_2 species would dominate in the closed system, with minor amounts of soluble species such as $UO_2(CO_3)_2^{2-}$.

The soil and water analyses show that by day 510, essentially all the corroded DU was associated with the soil ($100 \pm 4\%$) rather than the DU coupon and $<0.1\%$ U was in the solution phase. This provides further evidence that under waterlogged conditions, corrosion occurs by the oxidation of DU metal to uranyl with subsequent dispersion into the environment.

4.3.7 Microbial Community Profile in Field-moist and Waterlogged Soils

The open field-moist and closed waterlogged soils were selected for RISA to identify the impact of DU on the microbial community. The RISA results (Figure 4.5) show fewer bands in the DU-amended microcosm than in the field-moist controls, indicating a change in the microbial community. This change occurred during marked changes in the biogeochemical environment, with depletion of NO_3^-, and ingrowth of Fe(III) into the soils, as well as the presence of DU corrosion products. Under waterlogged conditions, an extra band pattern appeared in the DU-amended microcosm that was not observed in the control, also indicating a shift in the bacterial community composition. These changes warranted further investigation by DNA profiling and phylogenetic analysis, which were undertaken on selected samples.

The phylogenetic results obtained from DNA profiling are shown in Figure 4.6. In the control field-moist soil, the clone library (55 clones analysed, 15 RFLP types) was made up of a large number of novel, uncharacterised microorganisms and dominated by species of the Gammaproteobacteria genus *Rhodanobacter* (representing 38% and 44% of the 16S rRNA genes detected in the clone library, respectively). However, in the clone library from the field-moist DU-amended microcosm (55 clones analysed, 20 RFLP types) the Gammaproteobacterial group was greatly reduced (consisting of 4% of

83

the clones affiliated to *Rhodanobacter* species) while Gram-positive Bacilli, many of which can denitrify, dominated the clone library (48% of clones). The Bacilli phylogenetic class have been reported to thrive in soil exposed to U_3O_8 (RINGELBERG et al., 2004) and at heavily contaminated U sites (POLLMANN et al., 2006; SELENSKA-POBELL et al., 1999). DU oxides (U_3O_8) have previously been shown to alter microbial community structures and reduced diversity (RINGELBERG et al., 2004), although reduced diversity was not shown in this study. The dominant organism detected in the DU impacted microbial community was closely related to *Sporosarcina Soli strain 180* (98% match over 925 bases), characterised as Bacilli phylogenetic class, aerobic and NO_3^--reducing microoganisms.
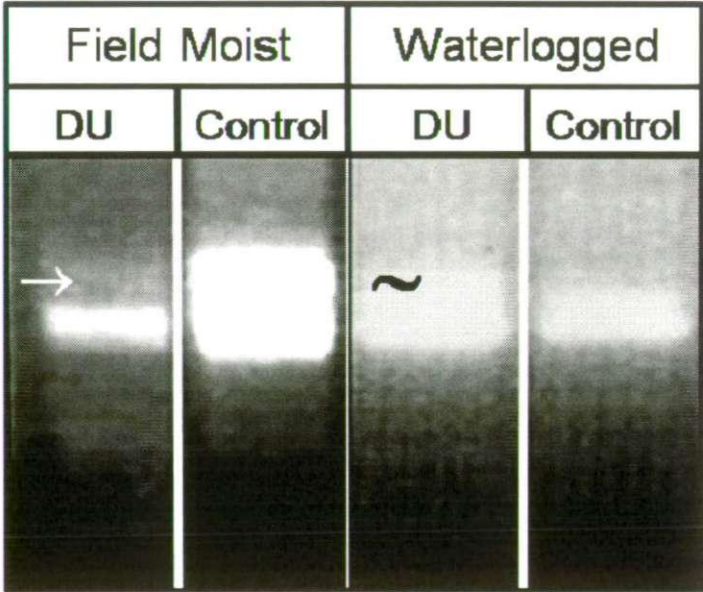
Figure 4.5 RISA results at day 435 on DU-amended field-moist (A) and progressively anoxic waterlogged microcosm, showing: missing bands ($\rightarrow$) in the DU-amended field-moist experiments and additional band ($\sim$) in the DU-amended closed waterlogged experiments.

In both the control and DU-amended waterlogged soils (Figure 4.6) the clone libraries were again dominated by a large number of novel uncharacterised microoganisms. In the DU-amended microcosm a loss in microbial diversity was suggested (24 compared to 31 RFLP types from 57 clones analysed from each soil); with the phylogenetic classes Alphaproteobacteria, Clostridia, Dehalococcoidete,

Nitrospiro and Sphingobacteria not detected in presence of DU. They were replaced by other organisms, including Gammaproteobacteria (12% of clone library) comprising mostly of an organism related to *Aquicella siphonis,* previously isolated from water samples in central Portugal (SANTOS et al., 2003).

The selection of different end-members of the community in both the field-moist and waterlogged soils, therefore, suggests either their resistance to toxic soluble uranium and/or particulate corrosion products, or adaptation to the chemical environment associated with the DU e.g. through changes in redox environment or even direct use of the DU itself as an electron donor.

(A) Control Field-moist Soil

(B) DU-amended Field-moist Soil

(C) Control Waterlogged Soil

(D) DU-amended Waterlogged Soil
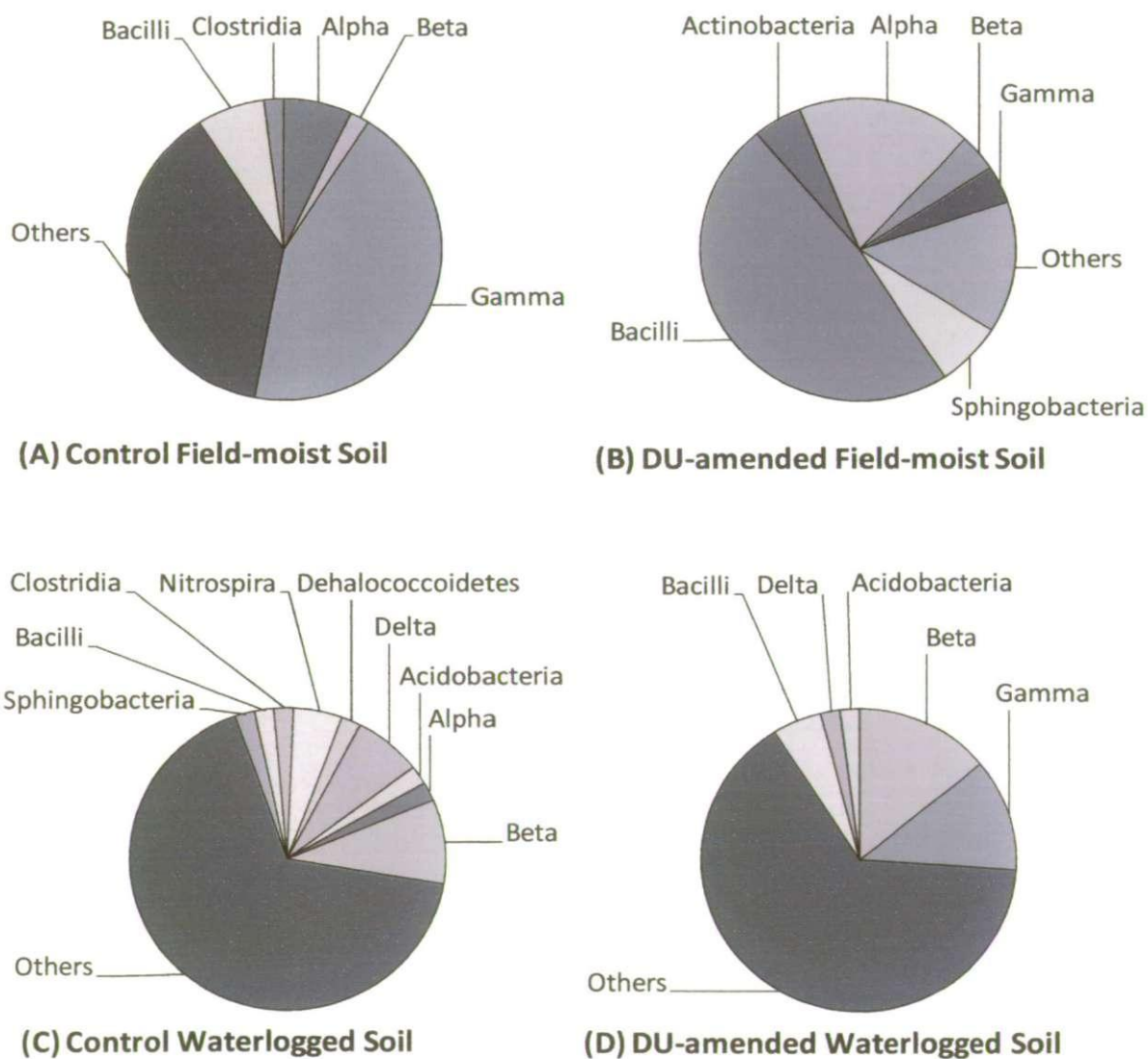
Figure 4.6 Phylogenetic affiliations of clones in field-moist (A-B) and the closed waterlogged (C-D) soils on day 435. Alpha, Beta and Gamma represent proteobacterial divisions.

4.4 Conclusions

The results from this study suggest that corrosion of DU penetrators fired into sub-surface soils is controlled by the biogeochemical conditions and the water status of the soil. Under oxic, field-moist conditions, the penetrator will corrode at approximately 0.49 ± 0.06 g cm^{-2} y^{-1}, with formation of a yellow metaschoepite product. These corrosion products are easily detached, and become dispersed heterogeneously in the soil. The generation of H$_2$ is hypothesised to drive changes in the local biogeochemical environment. Corroding DU also altered the microbial community composition significantly, with a shift to more DU-tolerant species. The dissolution of metaschoepite is likely to occur over a long time and U would then be transported away from the source in the soil solution.

Under waterlogged, NO$_3^-$-reducing conditions, the penetrator will corrode much more slowly at approximately 0.010 - 0.020 g cm^{-2} y^{-1}. Colloidal and particulate corrosion products are not an important source of DU entering the soil or aqueous phase under these conditions, and UO$_2$ oxidation to mobile UO$_2^{2+}$ species is the main mechanism for U release from the penetrator. However, the solubility of the UO$_2^{2+}$ species released from the DU will be highly dependent on the local Eh/pH conditions.

The corroding DU promoted reducing conditions and altered the microbial community composition significantly, with drastic loss in the microbial diversity and with at least one member of the microbial community that is able to adapt to the DU contamination. However once Fe(III) and SO$_4^{2-}$-reduction prevail, passivation of the penetrator surface organic occurred, slowing and preventing further corrosion.

Chapter 5

The Corrosion and Transport of Depleted Uranium Alloy in Sand Environments.

5.1 Introduction

The 1991 Gulf War alone resulted in the deposition of approximately 321 tonnes of DU into desert regions of Kuwait and Iraq. The test firing of DU weapons at military ranges has also resulted in the deposition of DU into a variety of sand-rich environments, such as the desert environment of the Yuma Proving Ground (FAN et al., 2005; JOHNSON et al., 2006) the dune sands of the QinetiQ Eskmeals range (TOQUE and BAKER, 2006) and the terrestrial and marine sediments of the Aberdeen Proving Ground (DONG et al., 2006; FAN et al., 2005). DU weapons have also been test fired into organic-rich, marine sediments of the Solway Firth (TOQUE and BAKER, 2007).

The fate and transport of DU in the environment is dependent on the corrosion products formed. DU readily corrodes to the U(IV) mineral uraninite (UO_2) (DONG et al., 2006; LAUE et al., 2004) which is highly immobile in the environment. Further oxidation to U(VI) is dependent on local redox and pH conditions (BAILEY et al., 2002), and results in to the formation of soluble species such as the uranyl ion (UO_2^{2+}), and/or U(VI) minerals.

The long term fate of DU-Ti alloy at the QinetiQ Eskmeals range has been investigated through *in situ* studies (TOQUE and BAKER, 2006). Loose uranium dioxide (UO_2) and schoepite ($UO_3.2H_2O$) corrosion products were observed with the reported corrosion rates of 0.080 - 0.17 g cm^{-2} y^{-1} (TOQUE and BAKER, 2006). A study from the Yuma Proving Ground, investigated the migration of U from corroding penetrators (BUCK et al., 2004; JOHNSON et al., 2004). Schoepite and metaschoepite were observed at 2 - 4 cm depth, while below 4 cm U was present as secondary U silicate species (BUCK et al., 2004; JOHNSON et al., 2004). Biogeochemical conditions have been shown to control DU corrosion in microcosm experiments containing undisturbed Solway Firth sediment and soil, with corrosion occurring under sub-oxic conditions and then ceasing under anoxic conditions due to passivation of the surface (see Chapter 3 & 4).

The transport of DU through the environment depends on the solubility of the corrosion products that form and the movement of particles. Column experiments can be used to quantify the movement of dissolved species through a homogenous porous medium, and this migration can then be modelled using codes such as k1D to generate kinetic data describing the interactions of the species with the solid phase (BRYAN et al., 2005; SCHÜßLER et al., 2001; WARWICK et al., 2000).

The large mass of DU fired into sand environments and the lack of clean up plans means that understanding the corrosion, transport and fate of the DU is important in terms of environmental contamination and human exposure. The hypotheses that the rates of DU corrosion, and the corrosion products formed, are dependent on the local biogeochemical conditions have held true (see Chapter 3 & 4). Therefore, laboratory microcosm and column experiments have been used to investigate the mechanisms and rates of DU corrosion and the transport of DU corrosion products in dune sand, modelling terrestrial and marine sand environments. The aims of these experiments were to investigate: (1) the corrosion of DU within oxic sand environments; (2) the dissolved and particulate products of the corrosion processes, and (3) the transport of DU corrosion products within a subsurface environment.

5.2 Experimental Section

5.2.1 Sampling and Characterisation

A terrestrial dune sand was sampled from Drigg Sands in Cumbria. Sub-samples of the sand were dried to determine the water content and the size distribution of the dried < 2 mm sand fraction. The organic carbon, inorganic carbon, cation exchange capacity and bulk chemical composition were determined. Seawater was sampled from Plymouth

Sound and the salinity, pH, inorganic carbon and anion concentrations determined. All methods were carried out as described in Section 2.3.

5.2.2 Microcosm Experiments

Experiments were designed to investigate the corrosion of DU within sand-rich environments. The dune sand was used in its field-moist state and with seawater to give two distinct environments, denoted here as field-moist and marine waterlogged. All experimental microcosm were prepared on the same day (n = 60) as described in Section 2.3.3. At selected intervals over a period of 510 days, microcosms were sacrificed in triplicate, along with three controls inside an anaerobic chamber (Section 2.3.4). The DU coupons, solution and sediment were then prepared for further analysis as described below; all errors stated are one standard deviation of three replicates.

5.2.3 Geochemical Methods

The oxygen content, pH and Eh of the solution phase were determined using calibrated electrochemical probes and a bench meter within the anaerobic chamber, using a sub-sample from each microcosm. The redox indicators, SO_4^{2-} and NO_3^-, were quantified by ion chromatography. Microbially-produced Fe(II) was extracted from the sediments and determined using the ferrozine method (STOOKEY, 1980). The uranium in the liquid phase was quantified by ICP-MS in two fractions, the colloidal + dissolved (< 0.45 μm) and the dissolved (< 10 kDa) and the geochemical speciation of uranium was modelled using experimental inorganic carbon, Eh and pH measurements. All methods were carried out as described in Section 2.4.

5.2.4 DU Coupon Analysis

The DU coupons were retrieved and rinsed to remove sand, air dried and stored in a desiccator to prevent further corrosion. Coupons were photographed and analysed by SEM-EDAX. The corrosion products were removed within 1 month to calculate the percentage mass loss. All methods were carried out as described in Section 2.6.

5.2.5 Sand DU Distribution and Particle Analysis

The distribution of radioactivity in the sand from the field-moist (day 332) and marine waterlogged (day 371) microcosm were determined using Phosphor Imaging Analysis. Areas of enhanced radioactivity or "hot" particles were subsequently isolated and analysed by Environmental SEM-EDAX. Particles from the field-moist sand contained enough uranium and were sufficiently crystalline to allow further analysis by XRD. All analyses were carried out as described in Section 2.7.

5.2.6 Transport Experiments

The discrete corrosion products formed in the field-moist system (metaschoepite $[(UO_2)_8O_2(OH)_{12}.(H_2O)_{10}]$) were suitable for inclusion in transport experiments. Synthetic rainwater was used as the mobile phase, to simulate the effect of rainfall on the dissolution and transport of the metaschoepite formed under field-moist conditions. Columns were prepared as described in Section 2.8.1. All calculations were performed using the k1-D coupled chemical transport code using 30 subdivisions of the column in the simulations. Two columns were prepared to investigate the oxic transport behaviour of aqueous UO_2^{2+} and DU corrosion products separately, and both were characterised physically using a conservative Br⁻ tracer. The eluent profiles from the columns were

used to define the k1D model parameters as shown in Table 5.1.

5.2.7 Transport of Uranium (UO_2^{2+})

The uranyl column was used to define the transport behaviour of dissolved uranyl and identify the kinetics of its interactions with the sand matrix. A U solution (1000 mg L^{-1}) was injected (50 µl) into the column. Eluent was collected continuously in 4 h fractions over 32 days for detailed transport data of the breakthrough curve and tail. Samples were prepared and analysed as described in Section 2.8.2. After the column experiment was complete, a tracer of KBr (2000 mg L^{-1}) was injected onto the column and analysed as described in Section 2.8.2.

5.2.8 Transport of DU Corrosion Product (Metaschoepite)

A column was prepared as described in Section 2.8.3, containing 50.8 mg of metaschoepite corrosion product. Fractions were collected from the sand column every 8 h over 98 days and prepared and analysed as described in Section 2.8.2 for detailed transport data of the breakthrough curve and tail. After the column experiment was complete, a tracer of KBr (2000 mg L^{-1}) was injected into the column, fractions were collected every 1 h and analysed as in Section 2.8.2. After the Br$^-$ tracer experiment was completed the column was opened and the sand was digested with nitric acid and analysed for U as described in Section 2.8.3.

Table 5.1 Parameters defined in the k1D transport code.

Parameter	Definition	Parameters defined from
Porosity	Measure of the void spaces in a packing material	The elution time of the Br⁻ peak
Dispersivity (m)	Spreading of a pulse due to different flow paths	The width of the Br⁻ peak
U input (mol L^{-1})		Known for the uranyl column; only variable parameter for the DU column, thus calculated by a process of iteration.
K_d	Ratio of contaminant associated with the solid and liquid phase at equilibrium	The modelled fit to initial U elution peak
Sorption kinetics	Kinetics of movement into and from non-exchangeable chemical fractions of the sand	A number of kinetic reactions can be added to define regions of the tail of the U elution peak.
Flow rate (mL h^{-1})	Measured flow rate	Calculated experimentally
Column dimensions (m)		Known
Column subdivisions	Sections within the column length	The transport of U defined at fixed subdivisions of the column. Thirty subdivisions were used

5.3 Results and Discussion - Microcosm Experiments

5.3.1 Biogeochemistry of the Microcosm

The field-moist sand was 13 % (w/w) water, 0.8 ± 0.1% by mass organic carbon, and had a particle size distribution of 98 % sand and 2% silt, cation exchange capacity of 1.3 ± 0.1 meq/100 g and an inorganic carbon content of 430 ± 30 mg kg^{-1}. Manganese and iron oxides comprised 0.02 % (m/m) and 1.4 % (m/m) of the sediment, respectively. The seawater was characterised as pH 8.0, salinity of 31.5 with an inorganic carbon content of 72 ± 1 mg L^{-1}, prior to mixing with the sediment. The anion concentrations (mg L^{-1}) in the sea water were: chloride 21000 ± 100, nitrate 92 ± 1; and sulfate 3100 ± 20.

In the field-moist microcosm and controls, the pH and Eh stayed fairly constant over the 510 day experimental period, from pH 7.2 - 7.5, and the Eh fluctuated between 570 - 610 mV. When comparing the control and DU-amended microcosm, differences were observed in the concentrations of the TEAs over time (Figure 5.1 A - C). In the control microcosm, the TEAs were not reduced over the experimental period, suggesting that oxic conditions were maintained. This is consistent with the visible air-filled macro-pores in the sand structure. However, in the DU-amended experiments depletion of NO$_3^-$ was observed from day 108 (220 ± 5 mg L^{-1}) to day 510 (19 ± 6 mg L^{-1}) and Fe(III)-reduction indicated by the depletion in Fe(III) was observed from day 332 to day 510 (0.22 ± 0.09 mg kg^{-1}). Sulfate-reduction was not observed in the controls or DU-amended microcosm. Overall, the presence of corroding DU resulted in the development of reducing conditions. This reduction of redox indicators has been observed in oxic field-moist soils (Chapter 4) and was attributed to abiotic reduction of redox indicators by the H$_2$ produced during DU corrosion. In the field-moist sand environment by 332 days, typically, 1.5 × 10^{-3} moles of U had oxidised to UO$_2$ in each

microcosm, potentially releasing 3.1×10^{-3} moles of H_2. This H_2 is sufficient to reduce 100 % of the total NO_3^- (7.3×10^{-5} moles) and bioavailable $Fe(III)$ (3.4×10^{-9} moles) abiotically.

In the marine waterlogged microcosm the pH and Eh changed slightly over the 510 day experimental period, the pH increased from 7.6 - 7.9 and the Eh decreased from 600 - 450 mV. Comparing the control and DU-amended microcosm, differences were observed in the concentrations of NO_3^- after day 371, with depletion of NO_3^- in the microcosm but not in the controls. No ingrowth of $Fe(II)$ into the sand was observed or SO_4^{2-}- reduction over the duration of the experiment. In the waterlogged marine sand environment by 500 days, typically, 4.3×10^{-4} moles of U had oxidised to UO_2 in each microcosm, potentially releasing 8.5×10^{-4} moles of H_2. This H_2 is sufficient to reduce 100 % of the total NO_3^- (7.3×10^{-5} moles) abiotically.
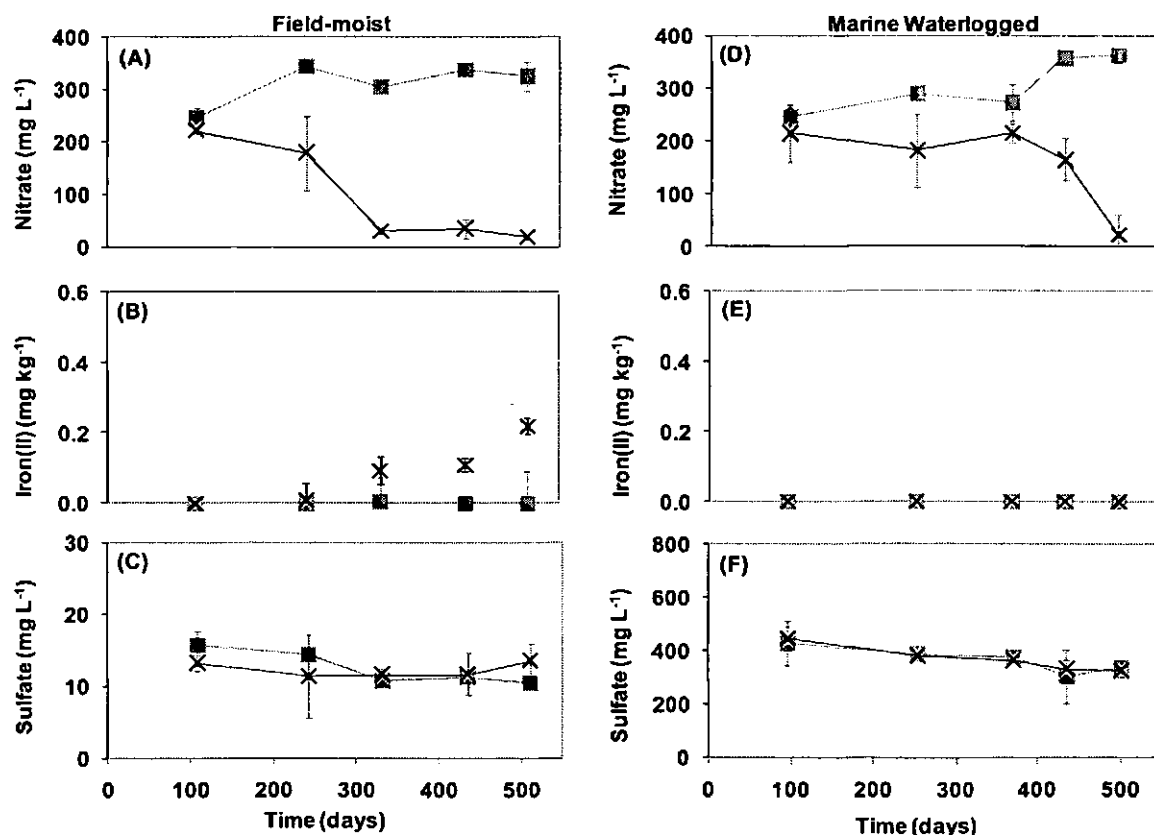
Figure 5.1 Biogeochemical time series data for DU-amended (x) and control (■) microcosm under field-moist (A - C) and marine waterlogged (D - F) conditions. Showing: nitrate concentrations (A & D), acid extractable Fe(II) (B & E) and sulfate concentrations (C & F) over time. Error bars show ± 1 s.d (n = 3).

5.3.2 Corrosion of DU Coupons in Field-moist and Waterlogged Sand

Coupons retrieved from the field-moist microcosm on day 108 and 242 are shown in Figure 5.2 A & B, respectively. The coupons showed localised pitting and cracking of the metal surface with some yellow product present by day 108, however by day 242 the coupon was covered with protruding, predominately yellow corrosion products; the coupon also had some black corrosion products. The corrosion of DU as indicated by % mass loss (Figure 5.3 A) increased linearly (r^2 = 0.98) over the duration of the experiment from 0.49 % on day 108 to 8.3 % on day 510. The intercept suggests that corrosion began after 88 days, highlighting a latent period prior to the onset of corrosion. Longer latent periods of 240 days (Chapter 4) have been observed previously for DU corrosion in soil.

DU coupons retrieved from the marine waterlogged microcosm on days 90 and 253 are shown in Figure 5.2 C & D, respectively. On day 90 the coupon showed small area of etched surface corrosion, however by day 253 deep localised pits developed on the surface of the alloy. The corrosion of DU as indicated by % mass loss (Figure 5.3 B) also increased linearly (r^2 = 0.98) over the duration of the experiment from 0.2 % on day 96 to 1.4 % on day 500. The intercept suggests that corrosion began after 11 days, suggesting a minimal latent period prior to the onset of corrosion, possibly due to the corrosive action of Cl⁻ on DU (TRZASKOMA, 1982).
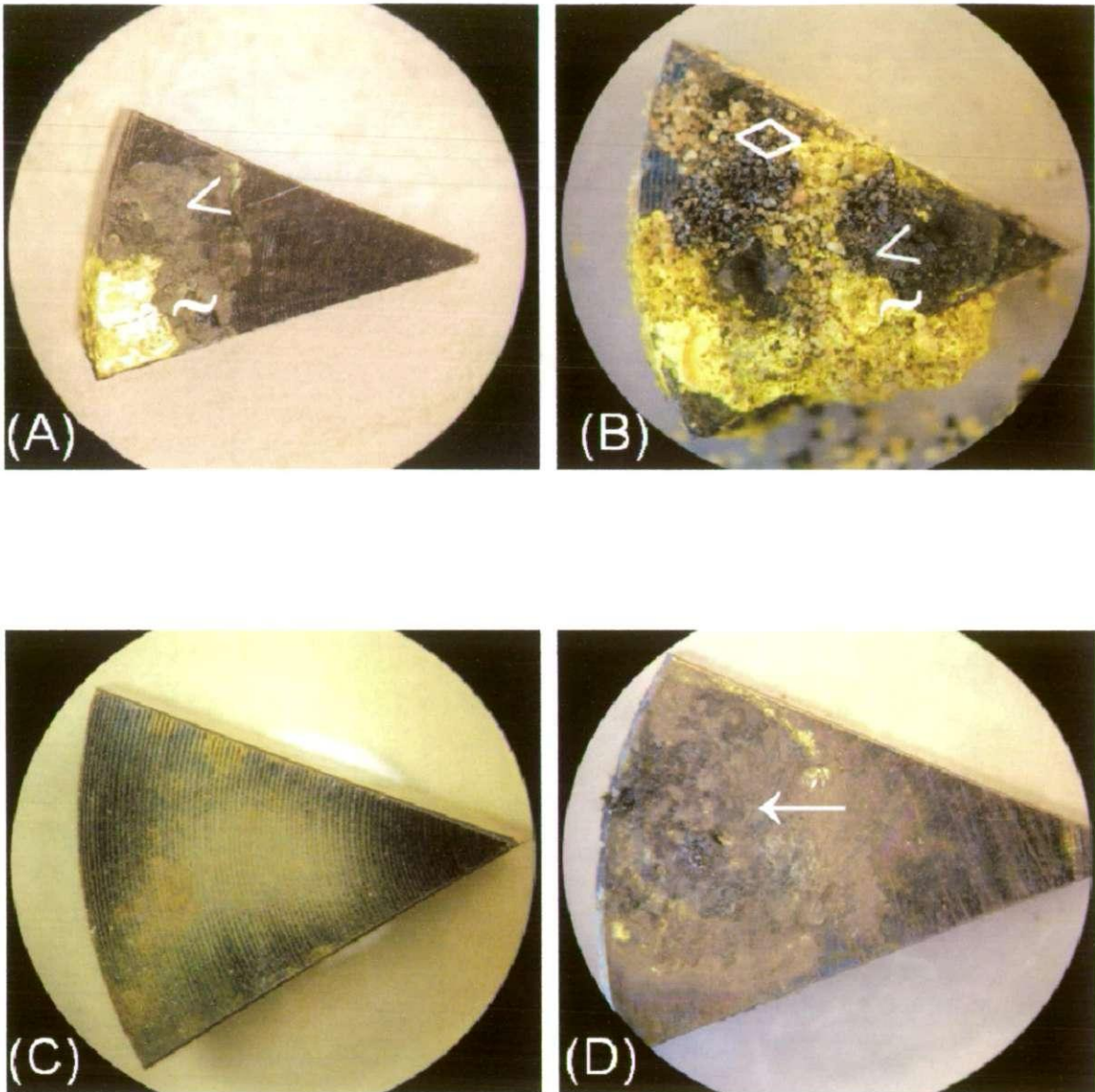
Figure 5.2 Colour photographs of DU coupons retrieved from field-moist and marine waterlogged microcosm. (A-B) show field-moist coupons from days 108 and 242, respectively and (C-D) show marine waterlogged coupon on days 90 and 253, respectively. Showing highlighted (~) areas of yellow and (<) black corrosion products, (◊) adhesive sand particles and (→) pitting corrosion.

The corrosion rates ($g \ cm^{-2} \ y^{-1}$) were calculated (see Equation 2.2; Section 2.6). Corrosion in the field-moist microcosm proceeded at a rate of $0.10 \pm 0.01 \ g \ cm^{-2} \ y^{-1}$. This rate falls within the range observed *in situ* at the Qinetic Eskmeals site of 0.08 - $0.17 \ g \ cm^{-2} \ y^{-1}$ (TOQUE and BAKER, 2006). Interestingly, the rate of DU corrosion is 5 times slower in this sand than in the field-moist soil used in Chapter 4 ($0.49 \pm 0.06 \ g \ cm^{-2} \ y^{-1}$). Parameters such as pH, moisture content, CEC and organic matter contribute to the corrosivity of an environment (MATTSSON, 1989) and the sand used in this study

had a less acidic pH (pH 7.4 vs. 5.5), lower moisture content (13 vs. 22 %), lower CEC

(1.3 vs. 21 meq/100 g) and a lower organic carbon content (0.8 vs. 12 %) than the soil

used in Chapter 4. The biogeochemical conditions are also a controlling factor in DU

corrosion (Chapter 3 & 4); however here and in Chapter 4 the field-moist matrices were

porous and allowed gaseous exchange, thus the reduction of redox markers was

attributed to the corroding DU rather than exhaustion of oxygen in the system through

microbially-driven redox processes.
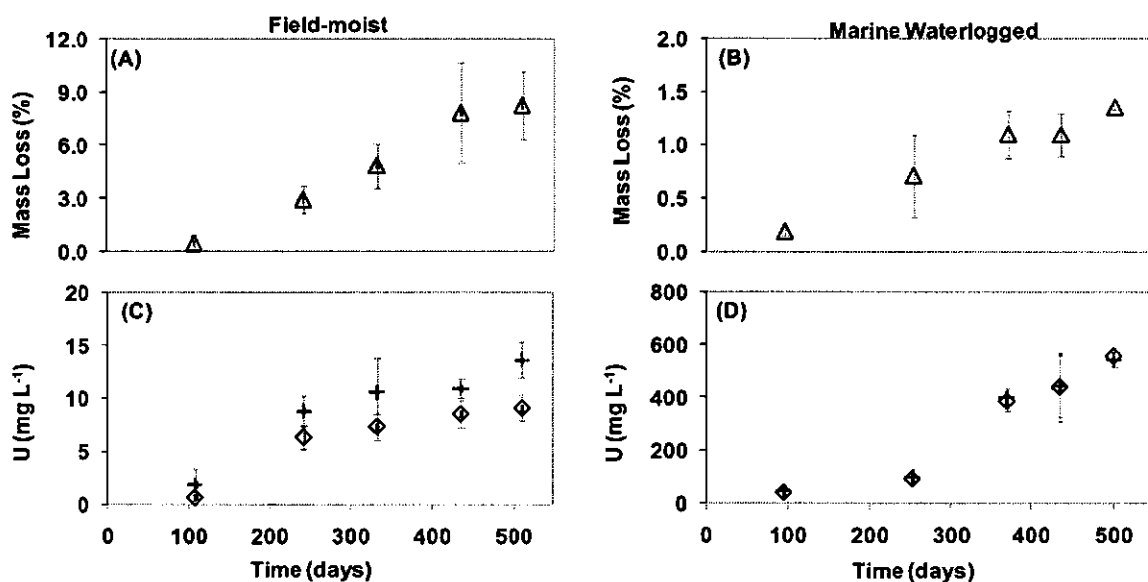
Figure 5.3 Time series data for DU corrosion in the field-moist (A & C) and the marine waterlogged (B & D) microcosm. Figures A & B show mass loss (%) of corroded DU from coupon (Δ) and figures C & D show changes in < 0.45 μm (+) and < 10 kDa (◊) U in the water. Error bars show ± 1s.d (n=3).

The corrosion rate of DU in the waterlogged marine microcosm was $0.020 \pm$

0.003 g cm^{-2} y^{-1}, which is an order of magnitude lower than the corrosion rate of 0.40 g

cm^{-2} y^{-1} (TRZASKOMA, 1982) observed for DU corrosion in NaCl solution of comparable

Cl$^-$ concentration. All factors that increase the corrosivity of an environment would be

enhanced in the marine sand vs a NaCl solution, with the exception of pH, which is less

acidic in the marine microcosm (pH ~ 7.8 vs pH ~ 5.5). This could indicate that pH is a

major control on corrosion rate. The corrosion rate of DU in the waterlogged marine microcosm is also lower than the sub-oxic corrosion rate of 0.056 ± 0.006 g cm^{-2} y^{-1} found in organic- rich sediments of the Solway Firth. The sand used in this study had a less acidic pH range (pH 7.6 - 7.9 vs. 6.4 - 8.0), lower cation exchange capacity (1.3 vs. 4.0 meq/100 g) and a lower organic carbon content (0.80 vs. 3.2) than the organic-rich sediments. Therefore the data strongly suggest that these sand/sediment properties are important and that corrosion rates based on dissolution in simple solutions are not sufficient to predict the fate of DU in the environment. Corrosion of DU in the Solway Firth sediments was observed during NO_3^--reduction (Chapter 3) and the intermediates of NO_3^--reduction (NO_2^-, N_2O, and NO) are known to oxidise UO_2 to the more mobile U(VI) (SENKO et al., 2002; 2005), potentially enhancing the corrosion process. However as conditions became anoxic in the Solway Firth sediments, the corrosion of DU ceased, thus the overall corrosion of DU is more stable in a low-organic system and will continue over longer timescales, as seen by the linear ($r^2 = 0.98$) rate of corrosion (Figure 5.3 B).

The corrosion rate (g cm^{-2} y^{-1}), mass and the mean surface area of a penetrator during corrosion were used to estimate the total corrosion time for a complete penetrator (see Equation 2.3; Section 2.6). Under field-moist sand conditions the total corrosion time for a penetrator was calculated to be between 250 - 350 years. Under marine waterlogged conditions the total corrosion time for a penetrator was calculated to be between 1300 - 1800 years.

5.3.3 Solution Phase Uranium

The dissolved U concentrations in the microcosm are shown in Figure 5.3 C-D. Colloidal U is important in the field-moist systems, since the U concentrations in the

<0.45 μm and < 10 kDa fractions are significantly different (p = 0.0036), and colloids comprise 33 % of the < 0.45 μm fraction on day 510. The concentration of < 0.45 μm U (Figure 5.3 C) correlated linearly with the % mass loss (r^2 = 0.94) (Figure 5.3 A), and on day 510, this fraction was 0.03 % of the total corroded DU. The low percentage of soluble U indicates the dominance of particulate corrosion products, however the soluble U would be present as mobile uranyl carbonates, such as $UO_2(CO_3)_2^{2-}$ under the measured conditions (pH 7.4, Eh +600 mV, inorganic carbon 430 ± 30 mg kg^{-1}).

In the waterlogged sea microcosm colloidal U not important (p = 0.17). On day 510, the dissolved U concentration was 550 ± 30 mg L^{-1} (8.1 % of the total corroded DU). The geochemical model Hydra/Medusa suggests that U would be present predominately as the soluble uranyl carbonates, such as $UO_2(CO_3)_3^{4-}$ under the measured conditions (pH of 7.7, Eh +600 mV, inorganic carbon 430 ± 30 mg L^{-1}).

5.3.4 Analysis of DU Particles from the Field-moist and Waterlogged Soils

The field-moist sand had a heterogeneous distribution of bright yellow corrosion products which correlated with intense radioactive hot spots on the Phosphor image. The corrosion products were partially covered in sand, but suitable for XRD analysis. XRD evidence suggested the presence of schoepite or a similar phase, as has previously been reported in surface and sub-surface soils (BUCK et al., 2004; TOQUE and BAKER, 2006) (Chapter 4). A representative ESEM image and EDAX spectrum of representative particle is shown in Figure 5.4 A - B, respectively. The ESEM image of a particle shows desiccation cracks, which is indicative of a dehydrated metaschoepite phase (BUCK et al., 2004). The ESEM-EDAX spectrum shows major peaks from U and O alongside minor peaks from elements (Si, C & Fe) commonly found in sand and also Ti, an element used in alloying DU.

Phosphor Imaging showed that the marine waterlogged sand also had a heterogeneous distribution, but with less intense radioactive hotspots. A representative ESEM image of the selected particles is shown with the EDAX spectrum in Figure 5.4 C - D. The spectra shows major peaks from U alongside peaks from elements (Si, Fe, Mg, Al, and C) commonly found in sands. These results indicate that the DU is present in the sand as sorbed ions, rather than as discrete oxidised corrosion products.

The corrosion products formed here are similar to those reported in Chapter 4. Under field-moist conditions predominately yellow metaschoepite was formed, whereas under waterlogged conditions there is sorption of uranyl to the soil/sand matrix. Therefore, saturation of a matrix has a significant effect on the mechanism of DU corrosion.
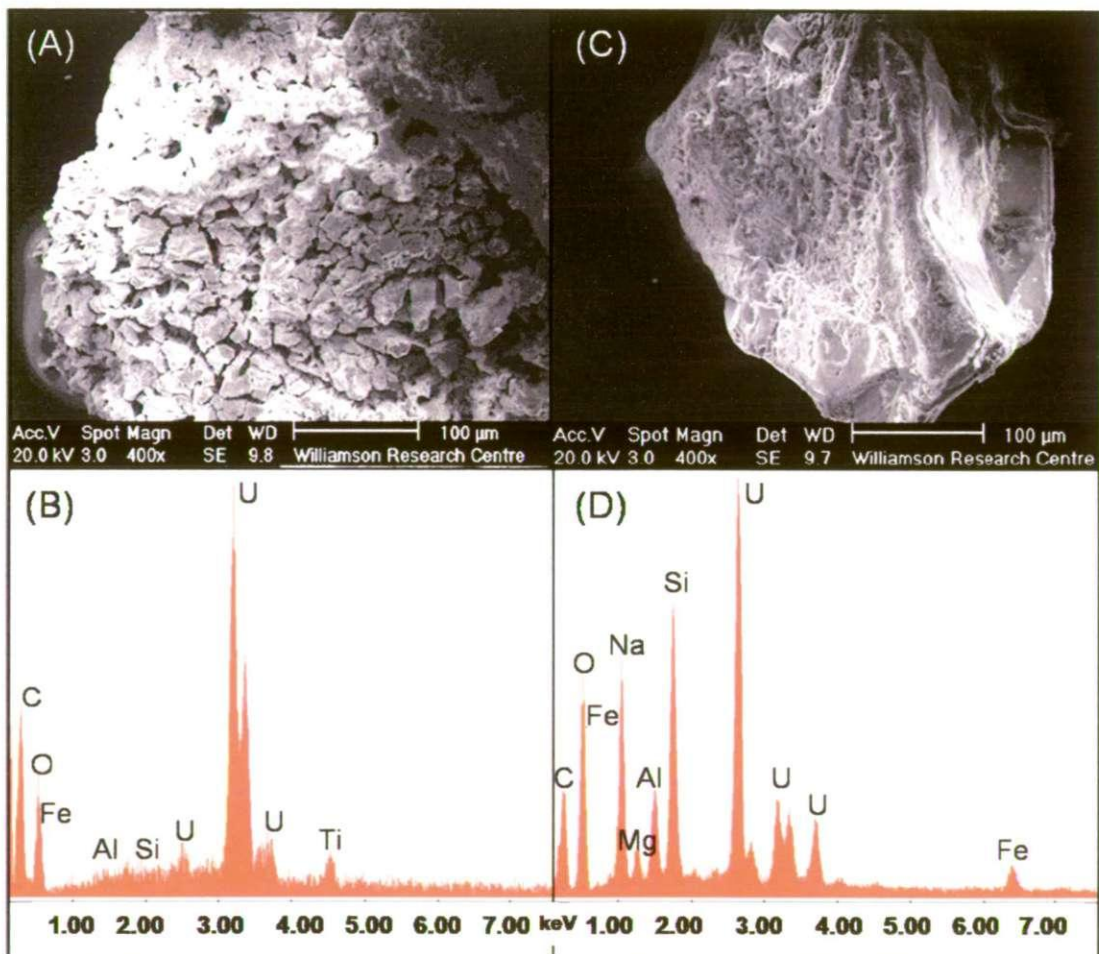
Figure 5.4 Representative backscattered electron image and SEM-EDAX spectrum of U-rich particles isolated from the field-moist (A - B) and marine waterlogged (C - D) marine waterlogged microcosm.

101

5.4 Results and Discussion - Transport Modelling

5.4.1 Column Characterisation

Columns used in the transport modelling were characterised using a bromide conservative tracer. Figure 5.5 shows the bromide elution data and the model fit; the porosities for the uranyl and DU columns were 0.54 and 0.53, respectively, and the dispersivities were 3×10^{-4} and 1×10^{-4} m. The agreement between the porosities indicates consistent column packing and the variation in dispersivity is in the range that would be expected for two similar but separately prepared porous columns (N Bryan [Manchester University] 2008, pers comm., 18-20 August). The linear flow velocity through the column was calculated to be 19.04 m y^{-1} and the time taken for the elution of the bromide peak (residence time) was 23 h. In all experiments the synthetic rainwater was buffered by the sand from pH 5.5 to pH 7.4.
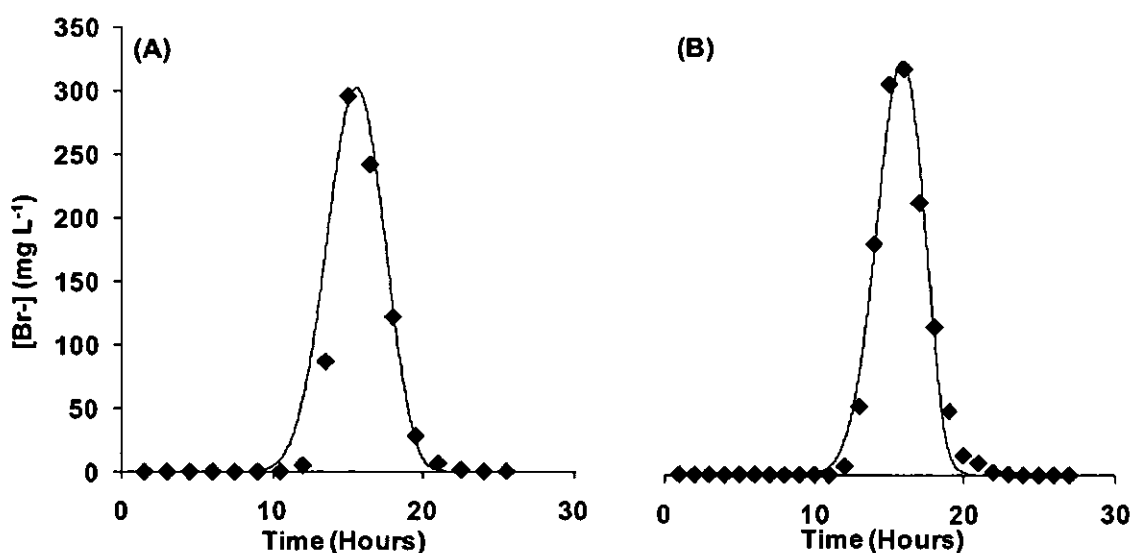
Figure 5.5 Time elution data for the transport of the bromide tracers in the (A) uranyl and (B) DU columns, showing the experimental ($\blacklozenge$) and modelled (—) data.

5.4.2 UO_2^{2+} Transport Modelling

The chemical reactions associated with the transport of uranyl species in the column were defined by modelling the uranyl column. The uranyl column was run for 32 days and the total eluant volume was 108 mL which is equivalent to 62 void column volumes and 192 samples. The experimental data for this U column are shown in Figure 5.6 along with the model fit. The U shows non-conservative behaviour on the column; the initial peak is retarded with respect to that of the conservative tracer (Fig 5.5 A), and there is a long elution tail.

Figure 5.6 Time elution data for the uranyl column, showing the experimental (•) and modelled (—) data. Column run for 32 days and 192 samples.
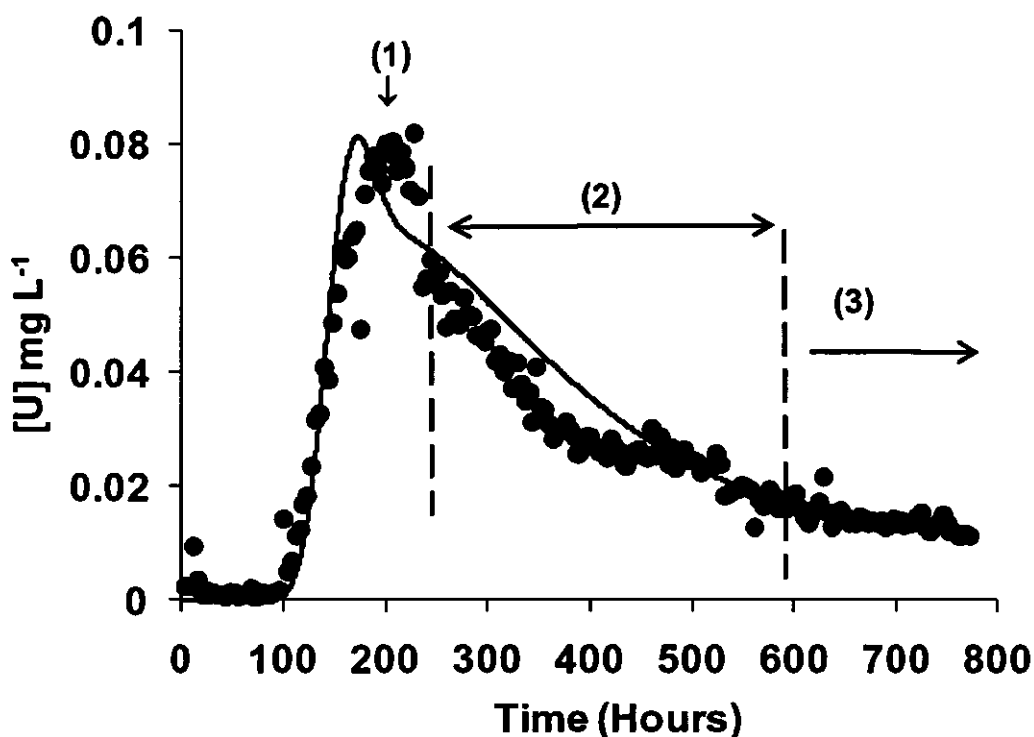
Three chemical interactions were required to produce a reasonable visual fit for the U data and these are illustrated in Figure 5.7. There is an initial rapid interaction

103

(Region 1) of the solution phase U [$U_{solution}$] with the sediment surface to produce an exchangeable sorbed U [$U_{Sorbed-exch}$], which may desorb instantaneously from the surface in order to maintain equilibrium with the solution phase U. This interaction has been defined by an equilibrium, K_d approach with a best fit value of 10.2.

The tail on the main elution peak (Regions 2 & 3) is the result of further chemical processes involving slow (kinetic) reactions. The changes in the concentrations of these fractions with time are described by two kinetic equations. For [$U_{Sorbed-slow1}$] (Equation 5.1), k_{f1} and k_{b1} are first order rate constants, which both have best fit values of 4.0 x 10^{-6} s^{-1}. For [$U_{Sorbed-slow2}$] (Equation 5.2), k_{f2} and k_{b2} are first order rate constants, which have best fit values of 5.5 x 10^{-6} and 5.0 x 10^{-8} s^{-1}, respectively.

$$\frac{d[U_{Sorbed-slow1}]}{dt} = k_{f1}[U_{Sorbed-exch}] - K_{b1}[U_{Sorbed-slow1}] \quad [5.1]$$

$$\frac{d[U_{Sorbed-slow2}]}{dt} = k_{f2}[U_{Sorbed-exch}] - K_{b2}[U_{Sorbed-slow1}] \quad [5.2]$$

Although the rate constants (k_{f1} and k_{f2}) for entry to these two fractions are similar, the dissociation constants (k_{b1} and k_{b2}) are quite different. Hence, the first [$U_{Sorbed-slow1}$] kinetic reaction is responsible for the first section of the tail (Figure 5.6, Region 2), whilst the second [$U_{Sorbed-slow2}$] kinetic reaction is responsible for the continuing tail at very long elution times (Figure 5.6, Region 3). At the end of the experiment (32 days) only a fraction of the U input (2.9 %) had been eluted, which is consistent with slow desorption causing the majority of U to be trapped within the column. In fact the model predicts the following distribution of the uranium on the column at the end of the experiment: $U_{solution}$ = 0.080 %, $U_{Sorbed-exch}$ = 0.81 %, $U_{Sorbed-slow1}$ = 0.88 % and $U_{Sorbed-slow2}$ = 98 %.
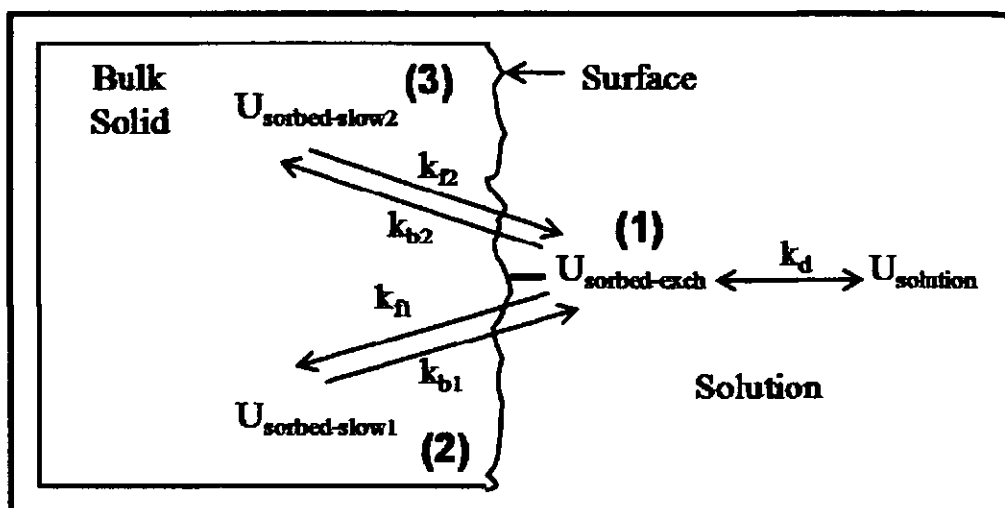
Figure 5.7 Schematic showing the chemical processes included in the transport modelling (equations are given in the text). All terms are defined in the text: ↔ represents equilibrium (instantaneous), and ⇌ kinetic (slow) reactions.

5.4.3 Corrosion Product (Metaschoepite) Transport Modelling

The reactions and associated parameters from the uranyl column were used to interpret the results for the DU column (Figure 5.8). The DU column was run for 98 days and the total eluent volume was 330 mL which is equivalent to 191 void column volumes and 194 samples. Firstly an iterative process was used to define the concentration of solution phase U [$U_{solution}$] produced by the dissolution of metaschoepite as a function of flow volume (Figure 5.9). The data show two phases of dissolution, an initial high concentration followed by a decrease, probably due to the rapid dissolution of a readily soluble fraction or hydrated species, and a later, long-term increase. These are apparent in regions A and B, respectively in Figure 5.8. In total, 15 mg of the metaschoepite was calculated to dissolve, and only 1.19 mg (8 %) of this eluted through the column by 98 days. Therefore, although a significant fraction of the metaschoepite has dissolved, the vast majority of the U is still trapped within the column. In fact the model predicts the following distribution of the uranium released from the metaschoepite at the end of the experiment: $U_{solution}$ = 0.40 %, $U_{Sorbed-exch}$ = 3.8 %, $U_{Sorbed-slow1}$ = 3.6 % and $U_{Sorbed-slow2}$ =

92 %. Column experiments have showed that the majority of dissolved U is held in a chemical fraction with very slow desorption kinetics and it is this behaviour that will dominate U transport in the environment. When modelling the transport of mobile DU species the tail in Region 3 (Figure 5.8) which was derived from constants controlling the $U_{Sorbed-slow2}$ had a particularly good fit. This modelling will therefore give a high level of confidence when making predictions for real environmental systems as it is it is this behaviour that will dominate U transport in the environment. The later increase in eluted U (Figure 5.8, Region B) from the dissolution of the metaschoepite, will eventually decrease once the metaschoepite source is exhausted.
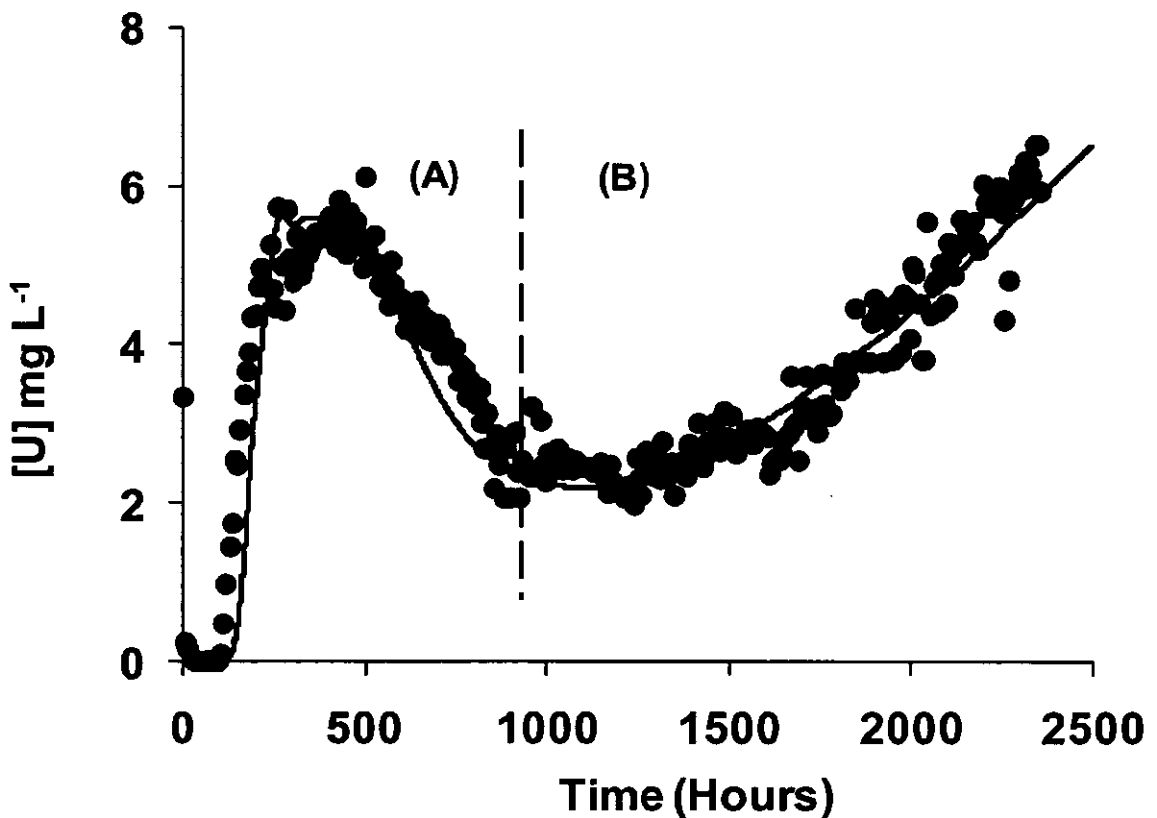
Figure 5.8 Elution data for the metaschoepite column, showing the experimental (•) and modelled (—) data.
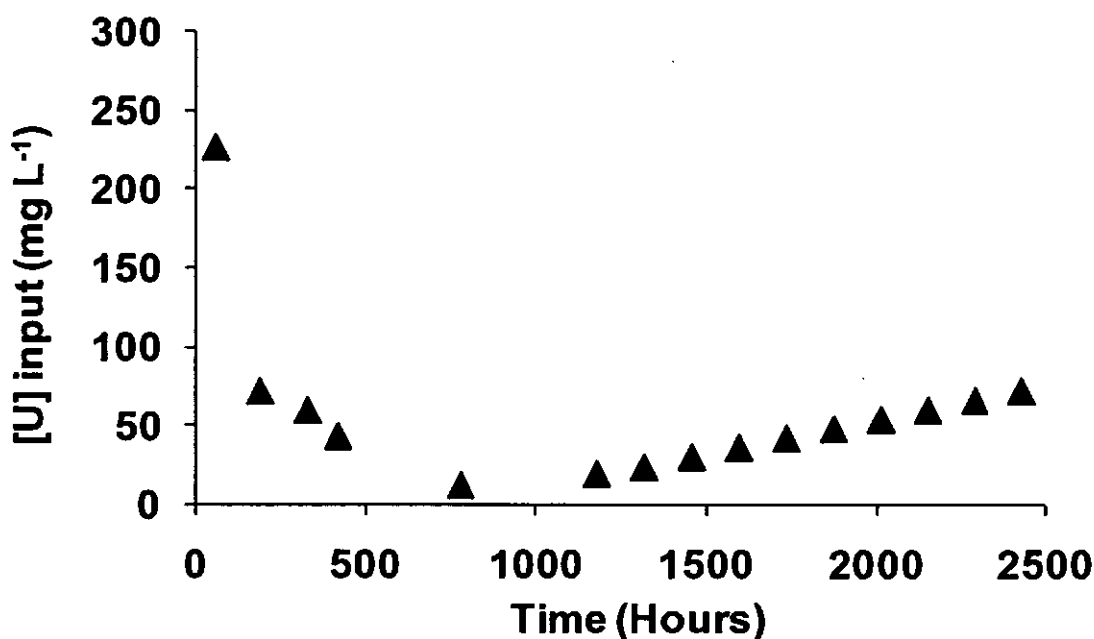
Figure 5.9 Variation in the solution phase U input to the DU column from the dissolution of metaschoepite.

To investigate the movement of DU further, the column was digested and analysed in 10 length fractions (Table 5.2). Most (88 %) of the DU was extracted from the first fraction (0 - 0.41 cm); however 10 % of the DU was extracted from the next three fractions (0.14 - 1.69 cm). The mass of U in the 0.14 - 1.69 cm region is not in excess of the predicted dissolution of the metaschoepite, however, there may be a contribution from migrating small particles or colloids. Colloids were seen to be important in the field-moist microcosm experiments, where colloids comprise 33 % of the < 0.45 μm fraction on day 510 (Figure 5.3 C); and the migration of metaschoepite and schoepite DU particles has previously been observed at depths of up to 4 cm in a sandy loam soils (BUCK et al., 2004; JOHNSON et al., 2004). In the 4.28 - 5.00 cm fraction, the DU concentration decreased to 5.0 ± 0.3 mg kg^{-1} which was comparable to the background sand U concentration of 5.2 ± 0.3 mg kg^{-1}.

107

Table 5.2 Results of the DU column digest, showing the transport of DU through the column. Error bars show ± 5% ICP-MS instrumental error.

Sand Fraction (g)	Column Fraction (cm)	U Concentration (mg kg⁻¹)	% U Fractions
0.41	0.00 - 0.41	6800 ± 400	87.4
0.24	0.41 - 0.65	240 ± 1	3.09
0.51	0.65 -1.16	310 ± 2	3.99
0.52	1.16- 1.69	280 ± 10	3.60
0.50	1.69 - 2.19	50 ± 3	0.643
0.55	2.19 - 2.74	29 ± 1	0.373
0.60	2.74 - 3.34	21 ± 1	0.270
0.59	3.34 - 3.92	22 ± 1	0.283
0.36	3.92 - 4.28	21 ± 1	0.270
0.72	4.28 - 5.00	5.0 ± 0.3	0.0643

5.4 Conclusions - Environmental Implications

The results of this study strengthen earlier hypotheses that the rates of DU corrosion and the corrosion products formed are dependent on the water content and geochemistry of the environment. In field-moist sand, penetrators will corrode at a rate of 0.10 ± 0.01 g cm^{-2} y^{-1}, predominately with the formation of yellow metaschoepite. The transport of this corrosion product, following rainfall, is dependent on its dissolution and subsequent interactions with the sand. Column experiments showed that the majority of dissolved U is held in a chemical fraction with very slow desorption kinetics and it is this behaviour that will dominate U transport in the environment. The concentrations of U eluting from the metaschoepite column were orders of magnitude higher than the World Health Organisation's recommended maximum admissible concentration for U in drinking

water of 15 µg L^{-1} (WHO, 2005), and were increasing at the end of the experiment. Therefore a high level of U contamination is predicted in proximity to a corroding penetrator.

In the low organic marine sand, penetrators corrode via pitting at the rate of 0.020 ± 0.003 g cm^{-2} y^{-1}. The rate of corrosion was significantly lower than observed in other experiments with similar salinity, showing the importance of the solid properties and geochemical conditions on DU corrosion. The rate of corrosion was linear due to corrosion occurring in an oxygenated environment. The main mechanism for U release from the penetrator is oxidation of UO_2 to U(VI) and its dispersion as uranyl species. This dissolved U will be transported away from the vicinity of the corroding penetrator.

Chapter 6

Conclusions and Future Work

6.1 Conclusions

The main aim of this project was to define the mechanisms and rates of DU-Ti alloy corrosion under contrasting environmental conditions. Additional aims were to investigate the effects of DU corrosion products on the microbial communities and the transport of these corrosion products within the environment. This work substantially contributes to the knowledge of DU corrosion under different biogeochemical conditions and with different water contents (field-moist and waterlogged); the dissolved and particulate products formed; the transport of corrosion products, and the impact of DU on the natural microbial community. The aims of these studies have therefore been achieved and the following conclusions bring together the findings in chapters 3 - 5.

6.1.1 Corrosion of DU-Ti Alloy Penetrators in Marine Environments

Two waterlogged marine environments were investigated, an organic-rich fine grained marine sediment and dune sand. Similar mechanisms of corrosion were observed in these systems, with localised pitting and the formation of black/grey UO_2 which adhered to the coupon. Colloidal and particulate DU corrosion products were not observed, indicating that oxidation of UO_2 and dissolution of uranyl ions from the DU penetrator were the main input of U into the surrounding environment. The uranyl species released were found to sorb to sediments to form secondary U species. Figure 6.1 shows a conceptual model of the mechanism of DU corrosion in the environment.

In the organic-rich sediments the rate of DU corrosion was not affected by the salinity of the water (31.5 and 16.5), at 0.056 ± 0.006 g cm^{-2} y^{-1}. Therefore the higher chloride concentration did not enhance the rate of DU corrosion. In the sand at a salinity

of 31.5, the corrosion of DU was slower at 0.020 ± 0.003 g cm^{-2} y^{-1}. Parameters such as pH, cation exchange capacity and organic matter contribute to the corrosivity of an environment (MATTSSON, 1989) and the sand used in this study had a less acidic pH range (pH 7.2 - 7.5 vs. 7.1 - 8.0), lower cation exchange capacity (1.3 vs. 4.0 meq/100 g) and a lower organic carbon content (0.80 vs. 3.2 %) than the sediment. These studies highlight the importance of sand/sediment properties and how corrosion rates based on dissolution in simple solutions are not sufficient to predict the fate of DU in the environment.
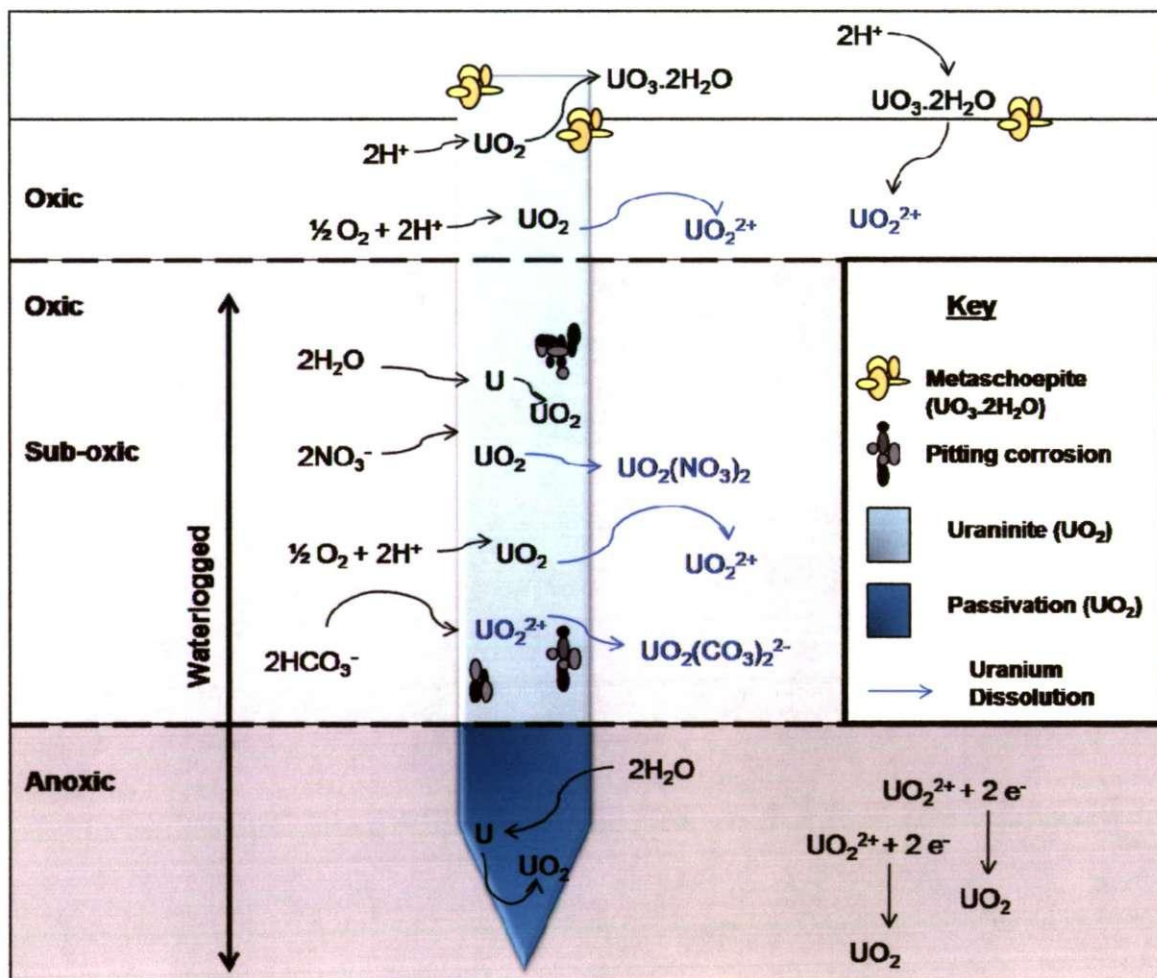

Figure 6.1 A conceptual model showing the mechanisms of DU corrosion in the terrestrial environment.

Corrosion of DU was only observed in marine sediments under oxic/sub-oxic conditions. Under increasingly anoxic conditions the corrosion of DU ceased. It was also observed that the geochemical environment can be affected by corroding DU, with a more rapid progression through the redox cascade in microbially active sediments and the reduction of redox indicators in the sand. In microbially active sediments the rapid progression through the redox cascade may be attributed to H_2 being used as an electron donor to support microbial reduction of NO_3^- (ACHTNICH et al., 1995), Fe(III) (CACCAVO et al., 1994) and SO_4^{2-} (OREMLAND and POLCIN, 1982) or H_2 abiotically reducing NO_3^-, Fe(III) and, to a lesser extent, SO_4^{2-} (MARSH and MCINERNEY, 2001). In an oxygenated environment the reduction of terminal electron acceptors may be mainly due to an abiotic process.

6.1.2 Corrosion of DU-Ti Alloy and its Transport in the Terrestrial Environment

Two terrestrial environments, a silty loam soil and a dune sand, were investigated under field-moist and waterlogged conditions. In the field-moist environments, latent periods of 88 and 242 days were observed prior to the onset of corrosion in the sand and soil, respectively. The DU corroded by deep pitting and eventually became covered with protruding, predominately yellow metaschoepite and black uraninite corrosion products. The presence of corroding DU again affected the geochemical environment with NO_3^-- and Fe(III)- reduction taking place despite the system remaining oxic. In the soil, the corrosion rate of DU was 0.49 g cm^{-2} y^{-1}, while in the sand the corrosion rate was lower at 0.10 g cm^{-2} y^{-1}. Again the results were consistent with the general corrosivity of the matrices; the sand used in this study had a less acidic pH (pH 7.4 vs. 5.5), lower moisture content (13 vs. 22 %), lower cation exchange capacity (1.3 vs. 21 meq/100 g) and a lower organic carbon content (0.80 vs. 12 %) than the soil.

In waterlogged soils shallow, crevice-shaped pits formed on the surface of the alloy. It was concluded that U was released into the surrounding environment by the oxidation of U(IV) at the DU surface and dissolution of uranyl species, which then sorbed to sediments. This process of corrosion is the same as in the marine microcosm and may be attributed to the waterlogged conditions. The presence of corroding DU again affected the biogeochemical environment with a more rapid progression through the redox cascade. The corrosion of DU only organic occurred under sub-oxic conditions at a rate of $0.010 - 0.020$ g cm^{-2} y^{-1}, which showed a correlation with the rate of nitrate reduction. Under anoxic conditions the corrosion ceased due to passivation of the metal (Figure 6.1).

Corrosion products such as metaschoepite can easily detached from the DU alloy and disperse in the environment; however the transport of corrosion products is mainly dependent on its dissolution and interaction with the soil/sediment. Column experiments showed that the majority of dissolved U is held in a chemical fraction with very slow desorption kinetics and it is this behaviour that will dominate U transport in the environment.

6.1.3 Impact of DU Corrosion Products on the Microbial Population

In marine sediments containing $\sim$ 7 g kg^{-1} of corroded DU, there was a marked reduction in microbial diversity. The phylogenetic affiliations found to be intolerant to the uranium released were Actinobacteria, Betaproteobacteria, Planctomycetacia, Clostridia, Spirochaetes, Bacteroidetes and Eudora. However there was also at least one member of the microbial community (Epsilonproteobacteria group) that was able to adapt and thrive in the DU contaminated sediment.

In the field-moist soil containing $\sim$76 g kg^{-1} of DU oxide (metaschoepite), there was also a distinctive change in the microbial community, with a reduction in the

114

dominant Gammaproteobacteria group, highlighting its intolerance to DU corrosion products. However the *Bacilli* phylogenetic group thrived in the presence of corroding DU and there was the appearance of two new phylogenetic groups Shingobacteria and Actinobacteria. The Betaproteobacteria and Alphaproteobacteria species also showed a tolerance to this level of DU contamination.

In the waterlogged soil containing ~2 g kg^{-1} of corroded DU, there was a marked reduction in microbial diversity. The phylogenetic affiliations found to be intolerant to the U released were Alphaproteobacteria, Shingobacteria, Clostridia, Nitrospira, and Dehalococcoidetes. Interestingly the Gammaproteobacteria group that was found to be intolerant to metaschoepite corrosion products in the field-moist soils showed tolerance in the presence of corrosion products produced in a waterlogged system.

Therefore these results demonstrate that corroding DU alters microbial community composition significantly, with drastic loss in the microbial diversity, and a shift to more DU-tolerant species. However changes in the microbial community will depend on the types of corrosion products formed.

6.1.4 Summary of Findings

These studies have made a significant contribution to the understanding of DU corrosion processes in a range of environments. The corrosion rates obtained from these studies (Table 6.1) can be applied to predict the fate of DU penetrators in the environment. From these studies a summary of general findings were:

(1) This work shows for the first time that corrosion rates are an order of magnitude higher in field-moist, oxic environments compared with waterlogged environments.

(2) Under field-moist conditions particulate and colloidal DU corrosion products are important, and these are typically metaschoepite and to a lesser extent uraninite or similar type phases. Corrosion under these conditions will lead to an increase risk of uranium dispersion into the terrestrial environment.

(3) Within soil/sediment, the transport of these DU corrosion products is mainly dependent on their dissolution and subsequent uranyl interactions with the solid phase.

(4) Under waterlogged conditions particulate and colloidal DU corrosion products are not significant. Corrosion involves the formation of adherent uraninite on the surface of DU, oxidation to U(VI) and dissolution.

(5) The formation of DU corrosion products affects the local geochemical environment. Under field-moist oxic environments the reduction of local geochemical indicators will occur, while under waterlogged environments progression through the redox cascade is more rapid.

(6) Corroding DU impacts the microbial community. Observed changes include a marked reduction in microbial diversity, intolerance and/or adaptation to corrosion products.

(7) Under anoxic conditions passivation of the DU metal occurs, preventing further corrosion. Therefore, DU deposited during conflict and test firing will be a legacy for future generation.

Table 6.1 The corrosion rates of DU-Ti alloy under characterised conditions.

Matrix	Rate $(g\ cm^{-2}\ y^{-1})$	Geochemical Conditions	Soil/ Sediment Properties
Waterlogged marine sediment (salinities of 31.5 and 16.5)	0.056 ± 0.006*	Sub-oxic	pH 6.4 - 8.0, 3.2 % organic carbon; cation exchange capacity 4.0 meq/100 g and inorganic carbon 370 mg kg^{-1}
Waterlogged sand (salinities of 31.5)	0.020 ± 0.003	oxic	pH 7.6 - 7.9 for waterlogged and 7.2 - 7.5 for field-moist, 0.8 % organic carbon; cation exchange capacity 1.3 meq/100 g and inorganic carbon 430 mg kg^{-1} and sand moisture content of 13 %
Field-moist sand	0.10 ± 0.01	oxic	
Waterlogged soil	0.010 - 0.020*	Sub-oxic	pH 5.0 - 6.5 for waterlogged and 5.0 - 6.5 for field-moist, 12 % organic carbon; CEC 21 meq/100 g and inorganic carbon 80 mg kg^{-1} and soil moisture content of 22 %
Field-moist soil	0.49 ± 0.06	oxic	

* Corrosion ceased under anoxic conditions

6.2 Future Work

Laboratory based microcosm studies have established that the rates of DU corrosion and the corrosion products formed are dependent on the water content and geochemistry of the environment and that corroding DU impacts the microbial community. Column experiments have shown that the transport of DU corrosion products in the environment is dependent its dissolution and subsequent interactions with the solid phase. Although the aims of the study were achieved there are several ways in which this work could be taken further; these include:

Nitrate Reducing Conditions

A relationship was observed between nitrate reduction and DU corrosion (Chapter 4). To investigate this relationship in more detail the NO_3^--reducing microcosm can be extended (poising) and analysed at multiple time points.

Corrosivity of the Soil/Sediment

Parameters such as pH, moisture content, anions, CEC and organic matter contribute to the corrosivity of an environment (MATTSSON, 1989). These soil/sediment properties were observed to affect the fate of DU corrosion (Chapter 4 and 5). To investigate soil/sediment properties and the corrosion of DU in more detail, microcosm studies could be carried out to investigate the importance of each individual parameter.

Abiotic and Biotic Reduction of Redox Indicator

Corroding DU was found to reduce redox indicators and/or increase progression through the redox cascade (Chapter 3 - 5). Experiments could be carried out to ascertain if H_2 is being used by microorganisms to support NO_3^-- (TILL et al., 1998) Fe(III)- (CACCAVO et al., 1994) and SO_4^{2-}-reduction (LIAMLEAM and ANNACHHATRE,

118

2007; OREMLAND and POLCIN, 1982) or if H_2 is abiotically reducing redox indicators (MARSH and MCINERNEY, 2001) or another process involved.

Chemical Oxidants

In the environment UO_2 can be chemially oxidised to the more mobile U(VI) species by O_2 (ABDELOUAS et al., 1999; MOON et al., 2007; ZHENG et al., 2002), NO_2^- (SENKO et al., 2002; 2005), the intermediates of NO_3^--reduction (N_2O, and NO) (SENKO et al., 2002) and Fe(III) (hydr)oxides (NEVIN and LOVLEY, 2000; SENKO et al., 2005). The effect of these oxidants on DU corrosion could be carried out to investigate in more detail how the chemical environment can influence the corrosion of DU.

Transport Experiments

The investigation into the transport of DU corrosion products was carried out using a simple matrix (sand) and solution (rainwater). To gain more knowledge on DU corrosion and transport other matrices should be used, possibly from regions impacted by DU and using more complex solutions, such as groundwater. More information on the dissolution and transport of DU corrosion products, will help in making predictions for real environmental systems.

DU particles have been observed at depths of up to 4 cm in a sandy loam soils (BUCK et al., 2004; JOHNSON et al., 2004) and colloidal DU particles were found to be important in a field-moist sand environment (Chapter 5). Therefore column experiments could be carried out to investigate the transport and fate of these nano sized particles and colloids in the environment.

References

Abdelouas, A., Lutze, W., and Nuttall, E. H., 1999. Oxidative dissolution of uraninite precipitated on Navajo sandstones. *J. Contam. Hydrol.* **36**, 353-375.

Achtnich, C., Bak, F., and Conrad, R., 1995. Competition for electron donors among nitrate reducers, ferric iron reducers, sulfate reducers, and methanogens in anoxic paddy soil. *Biol. Fert. Soils* **19**, 65-72.

Anderson, P., Davidson, C. M., Duncan, A. L., Littlejohn, D., Ure, A. M., and Garden, L. M., 2000. Column leaching and sorption experiments to assess the mobility of potentially toxic elements in industrially contaminated land. *J. Environ. Monit.* **2**, 234-239.

Bachmaf, S., Planer-Friedrich, B., and Merkel, B. J., 2008. Effect of sulfate, carbonate, and phosphate on the uranium(VI) sorption behaviour onto bentonite. *Radiochim. Acta* **96**, 359-366.

Bailey, M. R., Beral, V., Clayton, B., Darby, S. C., Goodhead, D. T., Hendry, J., Murray, V., Smith, B., Spratt, B., and Stoneham, M., 2002. The health hazards of depleted uranium munitions. Part II. Policy document 6/01; The Royal Society: London.

Begg, J. D. C., Burke, I. T., and Morris, K., 2007. The behaviour of technetium during microbial reduction in amended soils from Dounreay, UK. *Sci. Total. Environ.* **373**, 297-304.

Bem, H. and Bou-Rabee, F., 2004. Environmental and health consequences of depleted uranium use in the 1991 Gulf War. *Environ. Int.* **30**, 123-134.

Betti, M., 2003. Civil use of depleted uranium. *J. Environ. Radioact.* **64**, 113-119.

Bleise, A., Danesi, P. R., and Burkart, W., 2003. Properties, use and health effects of depleted uranium (DU): a general overview. *J. Environ. Radioact.* **64**, 93-112.

Borovec, Z., Kribek, B., and Tolar, V., 1979. Sorption of uranyl by humic acids. *Chem. Geol.* **27**, 39-46.

Brookins, D. G., 1988. *Eh-pH Diagrams for Geochemistry*. Springer-Verlag, Berlin.

Bruno, J., De Pablo, J., Duro, L., and Figuerola, E., 1995. Experimental study and modelling of the U(VI)-Fe(OH)$_3$ surface precipitation/coprecipitation equilibria. *Geochim. Cosmochim. Acta* **59**, 4113-4123.

Bryan, N. D., Barlow, J., Warwick, P., Stephens, S., Higgo, J. J. W., and Griffin, D., 2005. The simultaneous modelling of metal ion and humic substance transport in column experiments. *J. Environ. Monit.* **7**, 196-202.

Bryan, N. D., Jones, D. L. M., Keepax, R. E., Farrelly, D. H., Abrahamsen, L. G., Pitois, A., Ivanov, P., Warwick, P., and Evans, N., 2007. The role of humic non-exchangeable binding in the promotion of metal ion transport in groundwaters in the environment. *J. Environ. Monit.* **9**, 329-347.

Buck, B. J., Brock, A. L., Johnson, W. H., and Ulery, A. L., 2004. Corrosion of depleted uranium in an arid environment: Soil-geomorphology, SEM/EDS, XRD, and electron microprobe analyses. *Soil. Sed. Contam.* **13**, 545-561.

Burke, I. T., Boothman, C., Lloyd, J. R., Mortimer, R. J. G., Livens, F. R., and Morris, K., 2005. Effects of progressive anoxia on the solubility of technetium in sediments. *Environ. Sci. Technol.* **39**, 4109-4116.

Caccavo, F., Jr., Lonergan, D. J., Lovley, D. R., Davis, M., Stolz, J. F., and McInerney, M. J., 1994. *Geobacter sulfurreducens* sp. nov., a hydrogen- and acetate-oxidizing dissimilatory metal-reducing microorganism. *Appl. Environ. Microbiol.* **60**, 3752-3759.

Cardinale, M., Brusetti, L., Quatrini, P., Borin, S., Puglia, A. M., Rizzi, A., Zanardini, E., Sorlini, C., Corselli, C., and Daffonchio, D., 2004. Comparison of different primer sets for use in automated ribosomal intergenic spacer analysis of complex bacterial communities. *Appl. Environ. Microbiol.* **70**, 6147–6156.

Cerda, J., Gonzalez, S., Rios, J. M., and Quintana, T., 1993. Uranium concentrates bioproduction in Spain: A case study. *FEMS Microbiol. Rev.* **11**, 253-260.

Choppin, G. R., 1992. The role of natural organics in radionuclides migration in natural aquifer systems. *Radiochim. Acta.* **58/59** 113–120.

Choy, C. C., Korfiatis, G. P., and Meng, X., 2006. Removal of depleted uranium from contaminated soils. *J. Hazard. Mater.* **136**, 53-60.

De Zoubov, N., 1966. Establishment and interpretation of potential-pH equilibrium diagrams. In: Pourbaix, M. (Ed.), *Atlas of Electrochemical Equilibria in Aqueous Solution*. Pergamon Press, Oxford. Pages 198-212

DiSpirito, A. A. and Tuovinen, O. H., 1982. Uranous ion oxidation and carbon dioxide fixation by *Thiobacillus ferrooxidans*. *Arch. Microbiol.* **133**, 28-32.

Dionex, 2001. Determination of Inorganic Anions in Wastewater by Ion Chromatography: Application note 135. Dionex Corporation: Sunnyvale.

Dong, W., Xie, G., Miller, T. R., Franklin, M. P., Oxenberg, T. P., Bouwer, E. J., Ball, W. P., and Halden, R. U., 2006. Sorption and bioreduction of hexavalent uranium at a military facility by the Chesapeake Bay. *Environ. Pollut.* **142**, 132-142.

Duff, M. C., Coughlin, J. U., and Hunter, D. B., 2002. Uranium co-precipitation with iron oxide minerals. *Geochim. Cosmochim. Acta.* **66**, 3533-3547.

Echevarria, G., Sheppard, M. I., and Morel, J. L., 2001. Effect of pH on the sorption of uranium in soils. *J. Environ. Radioact.* **53**, 257-264.

EPA, 1986. SW-846 Method 9081. U.S Environmental Protection Agency: Washington DC.

EPA, 1999. Understanding variations in partition coefficients, K_d, values. U.S Environmental Protection Agency: Washington DC.

Fan, M., Thongsri, T., Axe, L., and Tyson, T. A., 2005. Using a probabilistic approach in an ecological risk assessment simulation tool: test case for depleted uranium (DU). *Chemosphere* **60**, 111-125.

Finch, R. J. and Ewing, R. C., 1992. The corrosion of uraninite under oxidizing conditions. *J. Nucl. Mater.* **190**, 133-156.

Fomina, M., Charnock, J. M., Hillier, S., Alvarez, R., Livens, F., and Gadd, G. M., 2008. Role of fungi in the biogeochemical fate of depleted uranium. *Curr. Biol.* **18**, R375-R377.

Gabriel, U., Gaudet, J. P., Spadini, L., and Charlet, L., 1998. Reactive transport of uranyl in a goethite column: an experimental and modelling study. *Chem. Geol.* **151**, 107-128.

Gates-Anderson, D.D., Laue, C.A., and Fitch, T.E., 2004. Dissolution treatment of depleted uranium waste. LLNL report no. UCRL-TR-202275, California.

Hamilton, E. I., 2001. Depleted uranium (DU): a holistic consideration of DU and related matters. *Sci. Total. Environ.* **281**, 5-21.

Hemond, H. F. and Fechner-Levy, E. J., 2000. *Chemical Fate and Transport in the Environment.* Academic Press, London.

Islam, F. S., Gault, A. G., Boothman, C., Polya, D. A., Charnock, J. M., Chatterjee, D., and Lloyd, J. R., 2004. Role of metal-reducing bacteria in arsenic release from Bengal delta sediments. *Nature* **430**, 68-71.

Jia, G., Belli, M., Sansone, S., Rosamilia, S., and Gaudino, S., 2004. Concentration, distribution and characteristics of depleted uranium (DU) in the Kosovo ecosystem: A comparison with the uranium behaviour in the environmental uncontaminated by DU. *J. Radioanal. Nucl. Chem.* **260**, 481-494.

Johnson, B. E., Medina, V. F., and Cunniff, D., 2006. Numerical simulation of depleted uranium transport in a desert environment using a distribution parameter watershed model. *Periodical of Haz., Toxic, and Radioactive Waste Mgmt.* **10**, 179-189.

Johnson, W. H., Buck, B. J., Brogonia, H., and Brock, A. L., 2004. Variations in depleted uranium sorption and solubility with depth in arid soils. *Soil. Sed. Contam.* **13**, 533-544.

Konhauser, K. O., Mortimer, R. J. G., Morris, K., and Dunn, V., 2002. The role of microorganisms during sediment diagenesis: Implications for radionuclide mobility. In: Keith-Roach, M. J. and Livens, F. R. (Eds.), *Interactions of Microorganisms with Radionuclides*. Elsevier, London. Pages 61 - 100.

Kornilovich, B. Y., Pshinko, G. N., and Koval'chuk, I. A., 2004. Effect of fulvic acids on sorption of U(VI) on clay minerals of soils. *Radiochemistry* 43, 528-531.

Langmuir, D., 1997. *Aqueous Environmental Chemistry*. Prentice Hall, New Jersey.

Laue, C. A., Gates-Anderson, D., and Fitch, T. E., 2004. Dissolution of metallic uranium and its alloys. *J. Radioanal. Nucl. Chem.* **261**, 709-717.

Liamleam, W. and Annachhatre, A. P., 2007. Electron donors for biological sulfate reduction. *Biotechnol. Adv.* **25**, 452-463.

Light, T. S., 1972. Standard solutions for redox potential measurements. *Anal. Chem.* **44**, 1038-1039.

Lo, D., Fleischer, R. L., Albert, E. A., and Arnason, J. G., 2006. Location, identification, and size distribution of depleted uranium grains in reservoir sediments. *J. Environ. Radioact.* **89**, 240-248.

Lovley, D. R. and phillips, E. J. P., 1986. Availability of ferric iron for microbial reduction in bottom sediments of the freshwater tidal Potomac River. *Appl. Environ. Microbiol.* **52**, 751-757.

Lovley, D. R. and Phillips, E. J. P., 1992. Reduction of uranium by *Desulfovibrio desulfuricans. Appl. Environ. Microbiol.* **58**, 850-856.

Lovley, D. R., Phillips, E. J. P., Gorby, Y. A., and Landa, E. R., 1991. Microbial reduction of uranium. *Nature* **350**, 413-416.

Lovley, D. R., Widman, P. K., Woodward, J. C., and Phillips, E. J., 1993. Reduction of uranium by cytochrome c3 of *Desulfovibrio vulgaris*. *Appl. Environ. Microbiol.* **59**, 3572-3576.

Lu, S. G., Tang, C., and Rengel, Z., 2004. Combined effects of waterlogging and salinity on electrochemistry, water-soluble cations and water dispersible clay in soils with various salinity levels. *Plant. Soil.* **264**, 231-245.

Mackay, D. M., Roberts, P. V., and Cherry, J. A., 1985. Transport of organic contaminants in groundwater. *Environ. Sci. Technol.* **19**, 384-392.

Marsh, T. L. and McInerney, M. J., 2001. Relationship of hydrogen bioavailability to chromate reduction in aquifer sediments. *Appl. Environ. Microbiol.* **67**, 1517-1521.

Mattsson, E., 1989. *Basic Corrosion Technology for Scientists and Engineers*. Ellis Horwood Limited, Chichester.

McIntyre, J. F., Lefeave, E. P., and Musselman, K. A., 1988. Galvanic corrosion behaviour of depleted uranium in synthetic seawater coupled to aluminium, magnesium, and mild steal. *Corros. Sci.* **44**, 502-510.

Meyer, M. C., Paschke, M. W., McLendon, T., and Price, D., 1998. Decreases in soil microbial function and functional diversity in response to depleted uranium. *J. Environ. Qual.* **27**, 1306-1311.

MOD, 2008. The UK Ministry of Defence, Depleted Uranium, http://www.mod.uk/DefenceInternet/AboutDefence/WhatWeDo/HealthandSafet y/DepletedUranium/DepletedUraniumdu.htm [viewed 30.09.08].

Moon, H. S., Komlos, J., and Jaffe, P. R., 2007. Uranium reoxidation in previously bioreduced sediment by dissolved oxygen and nitrate. *Environ. Sci. Technol.* **41**, 4587-4592.

Morris, K. and Raiswell, R., 2002. Biogeochemical cycles and remoblisation of the actinide elements. In: Keith-Roach, M. J. and Livens, F. R. (Eds.), *Interactions of Microorganisms with Radionuclides.* Elsevier, London. Pages 101-142.

Murphy, R. J., Lenhart, J. J., and Honeyman, B. D., 1999. The sorption of thorium (IV) and uranium (VI) to hematite in the presence of natural organic matter. *Colloid. Surf. A.* **157**, 47-62.

Nealson, K. H. and Saffarini, D., 1994. Iron and manganese in anaerobic respiration: environmental significance, physiology, and regulation. *Annu. Rev. Microbiol.* **48**, 311-343.

Nevell, W. and Wainwright, M., 1986. Increases in extractable sulphate following soil submergence with water, dilute sulphuric acid or acid rain. *Environ. Pollut. B.* **12**, 301-311.

Nevin, K. P. and Lovley, D. R., 2000. Potential for nonenzymatic reduction of Fe(III) via electron shuttling in subsurface sediments. *Environ. Sci. Technol.* **34**, 2472-2478.

Oremland, R. S. and Polcin, S., 1982. Methanogenesis and sulfate reduction: competitive and noncompetitive substrate in estuarine sediments. *Appl. Environ. Microbiol.* **44**, 1270-1276.

Papastefanou, C., 2002. Depleted uranium in military conflicts and the impact on the environment. *Health Phys.* **83**, 280-282.

Pollmann, K., Raff, J., Merroun, M., Fahmy, K., and Selenska-Pobell, S., 2006. Metal binding by bacteria from uranium mining waste piles and its technological applications. *Biotechnol. Adv.* **24**, 58-68.

POST, 2001. Parliamentary Office of Science and Technology, Depleted Uranium. Postnote number 154, www.parliament.uk/post/pn154.pdf [viewed 30.09.08].

Pourbaix, M., 1966. Corrosion. In: Pourbaix, M. (Ed.), *Atlas of Electrochemical Equilibria in Aqueous Solution*. Pergamon Press, Oxford. Pages 70-83.

Prichard, P. H. and Bourquin, A. W., 1984. The use of microcosm for evaluation of interactions between pollutants and microorganisms. In: Marshall, K. C. (Ed.), *Advances in Microbial Ecology*. Plenum Press, New York. Pages 133–215.

Priest, N. D., 2001. Toxicity of depleted uranium. *Lancet* **357**, 244-246.

Reeder, R. J., Nugent, M., Lamble, G. M., Tait, C. D., and Morris , D. E., 2000. Uranyl incorporation into calcite and aragonite: XAFS and luminescence studies. *Environ. Sci. Technol.* **34**, 638-644.

Reinoso Maset, E., Sidhu, S. H., Fisher, A., Heydon, A., Worsfold, P. J., Cartwright, A. J., and Keith-Roach, M. J., 2006. Effect of organic co-contaminants on technetium and rhenium speciation and solubility under reducing conditions. *Environ. Sci. Technol.* **40**, 5472-5477.

Ringelberg, D., Reynolds, C., and Karr, L., 2004. Microbial community composition near depleted uranium impact points. *Soil. Sed. Contam.* **13**, 563-577.

Santos, P.; Pinhal, I.; Rainey, F.; Empadinhas, N.; Costa, J.; Fields, B.; Benson, R.; Veríssimo, A.; da Costa, 2003. Gamma-proteobacteria *Aquicella lusitana* gen. nov., sp. nov., and *Aquicella siphonis* sp. nov. infect protozoa and require activated charcoal for growth in laboratory media. *Appl. Environ. Microbiol.* **69**, 6533-6540.

Schimmack, W.; Gerstmann, U.; Schultz, W.; Geipel, G., Long-term corrosion and leaching of depleted uranium (DU) in soil *Radiat. Environ. Biophys.* 2007, **46**, 221-227

Schippers, A., Hallmann, R., Wentzien, S., and Sand, W., 1995. Microbial diversity in uranium mine waste heaps. *Appl. Environ. Microbiol.* **61**, 2930-2935

Schüßler, W., Artinger, R., Kim, J. I., Bryan, N. D., and Griffin, D., 2001. Numerical modelling of humic colloid borne Americium (III) migration in column experiments using the transport/speciation code K1D and the KICAM model. *J. Contam. Hydrol.* **47**, 311-322.

Selenska-Pobell, S., Panak, P., Miteva, V., Boudakov, I., Bernhard, G., and Nitsche, H., 1999. Selective accumulation of heavy metals by three indigenous Bacillus strains, *B-cereus*, *B-megaterium* and *B-sphaericus*, from drain waters of a uranium waste pile. *FEMS Microbiol. Ecol.* **29**, 59-67.

Senko, J. M., Istok, J. D., Suflita, J. M., and Krumholz, L. R., 2002. In-situ evidence for uranium immobilization and remobilization. *Environ. Sci. Technol.* **367**, 1491-1496.

Senko, J. M., Mohamed, Y., Dewers, T. A., and Krumholz, L. R., 2005. Role for Fe(III) minerals in nitrate-dependent microbial U(IV) oxidation. *Environ. Sci. Technol.* **39**, 2529-2536.

Shanbhag, P. M. and Choppin, G. R., 1981. Binding of uranyl by humic acid. *J. Inorg. Nucl. Chem.* **43**, 3369-3372.

Sheppard, S.C., Sheppard, M.I., Tait, J.C., and Sanipelli, B.L., 2006. Revision and meta-analysis of selected biosphere parameter values for chlorine, iodine, neptunium, radium, radon and uranium. *J. Environ. Radioact.* **89**, 115-137.

Smith, K. A., 1980. A model of the extent of anaerobic zones in aggregated soils, and its potential application to estimates of denitrification. *J. Soil. Sci.* **31**, 263-277.

Stookey, L. L., 1970. Ferrozine - a new spectrophotometric reagent for iron. *Anal. Chem.* **42**, 779-781.

Sylwester, E. R., Hudson, E. A., and Allen, P. G., 2000. The structure of uranium (VI) sorption complexes on silica, alumina, and montmorillonite. *Geochim. Cosmochim. Acta.* **64**, 2431-2438.

Till, B. A., Weathers, L. J., and Alvarez, P. J. J., 1998. Fe(0)-supported autotrophic denitrification. *Environ. Sci. Technol.* **32**, 634-639.

Toque, C. C. L. and Baker, A. C., 2006. MOD DU program – the corrosion of depleted uranium in the Kirkcudbright and Eskmeals terrestrial environments. DSTL report no. DSTL/CR10978 V2.0, Alverstoke.

Toque, C. C. L. and Baker, A. C., 2007. MOD DU program - Report on the corrosion of depleted uranium in the Solway Firth. DSTL report no. DSTL/ CR11679 V1.0, Alverstoke.

Torok, S., Osan, J., Vincze, L., Kurunczi, S., Tamborini, G., and Betti, M., 2004. Characterization and speciation of depleted uranium in individual soil particles using microanalytical methods. *Spectrochim. Acta. B.* **59**, 689-699.

Trzaskoma, P. P., 1982. Corrosion rates and electrochemical studies of depleted uranium alloy tungsten fiber metal matrix composite. *J. Electrochem. Soc.* **129**, 1398-1402.

UNEP, 2001. Depleted uranium in Kosovo, post-conflict environmental assessment, United Nations Environment Programme, Imprimerie Chirat, France.

UNEP, 2002. Depleted uranium in Serbia and Montenegro: Post-conflict environmental assessment in the Federal Republic of Yugoslavia, United Nations Environment Programme, Imprimerie Chirat, France.

UNEP, 2003. Depleted uranium in Bosnia and Herzegovina: Post-conflict environmental assessment, United Nations Environment Programme, Imprimerie Chirat, France.

Waite, T. D., Davis, J. A., Payne, T. E., Waychunas, G. A., and Xu, N., 1994. Uranium(VI) adsorption to ferrihydrite: Application of a surface complexation model. *Geochim. Cosmochim. Acta.* **58**, 5465-5478.

131

Warwick, P. W., Hall, A., Pashley, V., Bryan, N. D., and Griffin, D., 2000. Modelling the effect of humic substances on the transport of europium through porous media: a comparison of equilibrium and equilibrium/kinetic models. *J. Contam. Hydrol.* **42**, 19-34.

WHO, 2001. Depleted uranium, sources, exposure and health effects, Department of protection of the human environment, World Health Organization, Geneva.

WHO, 2005. Uranium in drinking-water. Background document for development of WHO Guidelines for Drinking-water Quality. World Health Organization, Geneva.

Zheng, Y., Anderson, R. F., Geen, A., and Fleisher, M. O., 2002. Remobilisation of authigenic uranium in marine sediments by bioturbation. *Geochim. Cosmochim. Acta.* **66**, 1759-1772.